LOCALIZED CRUSHING IN ICE-STRUCTURE INTERACTION

RICHARD BENEDICT MEANEY, B.Eng., P.Eng.

LOCALIZED CRUSHING IN ICE-STRUCTURE INTERACTION

BY

RICHARD BENEDICT MEANEY, B.ENG., P.ENG

A THESIS SUBMITTED TO THE SCHOOL OF GRADUATE STUDIES IN PARTIAL FULFILLMENT OF THE REQUIREMENTS FOR THE DEGREE OF MASTER OF ENGINEERING

FACULTY OF ENGINEERING AND APPLIED SCIENCE

MEMORIAL UNIVERSITY OF NEWFOUNDLAND

JANUARY, 1992

ST. JOHN'S NEWFOUNDLAND CANADA

ISBN 0-315-73289-X

To my wife

Noeleen

Abstract

The National Research Council of Canada conducted a medium-scale ice-indentation test program on Hobson's Choice Ice Island in May, 1990. This test series was performed as an extension to a similar program of the previous year. A description of the 1990 test program along with an extensive characterization study of the observed failure surface is presented. More specifically, this study included measurements of the pulverized layer thickness, comparative density analysis of ice taken from the pulverized layer to undamaged ice, sieve analysis of ejected particles and microstructural studies of damage and pressure melting.

Ice samples, both undamaged multi-year sea ice and ice from the pulverized layer, were collected and transported to the Ice-Structures Laboratory of Memorial University of Newfoundland. Uniaxial compression tests, including constant strain rate tests and creep tests, were conducted. Estimates of peak stress, elastic strain, delayed elastic strain and permanent viscous creep were determined and comparisons were made between undamaged, predamaged and pulverized ice. Substantial creep enhancement was observed, that is total creep strain appeared to be heavily influenced by the damage state.

Utilizing measured parameters of the uniaxial compression test program, field observations and a damaging viscoelastic material model, finite element simulations were conducted. This finite element analysis focused on the behaviour of an intermediate layer of highly damaged ice at the ice-structure interface. Indentation test NRC-06 of the 1989 test program was chosen as the verification test.

Acknowledgements

The Guidance and assistance of Dr. I.J. Jordaan, NSERC/Mobil Industrial Research Professor in Ocean Engineering, Memorial University of Newfoundland, provided the motivation and challenges necessary to complete this work. His supervision and financial assistance is graciously acknowledged.

In relation to the Ice-Indentation tests on Hobson's Choice Ice Island, a note of appreciation must be extended to Dr. R. Frederking, National Research Council of Canada, and to Dr. N.K. Sinha, National Research Council of Canada. Both displayed a keen interest in this work and offered freely their advice and encouragement. The assistance of Mr. J. Xiao, Memorial University of Newfoundland, must also be acknowledged. Mr. Xiao contributed many hours of his time and reduced the burden of the finite element analysis. Furthermore, Mr. B. Stone, Memorial University of Newfoundland, provided assistance with the laboratory testing procedures and this is greatly appreciated.

Financial assistance for this work was made available through the Career Development Program of the Government of Newfoundland and Labrador and through the Center for Cold Ocean Resources Engineering of Memorial University of Newfoundland. Funding for travel to Canada's Ice Island was provided by the Northern Scientific Training Program.

Contents

List of Figures

List of Tables

Nomenclature

a_T	A constant defined by Sinha as 2.5×10^{-4} s^{-1} at 263 K.
d	Nominal grain diameter (mm).
d_1	Reference grain diameter (1 mm).
D	Damage parameter.
E	Young's modulus (MPa).
E_k	Spring constant of Kelvin unit (MPa).
E_m	Spring constant of Maxwell unit (MPa).
f	Frequency (Hz).
G	Shear modulus(MPa).
h	Thickness of idealized crushed layer (mm).
H_s	Desired stroke of hydraulic ram (mm).
K	Bulk modulus (MPa).
l	Length of indenter (m).
l_g	Actual gage length (mm).
N	Total number of cracks.
N_g	Crack density of one crack per grain.
$\dot{N}$	Crack rate.
NACL	Area of no apparent crushed layer (m^2).
NCA	Nominal contact area (m^2).
P_x	Contact pressure at location x (MPa).
Q	Activation energy (kJ/mol).
R	Universal gas constant (8.31 $kPa.L.mol^{-1}.K^{-1}$).
S	Deviatoric stress (MPa).
t	Time (s).
T	Temperature (K).
T_m	Melting temperature (K).
u	Indentation velocity (mm/s).
β	Creep enhancement parameter.
ϵ	strain (mm/mm).
ϵ_c, ϵ_{ij}^c	Permanent creep strain (mm/mm).
ϵ_d, ϵ_{ij}^d	Delayed elastic strain (mm/mm).
ϵ_e, ϵ_{ij}^e	Elastic strain (mm/mm).
ϵ_t, ϵ_{ij}^t	Total strain (mm/mm).
$\dot{\epsilon}$	Strain rate (s^{-1}).

$\dot{\epsilon}_{v_1}$	Permanent viscous creep parameter for unit stress. Defined by Sinha as 1.76×10^{-7} s^{-1} at 263 °K.
μ	Dynamic viscosity (MPa.s).
μ_k	Dynamic viscosity of Kelvin unit (MPa.s).
μ_m	Dynamic viscosity of Maxwell unit (MPa.s).
ρ_c	Density of crushed ice (kg/m^3).
ρ_i	Density of intact ice (kg/m^3).
σ	Stress (MPa).
σ_d	Stress applied to the Kelvin dashpot (MPa).
σ_s	Stress applied to the Kelvin spring (MPa.).
τ	Desired test period (s).

Chapter 1

Introduction

Energy self-sufficiency is considered by many western countries to be essential for sustaining economic development and maintaining wealth. Canada, with a vast supply of natural resources, has great potential for the development of both its hydroelectric power as well as its hydrocarbon reserves. Much of Canada's hydrocarbon reserves are located under arctic and sub-arctic oceans, hindering exploration and development efforts. The designers of exploration and production structures, as well as tankers and pipelines must consider environmental loads from high winds, waves and ice. This is especially true for those projects in the Beaufort Sea, the Labrador Sea and the North Atlantic Ocean off the East Coast of Newfoundland. Compounding the difficulty of developing these resources is the inherent volatility of the oil industry. Economically designed structures are essential for the successful development of Canada's offshore oil reserves.

The design process requires proper selection of ice loads. Over design will lead to excessive construction costs, reducing a project's feasibility, while underestimating design loads could result in catastrophic failure of the structure and extensive loss of life. Selection of design loads is a complex procedure; the forces which are generated

during the collision of an ice feature and a structure (ice-structure interaction) vary with the behaviour of both the structure and the ice feature. Structural compliance and geometry play a significant role. For example, the peak forces exerted on a structure are highly dependent on the structural design characteristics and their effects on ice failure mode. Artificial islands, with gently sloping beaches force bending failure of approaching ice sheets. Caisson retained structures are designed with rigid vertical walls and ice will typically fail by crushing or buckling. Arctic vessels such as ice breakers often ram ice features to force crushing and flexural failures. Additionally, the conceptual design of the Hibernia gravity based structure (GBS) incorporates a wedged ice belt which is intended to dissipate the kinetic energy of an colliding iceberg through ice crushing. Properties of the ice feature also affects the applied loads. The compressive strength of ice has been shown to be dependent on indentation rate, crystal structure, salinity, and temperature. The collision geometry must also be considered; total contact area and aspect ratio significantly contribute to the peak forces (Sanderson, 1988).

The focus of recent research efforts, at Memorial University of Newfoundland, has been directed towards three primary areas of interest, these are: pressure area relationships, ice-induced vibrations, and localized pressure gradients. Ice loads for early arctic structures were predicted from extrapolation of small scale laboratory test data to full scale designs. Contact areas for the actual structures were, in many cases, hundreds of times greater than that of the laboratory samples and the resulting ice loads were grossly overestimated. This pressure area relationship is often termed "scale effect". In cases where ice is failing by continuous crushing, fluctuations in load are frequently observed. These ice-induced vibrations can have

detrimental effects, even when peak forces do not exceed design specifications. An extreme example of the effects of ice-induced vibrations was seen with Gulf Canada Resources' Molikpaq on the Amauligak I-65 site in March 1986. Liquefaction, a form of fatigue of the structures sand berm foundation, resulted when dynamic loads persisted for approximately 30 minutes. It was estimated that the structure was within minutes of loosing lateral stability. Localized pressure gradients also raise concerns. During ice-structure interaction events, localized peak pressures, at the contact interface, have been determined to exceed five times the uniaxial compressive strength of ice. This observation appears to hold true even in cases where average global loads are surprisingly low.

An interesting characteristic of the Molikpaq incident was the existence of a 8 m high pile of crushed ice adjacent to the structure (Jefferies and Wright, 1988). This crushed ice appeared to be extruded from the ice-structure interface. The formation and extrusion of a pulverized layer of ice appears to accompany ice-structure interaction events, in which the ice is failing by continuous crushing and ice-induced vibrations are, in part, attributed to this activity. Kheisin et al. (1976), one of the first researchers to report the existence of this layer, postulated that the crushed material could behave as a highly viscous fluid and the crushed ice would be analogous to oil in a hydrostatic bearing. It is conceivable that a single crushing cycle may proceed as follows: the intermediate layer is squeezed causing the load to increase; if the stresses reach some critical level, damage processes spark the formation of microcracks which coalesce and create a new layer; this thicker layer can no longer support these high stresses and the load is reduced.

If ice-induced vibrations are to be understood, a fundamental knowledge of the

formation and behaviour of the intermediate crushed layer is essential. Presented herein is a comprehensive study of this crushed layer. This study encompasses field experimentation, laboratory testing, and mathematical modelling. More specifically, a characterization study of the ice failure zone was conducted on Hobson's Choice Ice Island, May 1990. Samples of intact and highly damaged ice were collected and brought to the Ice Structures laboratory of Memorial University of Newfoundland for uniaxial compression testing, and finally, finite element modelling was performed to investigate Kheisin's viscous fluid assumption. This thesis contains:

- A review of the literature pertaining to ice-structure interaction, including ice-induced vibrations, mechanical properties of ice and constitutive modelling.
- Field test data obtained on Hobson's Choice Ice Island including characterization of the ice failure zone.
- Details of the uniaxial compression test program with data analysis.
- Finite element analysis simulating the extrusion of a crushed layer.
- Discussions and concluding remarks.

Chapter 2

Literature Review

2.1 Ice-Induced Vibrations

The practical significance of ice-induced vibrations was brought to light on April 12, 1986 at 0800 hrs (Jefferies and Wright, 1988). Gulf's caisson retained structure "Molikpaq", while deployed at the Amauligak I-65 site, was subjected to an interaction with a multi-year ice floe. This floe, moving at 0.06 m/s, was continuously crushed against the vertical wall of the structure and dramatic vibrations resulted. Although the peak loads marginally exceeded the design load of 500 MN, prolonged vibrations (approximately 30 min. duration) led to partial fatigue (liquefaction) of the sand core foundation. The frequency of these vibrations was of the order of 1 Hz with a normalized dynamic amplitude of 45 % (Jefferies and Wright, 1988). Interestingly after a period of time the dynamic loads on the Molikpaq became phase-locked, that is the loads acting on various locations of the structure were in phase even though the amplitudes were not necessarily equal. Following the event, a uniform 8 m high pile of crushed ice had formed at the ice structure interface and this material consisted of blocks of reformed (sintered) ice powder. Jefferies and Wright (1988) highlighted two models which attempt to explain the physical pro-

cesses associated with ice-induced vibrations, these include the models of; Jordaan (1986) and Hallam and Pickering (1988).

The model proposed by Hallam and Pickering (1988) would see a typical load cycle proceed as follows: the ice floe approaches the structure and the structure begins to deflect; when the brittle ice strength is reached the ice crushes; the load is released and the structure springs back (and the ice floe springs forward) extruding the pulverized ice. It should be noted that the extrusion occurs as the load is reduced, i.e. on the down cycle. In this model, the ice is represented as a spring in series with a nonlinear dashpot and the dashpot is given a weak fracture link. Additionally the crushed layer is modeled as either a Mohr-Coulomb material or a Newtonian viscous fluid. Although this model produces reasonable results there are conceptual difficulties. If, for example, the crushed layer is to behave as a Newtonian fluid, the total load should be inversely proportional to h^3, where h is the crushed layer thickness. This model suggests that the load drops as the crushed layer is being extruded, thus contradicting the viscous fluid theory.

In the work of Jordaan (1986), ice is shown to be a creeping solid which is extremely brittle. Ice does not display a unique yield stress. Excluding hydrostatic states of stress, ice will creep under any loading condition. Furthermore, as ice fails by crushing, microcracks initiate, grow and coalesce to create discrete particles, thus degrading the mechanical properties of the ice. Plasticity theory requires a unique yield stress and as well, does not allow for degradation of the material behaviour. Plasticity theory simply does not apply to ice. Jordaan (1986) also highlights the formation and extrusion of a layer of crushed ice at the ice-structure interface and introduces the work of the Russian researcher Kheisin. Kheisin et

al. (1976), modelled this layer as a Newtonian fluid. The importance of numerical modelling techniques is also introduced. Sophisticated geometries coupled with complex material behaviour makes some closed form solutions impractical.

Following a series of laboratory indentation tests, Jordaan and Timco (1988) proposed that stored elastic energy and instability of the crushing process would prevent crushing from being continuous. Each crushing event would correspond to the pulverization of a finite volume of ice. The fluctuations in load were associated with periodic crushing followed by clearing of the pulverized ice. It was also noted that the clearing processes could continue throughout the crushing cycle. In an energy analysis, Jordaan and Timco (1988) showed that the pulverization process required very little energy relative to the total energy input. Similarly energy dissipation through elastic fluctuations were small. The greatest source of energy dissipation was associated with the clearing process, which in this work was assumed to be viscous extrusion of the crushed layer.

Full scale experiences with ice-induced vibrations are not restricted to the Molikpaq incident. Blenkarn (1970) presented data collected during the winter of 1963-64 from a Cook Inlet structure. This data clearly revealed a classic saw tooth load-time history. As well, crushing frequencies were recorded on the order of 0.5 to 2 Hz. Määttänen (1975a and 1975b) presented a study of the Kemi I and Kemi II single-pile tubular-steel lighthouses. These structures were extremely sensitive to ice-induced vibrations. The Kemi I collapsed in the winter of 1974, less than one year after its deployment. Määttänen suggested that ice crushing excited the natural frequency of the structure. Typical oscillating frequencies of the Kemi II were measured to be between 0.8 and 3.85 Hz. Engelbrektson (1977) instrumented

the Norströmsgrund lighthouse situated in the Gulf of Bothnia of the Baltic Sea. This concrete caisson structure experienced extreme vibrations in the winter of 1972-73. Again load fluctuations were measured to be at the natural frequency of the structure (approximately 2.3 Hz).

Björk (1981) summarized the response of several baltic lighthouses to ice loadings. The Nygrån was built in 1958 and collapsed in the winter of 1968-69; the cause of the collapse was not specified. The Vallinsgrund which was constructed in 1972 experienced equipment failures due to excessive vibrations and finally collapsed in April of 1979. Following their deployment in 1969, the lighthouses Björnklacken and Borussiagrund suffered horizontal displacements under heavy ice loads. During the winter of 1967 the Tainio lighthouse was displaced 14 m. The Kemi I concrete lighthouse was constructed in 1975. This structure was heavily instrumented with pressure cells and accelerometers. Load fluctuations were typically random although steady oscillations of approximately 2.9 to 3.1 Hz (the natural frequency of the structure) and 0.5 to 1.0 Hz were recorded.

2.2 Crushed Layer

D. E. Kheisin must be given credit for his pioneering work in the characterization of the ice failure zone. With an extensive drop-ball test program, Kheisin and his colleagues analyzed variations of the ice crystal structure in the vicinity of impact and presented mathematical models which describe the behaviour of the damaged material. These experiments were conducted in the winter and early spring of 1967 and included 200 individual tests. Hemispherical castings weighing 300 kg and 156 kg were dropped from various heights onto lake ice. Accelerations of the casting

and final impressions in the ice were recorded for each test.

Kheisin and Cherepanov (1973) reported that subjecting an ice cover to impact resulted in the formation of three characteristic layers within the ice column (see Figure 2.1). The first layer, with a thickness of 0 - 2 cm and opaque white appearance was shaped as a distorted lens and was considered to be a zone of total fracture and compression. As a result of partial melting the first 1 - 1.5 mm were smooth and more transparent. A clearly demarcated boundary indicated the beginning of layer II. Numerous radial macrocracks and fine microcracks along grain boundaries and basal planes typified this layer. At the centre of the impression, where the damage was greatest, small isometric crystals formed along intercrystaline boundaries. Crystal delamination could also be observed in this layer. Finally, layer III contained large radial cracks transecting crystals irrespective of their shape, size or orientation. Kheisin and Cherepanov speculated that the formation of the intermediate crushed layer resulted from basal plane shear and that the presence of submicroscopic ice particles and a small volume of liquid phase gave the crushed layer a viscous behaviour. Upon completion of a test, pressure reduction permitted instantaneous freezing. Furthermore, given the very short interaction time and the low thermal conductivity of ice this process was considered adiabatic and thus the heat liberated during the test would produce a local temperature rise. It was finally proposed that the crushed layer could be modelled as a very viscous Newtonian liquid.

Utilizing the drop-ball test data, Kheisin and Likhomanov (1973) determined the specific energy of crushing for ice. This parameter was defined as a ratio of the irreversible spent energy of the impact to the mass of ice in the volume of the

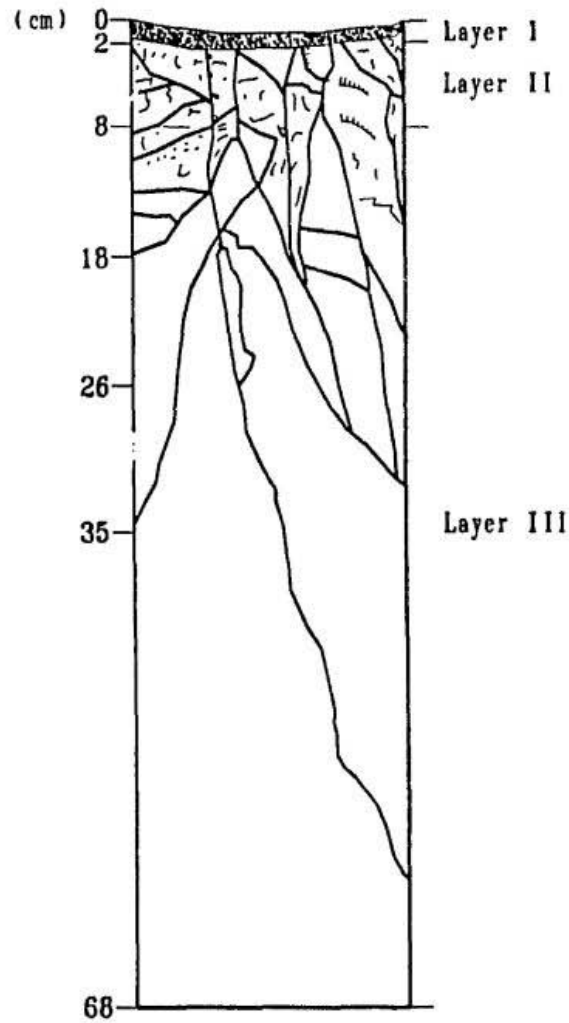

Figure 2.1: Distribution of damage from Kheisin and Cherepanov (1973).

indentation. The mean value of the specific energy of mechanical crushing was computed for spring ice and winter ice, 3 J/g and 14 J/g respectively, and these values were shown to be very stable.

Once again, Kheisin et al. (1976), expanded the analysis of the drop ball tests to include the presence of a uniform, viscous, intermediate layer. Recovery coefficients of not greater than 0.2 - 0.3 for fresh water winter ice and 0.1 for sea ice, indicated a nonelastic response and added support to such a viscous model. Using cylindrical coordinates to describe the particle motion within the layer and a simplified Reynolds equation, Kheisin et al. (1976) estimated the pressure distribution under the spherical indenter. This investigation also showed that peak contact pressures under the indenter could reach five times the standard compressive strength of ice.

2.3 Creep of Ice

As with metals at high temperatures, ice will creep under compressive or tensile loadings and it is usually considered to be a viscoelastic material. Calcote (1968) used a simple creep test to describe viscoelastic behaviour. The creep test had a constant load applied instantly at time t_0. In practice this is very difficult to achieve but where necessary dynamic test data is used to supplement the creep test data and a complete creep curve can thus be obtained.

Initially the material responds elastically, this instantaneous elastic strain ϵ_e is followed by time dependant creep. A typical creep curve, as shown in Figure 2.2, is comprised of three distinct sections: primary, secondary and tertiary creep. Examination of the curve reveals that for early stages of creep, the slope decreases with time indicating a declining strain rate, this is known as primary creep. Secondary

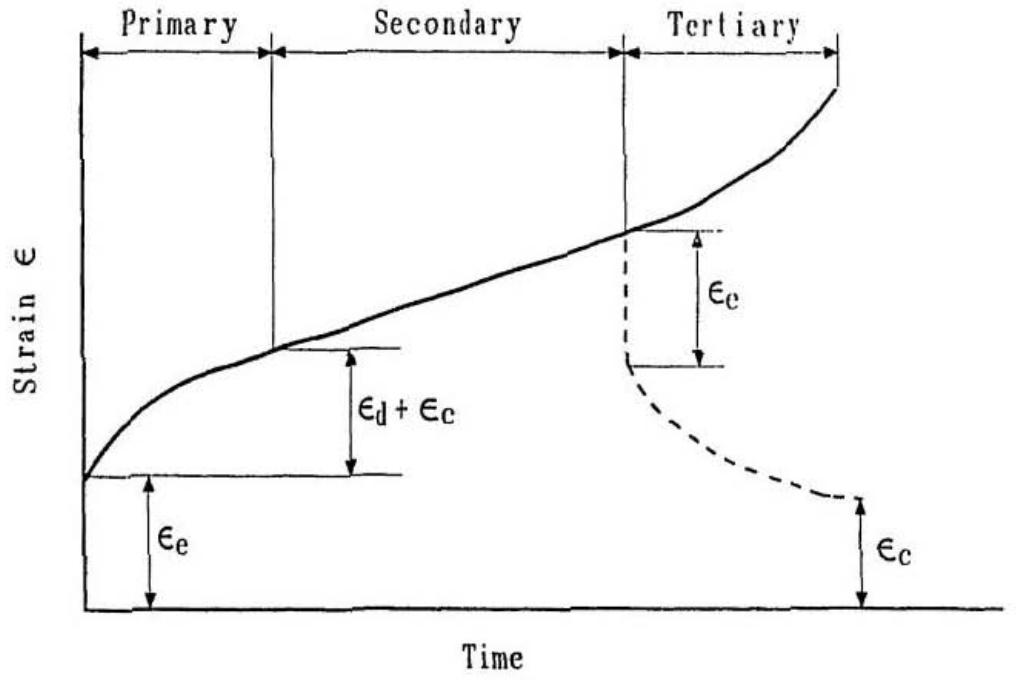

Figure 2.2: Typical creep curve for ice.

creep appears as the intermediate linear portion. Here the slope of the curve is minimum and the strain rate is constant. Tertiary creep is characterized by an increasing strain rate and this accelerating strain rate continues until fracture.

Most constitutive relationships for viscoelastic creep describe primary and secondary creep only (Calcote, 1968), this is also true in the case of ice. Furthermore these two stages of creep can be better represented if they are subdivided into delayed elastic strain and permanent viscous creep. Various techniques for modeling this behaviour will be introduced.

2.3.1 Power Law Creep

J.W. Glen pioneered the development of creep laws for ice. With his primary interest being the flow of glaciers, Glen (1955) conducted a series of compressive creep tests on polycrystalline equiaxed ice. Glen's law described the secondary creep of ice and showed that the minimum creep rate follows a power law of the form;

$$\dot{\epsilon} = k\sigma^n. \tag{2.1}$$

The exponent n was shown to be independent of temperature and was determined to be 3.17. Conversely, the value of k was influenced by temperature. Glen postulated that the value of k would take the form;

$$k = Bexp(-Q/RT) \tag{2.2}$$

where B is a constant, Q is activation energy, R is the universal gas constant and T is temperature on the absolute scale.

2.3.2 Sinha's Creep Equation

Sinha (1978) expanded the work of Glen to include primary creep or more specifically, delayed elastic strain. Sinha conducted compressive creep tests on columnar grained S2 type ice (columnar-grained ice with C-axis randomly oriented in the horizontal plane) with the loading direction perpendicular to the long axis of the grains. From this work, the total strain could be expressed as the sum of the elastic strain ϵ_e, the delayed elastic strain ϵ_d and the permanent viscous flow ϵ_c;

$$\epsilon_t(\sigma, T) = \epsilon_e(\sigma) + \epsilon_d(\sigma, t, T) + \epsilon_c(\sigma, t, T) \tag{2.3}$$

where σ is stress, t is time and T is temperature. From these tests Young's modulus was measured to be 9.3 GPa, giving good agreement with dynamic techniques. With a stress of 0.49 MPa and temperature of -20 °C, permanent viscous flow could not be measured before 800 s. The delayed elastic strain ϵ_d, was shown to behave as a decaying exponential;

$$\epsilon_d = c(\frac{\sigma}{E})^s[1 - exp\{-(a_T t)^b\}] \tag{2.4}$$

where b, c and s are constants and a_T is given by;

$$-ln(a_T) = \frac{Q}{R}(\frac{1}{T}) + m \tag{2.5}$$

m is a constant.

Sinha (1981 and 1984) described ice as a high-temperature material, with its working temperature typically greater than 0.85 T_M, where T_M is the melting temperature on the absolute scale. He also hypothesized that permanent viscous creep is associated with the mobility of defects, such as vacancies and dislocations, while delayed elasticity is governed by grain boundary sliding. Throughout this work, Sinha (1981) showed that delayed elasticity is strongly dependent upon grain size and modified his expression for delayed elastic strain to read;

$$\epsilon_d = c_1(\frac{d_1}{d})(\frac{\sigma}{E})^s[1 - exp\{-(a_T t)^b\}] \tag{2.6}$$

d_1 and d are the reference and actual grain sizes respectively. Permanent viscous creep was shown to be insensitive to grain size. Sinha's relationship for the behaviour of ice in uniaxial compression was then expressed as;

$$\epsilon_t = \frac{\sigma}{E} + c_1(\frac{d_1}{d})(\frac{\sigma}{E})^s[1 - exp\{-(a_T t)^b\}] + \dot{\epsilon}_{v_1} t(\frac{\sigma}{\sigma^1})^n. \tag{2.7}$$

The elastic strain followed Hooke's law while the permanent viscous creep is modeled after Glen's law. Note, c_1 and $\dot{\epsilon}_{v_1}$ are constants while σ^1 represents unit stress.

This creep law accurately describes the mechanical behaviour of ice under constant compressive loading. In practice, such a law must be capable of predicting the strain path for a variable stress history. Using the principal of superposition, Sinha (1981 and 1983) demonstrated the ability of his creep law to make such predictions. By applying the load in a series of incremental steps, a variable load history can be approximated, in doing so, Sinha's relationship became;

$$\begin{aligned} \epsilon_t &= \frac{1}{E}\sum_{i=1}^{n+1}\Delta\sigma_i + \frac{c_1}{E}[\frac{d_1}{d}]\sum_{i=1}^{n+1}\Delta\sigma_i[1-exp\{-(a_T[n+1-i]\Delta t)^b\}] \\ &\quad +\dot{\epsilon}_{v_1}\Delta t\sum_{i=1}^{n}[\frac{1}{\sigma^1}\sum_{j=1}^{i}\Delta\sigma_j]^n. \end{aligned} \tag{2.8}$$

Although Sinha has shown that this technique yields favorable results, it required the storage of the complete material response history.

2.3.3 Viscoelastic Model

As with Sinha's creep equation, viscoelastic models subdivide total strain into elastic strain, delayed elastic strain and permanent viscous creep. Additionally, the elastic and permanent viscous creep components are equivalent to those presented in Sinha's relationship but differences arise in the expression of delayed elastic strain. While the predicted strain-time curves of viscoelastic models are similar to those of Sinha's relationship, they lend themselves more easily to the time-stepping routines utilized by present day digital computers.

Figure 2.3 can be used to conceptualize the viscoelastic model. This Burgers body (Calcote, 1968) consists of a Maxwell unit and Kelvin (or Voigt) unit. The

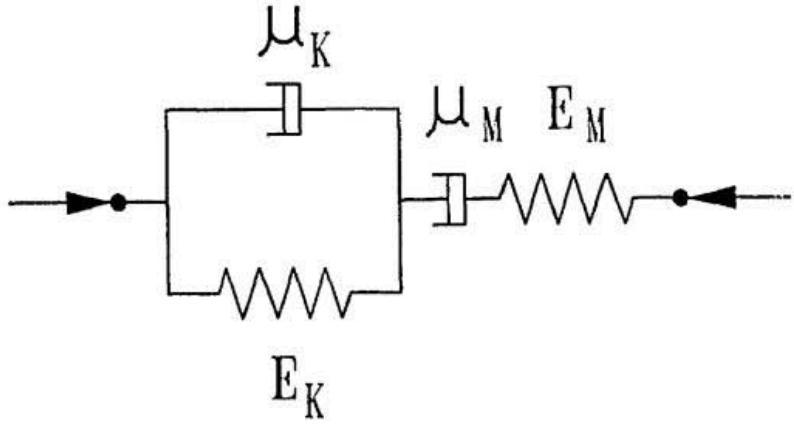

Figure 2.3: Viscoelastic model for ice (Burgers body).

Maxwell unit, which comprises a spring and dashpot in series, represents the elastic and permanent viscous creep components, while the Kelvin unit, utilizing a spring and dashpot in parallel, can model the delayed elastic strain. Applying a constant compressive load σ results in an instantaneous compression of the Maxwell spring and a time dependent, nonrecoverable, compression of the Maxwell dashpot. Additionally, the Kelvin unit produces a recoverable, time dependent, response.

Development of the constitutive relation of a viscoelastic model for ice must begin with a description of a linear spring and dashpot. A linear spring obeys Hooke's law, that is:

$$\sigma = E\epsilon, \tag{2.9}$$

while a linear dashpot behaves as a newtonian fluid:

$$\sigma = \mu\dot{\epsilon}. \tag{2.10}$$

Stress in each component of the Maxwell unit (a Hookean spring and Newtonian

dashpot connected in series) is equivalent, while the total strain of this model is the sum of the elastic and viscous strain:

$$\epsilon = \epsilon_e + \epsilon_c. \tag{2.11}$$

Substitution of equations 2.9 and 2.10 gives:

$$\epsilon = \frac{\sigma}{E_m} + \frac{\sigma}{\mu_m} t. \tag{2.12}$$

In contrast to the Maxwell model, the strain of each component of the Kelvin unit (a Hookean spring and Newtonian dashpot connected in parallel) is equivalent, while the total stress in the body is the sum of the stress in each component, therefore:

$$\sigma = \sigma_s + \sigma_d. \tag{2.13}$$

Once again, substituting equations 2.9 and 2.10 yields:

$$\sigma = E_k \epsilon + \mu_k \dot{\epsilon}. \tag{2.14}$$

Solving this differential equation for ϵ produces:

$$\epsilon_d = \frac{\sigma}{E_k}[1 - e^{(-\frac{E_k t}{\mu_k})}]. \tag{2.15}$$

Combining equations 2.12 and 2.15 thus gives the constitutive relationship for a linear viscoelastic model:

$$\epsilon_t = \frac{\sigma}{E_m} + \frac{\sigma}{\mu_m} t + \frac{\sigma}{E_k}[1 - e^{(-\frac{E_k t}{\mu_k})}]. \tag{2.16}$$

Refer to Calcote (1968) and Fung (1969).

2.3.4 Damaging Viscoelastic Model

A simple Burgers body comprised of linear springs and dashpots cannot accurately reproduce the creep in ice. It is widely accepted that a power law relationship produces acceptable results for secondary creep but difficulties arise when describing delayed elastic strain. Jordaan and McKenna (1988) suggested that delayed elastic strain could be represented by a chain of linear Kelvin units or by a single Kelvin unit with a nonlinear dashpot. It is also conceivable that a chain of nonlinear Kelvin units could be used to model delayed elastic strain in ice.

McKenna et al. (1990a and 1990b) presented a damaging viscoelastic model for ice. In this work isotropic behaviour was assumed. Once again, the total strain was expressed as a sum of three components: elastic, delayed elastic and permanent creep strain. When expressed in the general form this expression became:

$$\epsilon_{ij}^{t} = \epsilon_{ij}^{e} + \epsilon_{ij}^{d} + \epsilon_{ij}^{c}. \tag{2.17}$$

The elastic behaviour followed Hooke's law and was expressed as:

$$\epsilon_{ij}^{e} = C_{ijkl}\sigma_{kl}, \tag{2.18}$$

where C_{ijkl} is the elastic stiffness tensor. Permanent creep was expresses as a power law of the form:

$$\dot{\epsilon}_{ij}^{c} = \dot{\epsilon}_{0}^{c}\frac{(S)^{n-1}}{(\sigma_0)^{n}}S_{ij}, \tag{2.19}$$

where $\dot{\epsilon}_0^c$ is a creep constant, σ_0 is a normalized stress, n is a positive exponent and S is the applied load.

The delayed elastic strain was modelled as a Kelvin unit with a nonlinear dashpot and a linear spring. McKenna et al. (1990a and 1990b) expressed the delayed

elastic strain for this nonlinear Kelvin unit as:

$$\dot{\epsilon}^d = \frac{S^d}{\mu(S^d)}, \tag{2.20}$$

where the dashpot viscosity μ is a function of the internal stress S^d and is expressed as:

$$S^d = S - 2G_k\epsilon^d, \tag{2.21}$$

with $2G_k$ being defined as the spring stiffness of the Kelvin unit, while ϵ^d, the accumulated delayed elastic strain was given by:

$$\epsilon^d = \int_0^t \dot{\epsilon}^d dt. \tag{2.22}$$

Additionally, the effective viscosity of the Kelvin unit was written as follows:

$$\mu(S^d) = \frac{(\sigma_0)^n}{\dot{\epsilon}_0^d (S^d)^{n-1}}. \tag{2.23}$$

The above expressions apply to undamaged ice only. The formation of cracks within the solid i.e. damage, can alter the properties of each component of the Burgers body. Crack formation was derived from rate theory and the rate of cracking was determined from the expression:

$$\dot{N} = \dot{N}_0 [\frac{(\sigma_q - \sigma_c)}{\sigma_0}]^m, \tag{2.24}$$

where $\dot{N}_0$ and m are constants, σ_q is the equivalent von Mises stress and σ_c is the critical stress for crack initiation.

An isotropic damage parameter was taken from the work of Budiansky and O'Connell (1976) which assumed the form:

$$\lambda = a^3 N, \tag{2.25}$$

where N is the total number of cracks and a is the average crack radius. Each crack is assumed to be penny shaped and the crack size is equivalent to the grain size:

$$\lambda = \frac{N}{8N_g};\ N_g = (d_g)^{-3}, \tag{2.26}$$

where d_g is the average grain diameter and N_g represents a density of one crack per grain.

Following the work of Horii and Nemat-Nasser (1983), McKenna et al. (1990a and 1990b) expressed the shear and bulk moduli of the damaged ice as:

$$\frac{G'}{G} = g(\lambda, \frac{\sigma_m}{\sigma_q}, C_f) \tag{2.27}$$

and

$$\frac{K'}{K} = k(\lambda, \frac{\sigma_m}{\sigma_q}) \tag{2.28}$$

respectively, where C_f is the coefficient of friction across the crack faces. Also, σ_m is the mean pressure and σ_q is the von Mises equivalent stress and these are expressed as:

$$\sigma_m = \sigma_{ii}/3 \tag{2.29}$$

and

$$\sigma_q = (1.5 S_{ij} S_{ij})^{1/2}, \tag{2.30}$$

where S_{ij} is the deviatoric stress.

Finally, McKenna et al. (1990a and 1990b) expressed damage enhancement of permanent creep and delayed elastic strain rates as:

$$\dot{\epsilon}_0^{c\prime} = \dot{\epsilon}_0^c exp(\beta N/N_g) \tag{2.31}$$

and

$$\dot{\epsilon}_0^{d\prime} = \dot{\epsilon}_0^d exp(\beta N/N_g) \tag{2.32}$$

respectively, where β is a constant enhancement parameter. Note that for the expressions, the primes denote the influence of damage.

2.4 Mechanical Properties

2.4.1 Sea Ice

Before a discussion of the mechanical properties of sea ice can commence, it is essential that a summary of the factors which influence its behaviour be presented. Typically test programs on sea ice show significant scatter. The mechanical properties of ice have been shown to vary with temperature, salinity, strain rate, crystal structure and orientation as well as a host of other factors. Sea ice is a naturally occurring material and its crystal structure is influenced by the method of formation, age, salt content and the influence of surrounding ice fields. An individual ice crystal is anisotropic although for special cases, such as polycrystalline equiaxed ice, isotropic behaviour can be assumed. Ice behaves as a viscoelastic material, i.e. it exhibits properties of both elasticity and creep. Furthermore it should be noted that ice, as it is found in nature, must be considered to be a high-temperature material. That is a ratio of its ambient temperature to its melting temperature, on the absolute scale, normally exceeds 0.85 ($T/T_m > 0.85$).

An extensive data set for mechanical properties of multi-year (second-year or older) sea ice is reported in Richter-Menge and Cox (1986) and Cox et al. (1984). This was a two-phase program. Phase I consisted of 282 uniaxial compression, tension and confined compression tests on samples collected from the Southern Beaufort Sea and Phase II was comprised of 188 tests on samples collected from the Alaskan Beaufort Sea. The ice crystal structure was considered to be highly

variable consisting of granular ice, columnar ice and mixed granular and columnar ice. As a result of ridge formation and consolidation, not all columnar grains were vertical. Salinities ranged between 0.40 and 2.40 ‰ while densities varied from 835 to 890 kg/m^3. The uniaxial tests covered strain rates of 10^{-5} s^{-1} to 10^{-2} s^{-1} and temperatures of -5 °C and -20 °C. These test results showed the ductile to brittle transition to be between the strain rates of 10^{-3} s^{-1} and 10^{-2} s^{-1}. It should be noted that values of elastic modulus were estimated from the initial tangent modulus and are therefor subject to criticism.

Timco and Frederking (1982) have also presented data for multi-year ridge ice, collected from the polar pack in October, 1979. These tests were constant stress rate tests, although the authors suggested a nominal strain rate of $\dot{\epsilon} = 2.5 \times 10^{-4}$ s^{-1}. The range of stress rates ($\dot{\sigma}$) for the test series was 0.13 MPa.s^{-1} to 0.24 MPa.s^{-1} and the compressive strength varied between 4.4 MPa and 12 MPa.

Small scale test data on the compressive strength of first year sea ice is readily available in the literature and for comparative purposes the work of Schwarz (1970), Frederking and Timco (1983) and Frederking and Timco (1984) have been presented in Figure 4.8 of Chapter 4. Furthermore, authors such as Butkovich (1959), Dykins (1971) and Lainey and Tinawi (1984) have compiled a wide range of data for various ice types and loading configurations.

Elastic modulus data is typically determined through either static or dynamic techniques. Static measurement of elastic modulus have been determined by estimating the slope of stress-strain curves of uniaxial compression tests or by measuring deflections of beams (Weeks and Anderson, 1958; Dykins, 1971; Schwarz, 1975; Lainey and Tinawi, 1981). Typical values are found to be between 0.5 GPa and 10

GPa. These tests typically require relatively large loads and finite time intervals. Given the viscoelastic behaviour of ice, the inelastic components of strain cannot be neglected and these measurements have therefore been subject to criticism. These test techniques do have the benefit of simplicity and can be performed in almost any ice structures laboratory, therefore making estimates of elastic modulus available in cases where they would not otherwise be performed.

Dynamic measurements of elastic modulus have been determined through seismic techniques, that is the measurement of propagation of vibrations through an ice sheet. The velocity of elastic waves within the ice can be used as a measure of Young's Modulus. The relative movement of the ice molecules is extremely small thus allowing inelastic properties to be neglected. Dynamic measurements show characteristically less scatter than static measurements, however temperature gradients within the ice sheet produce variations in the measured values. Elastic modulus values have been reported to range between 5.5 GPa and 10 GPa (Anderson, 1962; Langleben, 1962; Abele and Frankenstein, 1967).

2.4.2 Crushed Ice

The existence of an intermediate layer of crushed or pulverized ice has been identified, at the ice-structure interface, during interaction events in which the ice is failing by crushing. When modelling such events a knowledge of the mechanical properties of this intermediate layer is essential. Although this information is scarce, several researchers have investigated the behaviour of crushed or broken ice.

With an objective to study the interaction processes of ice rubble fields with offshore drilling structures, Gale et al. (1986) conducted a series of large scale

direct shear box tests. These tests were conducted at -2 °C with various particle size gradations. Furthermore, for comparative purposes tests were conducted on silica sand. Shear stress-displacement curves of the broken ice displayed a strong dependence on normal stress, and interestingly the broken ice showed a continuously increasing shear resistance. Conversely, the silica sand reached a maximum shear stress after relatively small displacements. The measured angle of internal friction of the broken ice ranged between 36° and 45° and it was proposed that this material exhibited a linear Mohr-Coulomb failure envelope.

Wong et al. (1987) expanded the previous work to include the presence of brine and to investigate the effect of increasing shear rate. Although immersion of the crushed ice, in a brine solution, effectively reduced the shear strength, the force-displacement curves of the immersed broken ice displayed the same characteristic behaviour as the non immersed broken ice. That was a continuously increasing shear stress with displacement. Deformation rates of 2.8 mm/min and 5.9 mm/min, were included in the test program. However no significant differences were noted between these strain rates. Conceding that the shear box tests do not give accurate measurements of volume change, Wong et al. (1987), suggest that volumetric deformation is predominantly dilatant. Furthermore a cautionary note is directed towards the use of a Mohr-Coulomb failure criteria, in the analysis of crushed ice, since a maximum failure stress could not be identified.

As a supplement to the shear box tests, Gale et al. (1987) conducted a series of triaxial compression tests on broken ice. These tests were conducted on right circular cylinders (cylinder dimensions measured 150 mm high with a 70 mm diameter) at -2.5 °C with a displacement rate of 0.5 mm/min. The authors concluded that

Table 2.1: Friction coefficients between sea ice and selected of materials from various authors. Note 's' and 'r' denote smooth and rough respectively.

Author	Material	Static	Dynamic
Enkvist (1972)	Stainless Steel	-	0.025
	Painted Steel	-	0.041
	Sandblasted Steel	0.340	0.045
	Scrap Steel	-	0.109
Grothues-Spork (1974)	Smooth Steel	0.01-0.05	-
	Rough Steel	0.30-0.50	0.10-0.20
Airaksinen (1974)	Smooth Steel	0.45	0.07-0.18
	Rough Steel	0.60	0.18-0.23
Tusima & Tabata (1979)	Stainless Steel, s	-	0.013-0.07
	Stainless Steel, r	-	0.134-0.28
	Aluminum	-	0.015-0.14
	Carbon Steel	-	0.051-0.14
Tabata & Tusima (1981)	Stainless Steel, s	-	0.017-0.025
	Stainless Steel, r	-	0.081-0.14
	Teflon	-	0.019-0.031
	Epomarine	-	0.017-0.019
		-	

a bi-linear deviatoric stress-strain curve characterized the broken ice behaviour, and that the breakover stress (i.e. stress at which the slope changed) appeared to suggest a possible failure envelope. Furthermore, as with the shear box tests, the triaxial tests displayed a continuously increasing shear stress with displacement.

2.5 Friction

Like many other physical properties of ice, friction coefficients, both static and dynamic, exhibit significant scatter. Temperature, normal stress and velocity directly affect the coefficients of friction, as does salinity and surface topography. While an explanation for this behaviour will not be explored at this time, typical values are presented in Table 2.1. These values were used to establish a reasonable working range of friction coefficients, between a rigid indenter and the ice surface, in the finite element analysis.

More recently, Molgaard (1989a and 1989b), measured dynamic coefficients of friction between freshwater ice and steel. With his unique apparatus, Molgaard determined coefficients of friction over a range of temperatures and velocities. Generally, increasing velocity gave a decrease in friction as did increasing temperature. At -10 °C coefficients of dynamic friction varied between 0.030 to 0.080 for sliding speeds of 5.95 cm/s to 82.35 cm/s.

Chapter 3

The Field Test Program on Canada's Ice Island (1990)

Small-scale laboratory testing, of ice samples, provides invaluable information for the development of damage models and constitutive relationships. These tests also provide insight to the mechanisms which govern fracture and damage of ice. Although such experiments can be performed in highly controlled surroundings, difficulties arise when extrapolating this data to full scale structural designs. Previous field experience has shown that laboratory test data grossly overestimates design loads for structures, which typically have contact areas hundreds of times greater than the laboratory samples. Economical structural designs require reliable and realistic ice load predictions. Medium to full scale test programs allow the collection of data pertaining to the scale effect, failure processes and structural behaviour, which cannot otherwise be reproduced.

Following successful field test programs at Pond Inlet, 1984, and on Hobson's Choice Ice Island, 1989, an ambitious medium-scale ice indentation test program was planned for the spring of 1990. This program was designed to collect data which would lead to the determination of more realistic design ice loads for arctic struc-

tures and vessels. The comprehensive test matrix in conjunction with sophisticated apparatus and data acquisition equipment would allow the program participants to better understand ice failure processes. More specifically, this test series was designed to address: scale effect, vibrations attributed to ice crushing (ice-induced vibrations), variations in local and global loads, and the influence of structural compliance and geometry.

The test apparatus was heavily instrumented. Load cells in the hydraulic actuators and pressure transducers on the face of an indenter gave force-time histories and identified localized crushing events. Temperature variations at the ice-indenter interface were monitored and a view-port in one indenter allowed several events to be captured on video cassette. Acoustic emissions were recorded for various indentation tests and physical measurements were taken to characterize the final ice failure surface.

As with many other test programs of this nature, the primary characteristics of the load-time curves are proprietary and will remain so for a two-year period. Therefore data pertaining to peak forces, pressure distributions, or force-time histories cannot be presented at this time. Supplementary information, such as microstructural analysis and characterization of the failure surface may be presented.

3.1 Test Site

Canada's Ice Island is a massive feature. With an areal extent of eight by four kilometers, and a thickness of forty meters, this billion tonne iceberg behaves as a very stable floating platform. After calving from the Ward Hunt Ice Shelf on the northern coast of Ellesmere Island in 1982, the ice island began drifting Southwest

along the continental margin of the Queen Elizabeth Islands. By the spring of 1990, it had reached Ellef Ringnes Island and moved into the Perry Channel.

Hobson's Choice Ice Island provides an ideal platform from which scientists can study Canada's arctic and as well provides an opportunity for the Canadian government, through science, to exercise sovereignty over the region. Movement of the island has been monitored since 1983 and scientific studies have been performed on the island from 1985 onwards. A camp situated on the island is operated and maintained by Energy, Mines and Resources Canada, and is occupied primarily by scientists from the Atlantic Geoscience Centre of the Geological Survey of Canada. The infrastructure resulting from these previous expeditions made the ice island an attractive site for ice indentation testing. The first ice indentation test program was conducted on the island in 1989 and it laid the foundation for the 1990 field test program.

The ice features which pose the most significant threat to structures in the Beaufort Sea are multi-year pressure ridges. Access to multi-year sea ice is therefore an essential component to any field test program. As can be seen from Figure 3.1, the ice island consists of a large central portion of shelf ice (granular fresh water ice) with multi-year sea ice consolidated to its sides. It is within this sea ice, which has consolidated since the island calved in 1982, that the indentation tests were performed. Crystallographic studies revealed that the ice could be classified as transitional, that is it contained both columnar and frazil ice. In addition, the axis of the columnar grains were not necessarily vertical, a result of the rafting and consolidation process. Furthermore, salinity varied from 0 ‰ to 4 ‰ (Gagnon and Sinha, 1991). These characteristics are typical of multi-year pressure ridges.

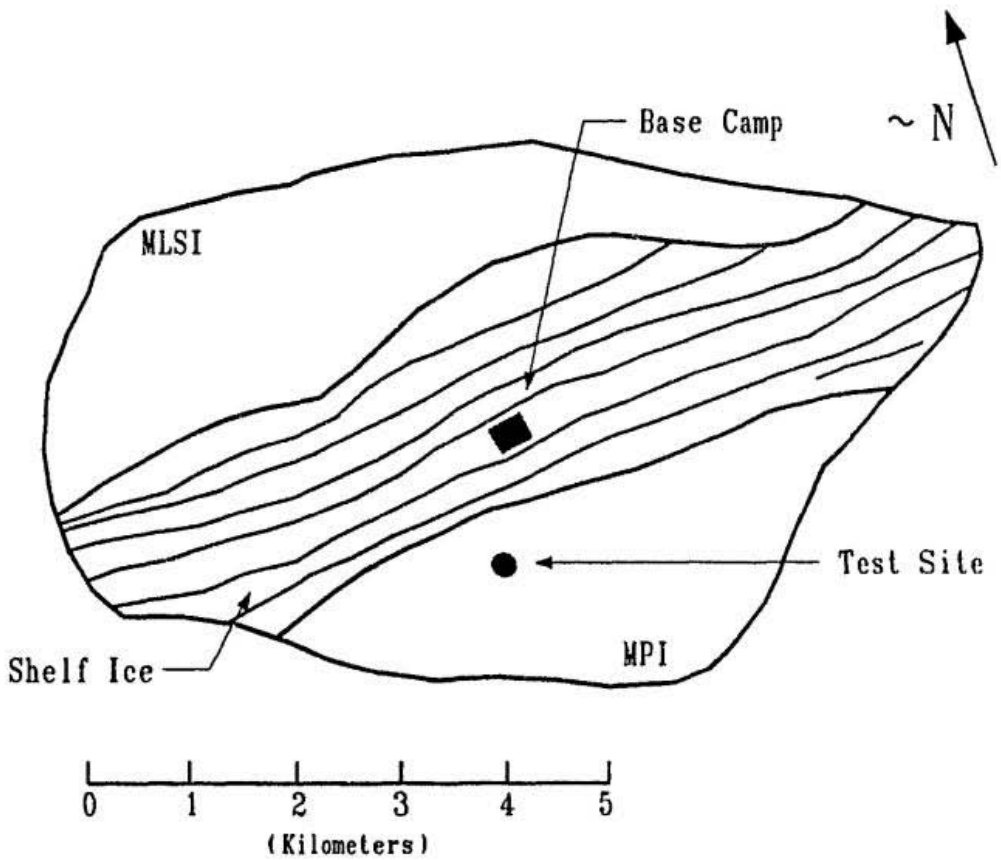

Figure 3.1: Plan view of Hobson's Choice Ice Island, from Kennedy (1991).

3.2 Test Plan

The peak forces exerted on a structure are highly dependent on the structural design characteristics and ice failure mode. Artificial islands, with gently sloping beaches force bending failure of approaching ice sheets. Caisson retained structures are designed with rigid vertical walls and ice will typically fail by crushing or buckling. Arctic vessels such as ice breakers often ram ice features to force crushing and flexural failure. Conceptual design of the Hibernia gravity based structure (GBS) incorporates a wedged ice belt which is intended to dissipate the kinetic energy of an imposing iceberg through ice crushing.

To investigate the significance of structural geometry, the test plan embodied three general classes of indenter; flat rigid, flat flexible, and wedge; with the dominant failure mode for each class being predicted as crushing. The flat flexible indenter was designed and constructed to simulate the structural behaviour of an icebreaker, while the wedge indenters modelled the conceptual design of the Hibernia GBS. There were five indenters in total:

- TFF – Flat flexible indenter, triple actuator configuration,
- TRF – Flat rigid indenter, triple actuator configuration,
- TW1 – Wedge indenter # 1, triple actuator configuration,
- TW2 – Wedge indenter # 2, triple actuator configuration,
- SFF – Flat flexible indenter, single actuator configuration.

The triple actuator configuration had a nominal indentation rate of 100 mm/s while the nominal speed of the single actuator system was 400 mm/s. Various test

face geometries were also investigated, these included horizontal and vertical wedges along with truncated pyramids. In total 18 indentation tests were conducted.

3.3 Test Apparatus

The mechanical and hydraulic system for the 1990 field test program was initially designed and fabricated by Geotechnical Resources Limited (Geotech) of Calgary, under contract from Mobil Oil, for the 1984 Pond Inlet test series. Following this program the equipment was donated to Memorial University of Newfoundland and subsequently utilized in the 1989 and 1990 field test programs on Hobson's Choice Ice Island. Although minor modifications have been performed, the system is essentially unchanged.

At the heart of the indentation system was a series of hydraulic actuators; the configuration of which could be altered to suite the requirements of each test. A bank of accumulators which provided the hydraulic supply to the actuators were charged with compressed air prior to testing. With this system, the only required electrical power at the time of testing, was that power necessary for operation of the data acquisition and feedback control system. A schematic illustration of this system and test set-up can be found in Figure 3.2.

Each actuator was rated for 4.6 MN of static thrust giving the triple actuator system a total of 13.8 MN. All tests with the triple actuator configuration were performed with an indentation rate of 100 mm/s, while the single actuator configuration had an indentation rate of 400 mm/s. Actuator stroke for either arrangement was limited to 300 mm.

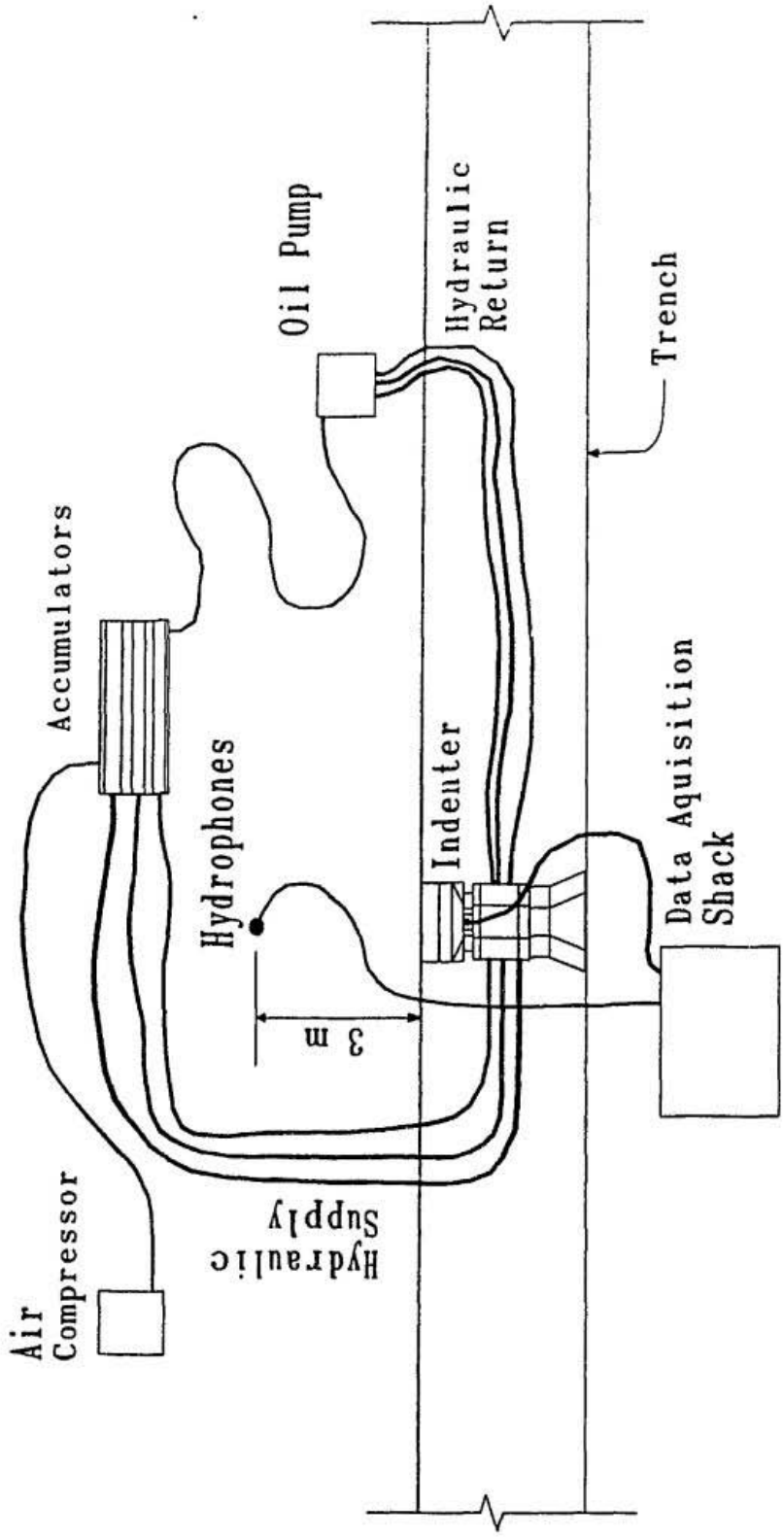

Figure 3.2: Schematic of indentation system.

3.4 Characterization of the Failure Zone

Crushing with subsequent ejection of ice particles was identified as the dominant mode of failure for all tests and in the case of test TFF-01 spalling or flaking, associated with the formation of macrocracks, was observed. Common to all failure surfaces were several characteristic features. These attributes were noticeable even with varying indenter compliance or ice face geometry. From Figure 3.3 it can be seen that there are essentially three regions associated with the failure zone, first, spall areas on the periphery of the contact surface, second, zones of crushed or pulverized ice generally associated with lower pressures and third, regions where a distinct crushed layer does not exist. Macroscopically the ice in this region of no distinct crushed layer appeared to be undamaged but this was not necessarily true (Kenny et al., 1991).

Preliminary analysis of the load histories indicated a dynamic fluctuation in local peak pressures with a highly varied spatial distribution and steep pressure gradients across load cells. Although the features of the failure surface tend to suggest that peak pressures should correlate with the zones of no distinct crushed layer, superimposing the final recorded pressures on the interface failed to reveal such a phenomena (Frederking, 1990).

3.5 Density Measurements

As part of the characterization process of the failure surface, a comparison of density of the crushed layer to that of the parent ice was performed. Values of density were determined by cutting samples into right rectangular prisms, measuring dimensions

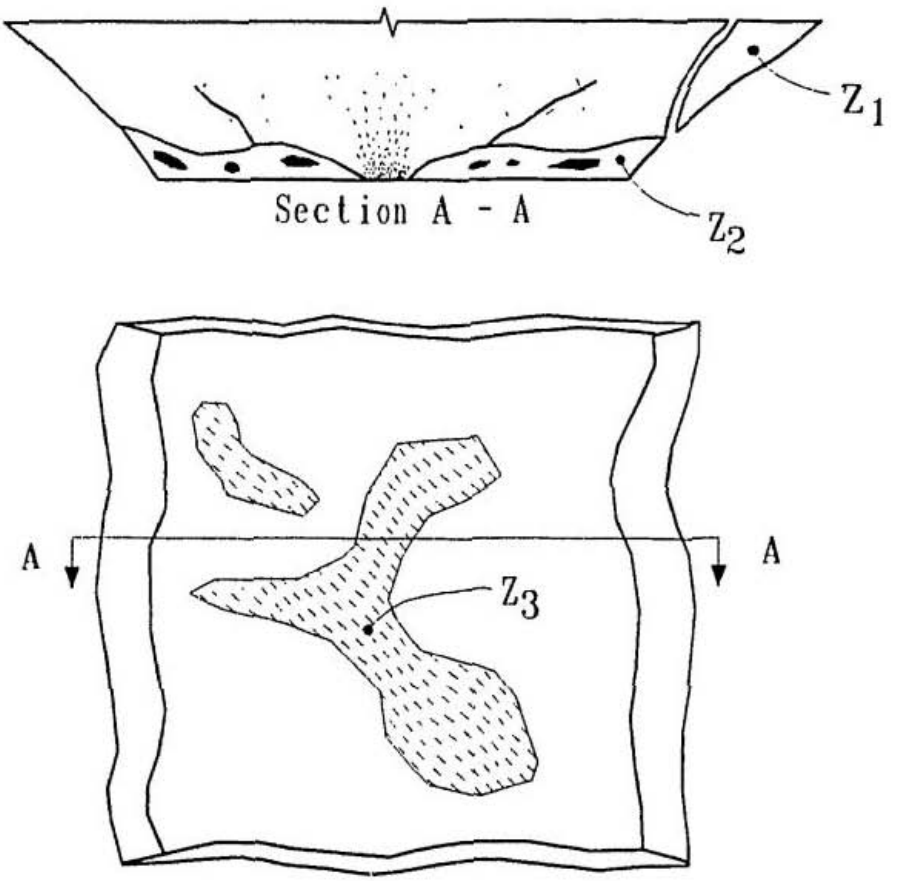

Figure 3.3: Typical front view of test face following indentation. The failure region is divided into three general zones; (i) spall areas Z_1, (ii) zones of pulverized ice Z_2 and (iii) zones of no distinct pulverized layer Z_3.

to find volume and weighing the samples on an electronic scale. To minimize random errors at least four measurements of each dimension were recorded. The location of each sample within the test face was essentially arbitrary, with the only constraint being crushed ice layer thickness. To enable a sufficiently large sample to be cut, a minimum layer thickness of 20 mm was required.

Density measurements of the parent ice were conducted in the same manner. The location of these samples was chosen to be as close as possible to the crushed ice samples, generally immediately behind the crushed layer. Due to the presence of microcracks within the parent ice, these density measurements cannot always be considered to be the density of the virgin material. Gagnon and Sinha (1991) have reported that the density of the parent structure varied from 875 kg/m^3 to 886 kg/m^3.

From Table 3.1 it can be seen that the crushed ice layer density varied between 749 kg/m^3 and 864 kg/m^3. The parent ice density was found to be greater than that of the crushed material and varied between 858 kg/m^3 and 890 kg/m^3. The maximum error of observation for all density measurements is estimated as ± 13 kg/m^3 and is associated with difficulties machining and measuring each sample.

During the test program it was observed that the crushed material at the periphery of the contact face appeared to be less consolidated than the material at the center. To quantify this observation a series of density measurements were taken along a horizontal section of test face TFR-03. Across the width of the test face ten samples, each with a length of approximately 100 mm, were removed. Several samples, selected from the central portion of the failure surface, consisted of ice obtained from the region of no distinct crushed layer. For example, although the

Table 3.1: Density measurements of crushed layer and parent ice.

Test Face	Indentor Type	Crushed Layer ρ_c (kg/m^3)	Parent Ice ρ_i (kg/m^3)
TFF-01	Flat, Flexible	864	879
TFF-02	Flat, Flexible	807	884
TW1-01	90° Wedge	776	858
TFR-01	Flat, Rigid	749	890
TFR-01	Flat, Rigid	784	882
TFR-02	Flat, Rigid	842	874

ice near the center of the horizontal thick section through TFR-01, shown in Figure 3.7, is in a damaged state, a discrete crushed layer does not exist. For the purposes of this investigation all samples were treated as being part of the pulverized layer. The density of the crushed layer along the horizontal section of TFR-03 ranged from 813 kg/m^3 to 874 kg/m^3, and as expected, the density tended to increase toward the center. Figure 3.4 shows this trend. It is suspected that substantially greater confining pressures at the center of the indenter contributed to this observation.

3.6 Crushed Layer Thickness

Following tests TFF-01 and TFR-01, crushed layer thicknesses were measured in detail. The initial test face geometries of each test were similar but the indentor compliance varied. The indentation surface was a truncated vertical wedge with a 300 mm wide flat face with the sides sloping at 1:3. Test TFF-01 incorporated a flat flexible indenter while test TFR-01 was performed with a flat rigid indenter.

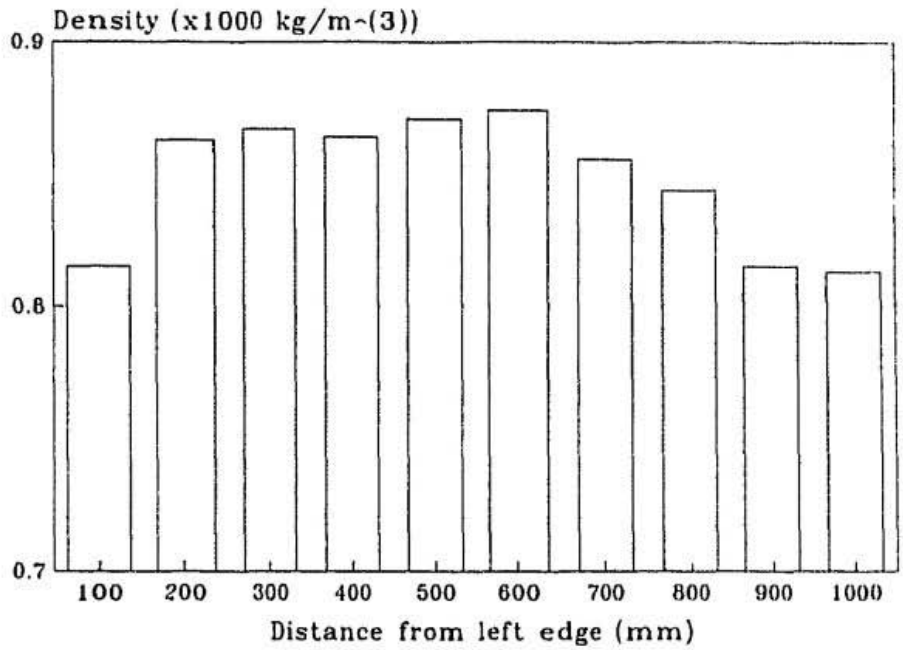

Figure 3.4: Density variation of crushed layer: Test TFR-03.

Crushed ice layer thicknesses were determined in the following manner: a 50 mm grid was superimposed on the test face. The first 50 mm thick horizontal section was cut from the test face and at each 50 mm increment along this section, the crushed-ice layer was measured. Once complete, the next horizontal section was cut and the process continued until the entire face was sectioned. It should be noted that the crushed ice layer thickness was measured to the nearest millimetre.

As with the density measurements, there were several instances where no distinct boundary between the crushed layer and the parent structure could be found. Consequently, it was decided that for a particle to be considered as part of the crushed layer it would have to be isolated from the parent ice by a crack or network of cracks.

Figures 3.5 and 3.6 give three dimensional representations of the crushed layer profiles of test faces TFF-01 and TFR-01. It should be noted that these surfaces show the test faces with the crushed layer removed. Furthermore, the high points represent areas where the crushed layer thickness goes to zero.

The crushed layer of test face TFF-01 had a mean thickness of 41 mm with the maximum thickness reaching 173 mm. The flat flexible indenter was constructed with a steel plate on horizontal ribs and was designed to simulate a ship's hull. The added stiffness associated with the presence of the ribs can be seen in the crushed layer profile as the crushed layer appears thinner in the presence of the stiffening ribs.

Test face TFR-01 had a much more uniform appearance than TFF-01. TFR-01 showed a thin line of no distinct crushed layer along a vertical axis through the center of the face, see Figure 3.6, with the crushed layer thickness increasing

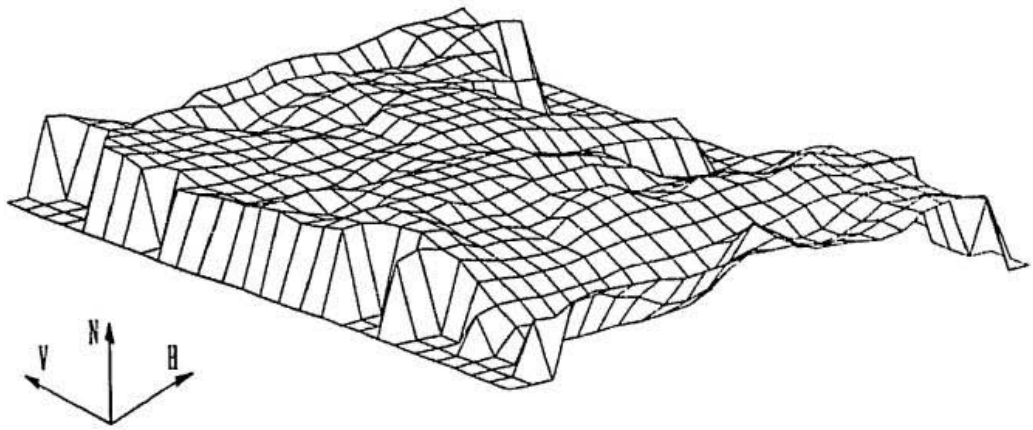

Figure 3.5: Crushed layer profile: Test TFF-01. Note that V represents the vertical axis, H represents the horizontal axis and N is normal to the test face with the arrow pointing out of the trench wall.

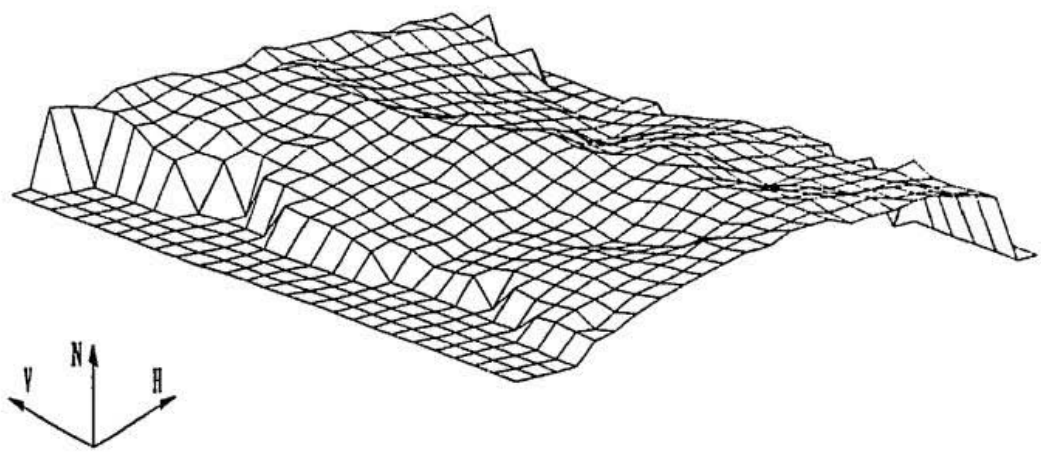

Figure 3.6: Crushed layer profile – Test TFR-01. Note that V represents the vertical axis, H represents the horizontal axis and N is normal to the test face with the arrow pointing out of the trench wall.

toward the perimeter. The average thickness of the crushed layer was 57 mm with the maximum thickness reaching 155 mm. This region of no discernible crushed layer was observed for all indentation tests and its presence provides additional support to the hot spot or contact line phenomenon as postulated by Lindholm et al. (1990), Riska (1989) and Jordaan et al. (1990).

The crushed layer typically contained large ($\geq$ 25 mm) relatively undamaged particles surrounded by a matrix of finely pulverized ice, suggesting a grinding action as the larger particles slide and rotate during extrusion. This effect was exaggerated with the wedge indenters, the geometry of which gave rise to a greater degree of spalling. The appearance of the crushed layer formed in the wedge indentation tests also suggested substantially less confinement.

3.7 Contact Area

The final nominal contact areas (NCA) for selected tests are presented in Table 3.2. Additionally, an estimate of the areas of no apparent crushed layer (NACL) are presented as a ratio of the final nominal contact area. The nominal contact area is the area estimated from the indenter penetration and the test face geometry, while the area of no apparent crushed layer is the portion of the test face which appeared to be blue in colour following each indentation test.

The data in Table 3.2 would suggest that the area of contact is approximately 35 % of the nominal contact area. It has been proposed that the bulk of the load is carried by ice in zones where the crushed layer is thinnest and that ice in this zone is behaving elastically. An investigation of this hypothesis will be presented in Chapter 5.

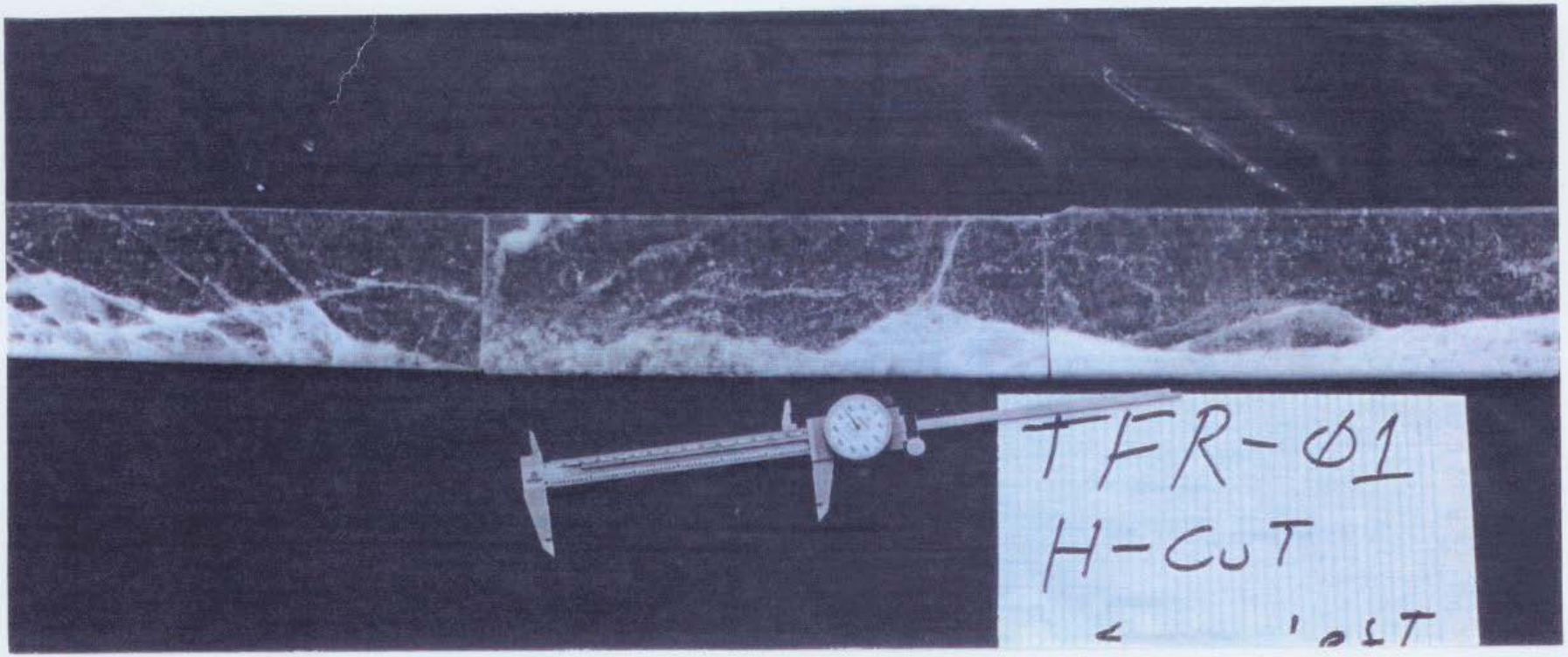

Figure 3.7: Horizontal thick section of TFR-01. To give an indication of the scale the calipers are extended to 150 mm.

Table 3.2: Estimates of contact area.

Test	NCA (m^2)	NACL / NCA
TFF-01	1.35	0.25
TFR-01	1.35	0.22
TFR-02	0.49	0.47
TFR-03	1.21	0.24
TFR-04	0.49	0.40
TFR-05	1.21	0.32
SFF-01	0.70	0.41
SFF-02	0.70	0.56

3.8 Particle Examination: Sieve Analysis, Sintering and Pressure Melting

In an attempt to understand better the dynamic activity associated with ice-structure interactions, several researchers have turned their attention to the physical processes associated with the formation and subsequent extrusion of the crushed layer. Previous researchers have shown that the majority of the energy dissipation occurs during viscous extrusion of the pulverized layer (Timco and Jordaan, 1987; Jordaan and Timco, 1988). Past experience has also shown that very high local peak pressures and large pressure gradients exist across the indentor interface. Furthermore, the actual contact area between ice particles in the crushed layer would be far less than the apparent contact area and therefore inter-particle pressure would tend to exceed these high local pressures. When these loads are coupled

with rapid extrusion and particle movement within the crushed layer friction and pressure melting become very real possibilities. In addition, rapid pressure drops may allow refreezing and sintering to occur which can give rise to a stick-slip type phenomenon.

Following several indentation tests, ejected particles were collected and examined. Particle size distributions of the extruded crushed ice were determined through sieve analysis using nine sieves with mesh sizes ranging from 50.8 mm to 0.841 mm. The surface appearance of discrete particles was also examined, under a microscope, for signs of pressure melting and sintering.

For the initial test TFF-01, the sample size totalled 37.44 kg, representing greater than 30% of the total crushed material. An estimate of the crushed volume was calculated by knowing the initial face geometry and the distance which the indenter penetrates the surface. For the remaining tests, smaller representative samples were taken. All tests show similar distributions as can be seen in Figure 3.8; however the mean particle size varied slightly. Test TFF-03 showed the smallest mean particle size, 15 mm, while TW1-01 gave the greatest mean particle size, 34 mm. Tests TFF-01, TFF-02, and TFR-01 had mean particle sizes varying between 21 mm and 28 mm. If the particle size distribution curve of TW1-01 is examined, it can be seen that only 57.7 % of the sample passed the 50.8 mm sieve and that the curve is offset to the right. This can be attributed, in part to the greater degree of spalling associated with the wedge indenter.

Extruded particles were collected following several of the indentation tests and examined under a microscope. In all cases the surfaces appeared to be wetted and neither particle displayed rough edges nor sharp corners, thus suggesting melting

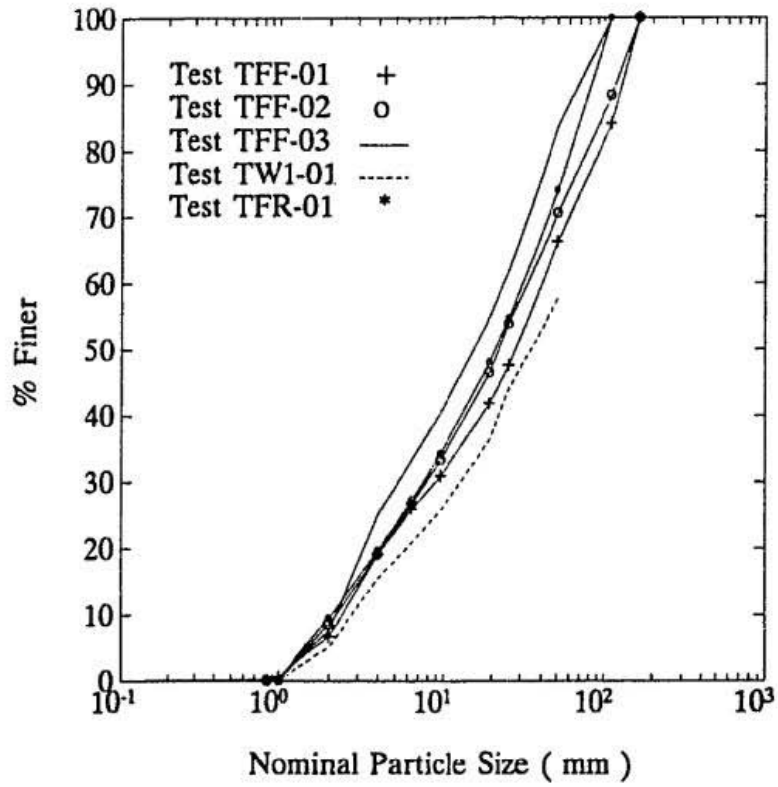

Figure 3.8: Particle size distributions.

of the ice particles and the presence of liquid. Figure 3.9 is a photomicrograph of a typical extruded ice particle which appeared as a conglomerate of small particles sintered into a larger mass. Other particles appeared as one large particle with smaller particles sintered to its surface. This microscopic examination, when coupled with the observations of Gagnon and Sinha (1991), provided further support to pressure melting, friction melting and sintering as active phenomena during the dynamic crushing and extrusion process.

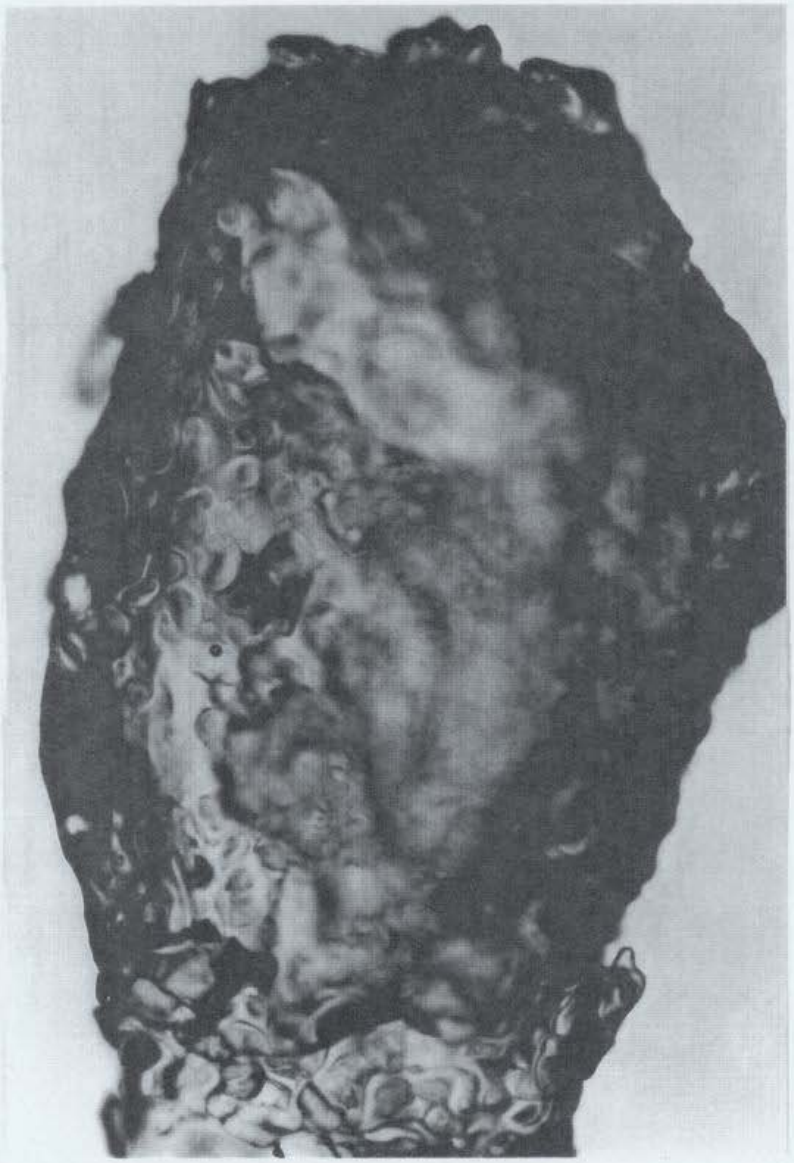

Figure 3.9: Photomicrograph of an extruded particle; ×35 magnification factor.

Chapter 4

Laboratory Test Program

Development and refinement of constitutive relationships for ice requires a thorough knowledge of the mechanical behaviour of the material. Mechanical properties, such as Young's modulus and compressive strength can be determined through uniaxial compression tests. These tests also allow the influence of strain rate and other variables such as grain size and temperature to be investigated. Furthermore, creep constants and damage parameters can be determined through uniaxial compression testing. This chapter contains a description of the test set-up and procedures as well as presents the test data and subsequent analysis.

4.1 Test Plan

During the field test program of 1990, ice samples were collected and brought to Memorial University of Newfoundland for analysis. These ice samples included intact relatively undamaged multi-year sea ice and highly damaged crushed ice from the intermediate layer. This uniaxial compression test series was designed to determine and compare the mechanical properties of both the undamaged and the crushed ice.

Table 4.1: Uniaxial test plan.

Test Number	Test Date	Sample	Planned Load Sequence
II1	Sept 5	SFR-01 H	Strain Control 1. $\dot{\epsilon} = 5 \times 10^{-5}$ s^{-1} to 2 % 2. $\dot{\epsilon} = 5 \times 10^{-5}$ s^{-1} to 4 %
II2	Sept 6	SFR-01 H	Strain Control 1. $\dot{\epsilon} = 2.5 \times 10^{-4}$ s^{-1} to 1 % 2. $\dot{\epsilon} = 2.5 \times 10^{-4}$ s^{-1} to 2 % 3. $\dot{\epsilon} = 2.5 \times 10^{-4}$ s^{-1} to 3 % 4. $\dot{\epsilon} = 2.5 \times 10^{-4}$ s^{-1} to 4 %
II3	Sept 10	SFR-01 V	1. Load Control $P_{max} = 0.75$ MPa 2. Strain Control $\dot{\epsilon} = 2.5 \times 10^{-4}$ s^{-1} to 2 % 3. Load Control $P_{max} = 1.0$ MPa
II4	Sept 13	SFR-01 V	1. Strain Control $\dot{\epsilon} = 5 \times 10^{-4}$ s^{-1} to 1 % 2. Strain Control $\dot{\epsilon} = 5 \times 10^{-4}$ s^{-1} to 2 % 3. Load Control $P_{max} = 1.0$ MPa
CI1	Sept 19	TFF-01	Strain Control 1. $\dot{\epsilon} = 5 \times 10^{-4}$ s^{-1} to 1 % 2. $\dot{\epsilon} = 5 \times 10^{-4}$ s^{-1} to 1 % 3. $\dot{\epsilon} = 1 \times 10^{-3}$ s^{-1} to 1 % 4. $\dot{\epsilon} = 1 \times 10^{-3}$ s^{-1} to 1 %
CI2	Sept 20	TFF-01	Load Control $P_{max} = 1.0$ MPa.
CI3	Sept 24	TFF-01	Strain Control 1. $\dot{\epsilon} = 2.5 \times 10^{-4}$ s^{-1} to 1 % 2. $\dot{\epsilon} = 2.5 \times 10^{-4}$ s^{-1} to 1 % 3. $\dot{\epsilon} = 1 \times 10^{-3}$ s^{-1} to 1 % 4. $\dot{\epsilon} = 1 \times 10^{-3}$ s^{-1} to 1 %

II - Intact ice CI - Crushed ice

The number of samples were limited by the ability to transport this ice safely from the field to the Thermal Laboratory of Memorial University of Newfoundland. It is for this reason that the tests were conducted in a manner which allowed the collection of as much information as possible. Each test was conducted as either a creep test or a constant strain rate test, with several tests incorporating both. The test plan is presented in Table 4.1. Due to brittle failure or extreme deformation of several samples, some tests could not be run to completion, these included tests CI1 and CI2.

4.2 Creep Test

In the classical creep test, for example those used in the testing of concrete or rock, a constant load is applied to the sample for long periods of time, months or even years. In contrast, the creep tests of this test series require relatively short loading times. For structural design purposes, long term creep data, for materials such as concrete, is essential. The service life of offshore structures can often exceed 10 or even 20 years and designers of such structures must understand how the construction materials will perform throughout their lifetime. Similarly when determining ice loadings, the engineer must acquire the knowledge necessary to predict the behaviour of the ice feature for the duration of the ice-structure interaction. An extreme crushing event, for example the Molikpaq in 1986, would last 30 minutes and estimates of iceberg collision times for the Hibernia project range between 0.7 and 15 s. Moreover, in full scale crushing events where the load may fluctuate at 15 Hz, the ice is subjected to a series of 0.07 s load pulses. It is for these reasons that this test series is aimed at determining the short term creep

behaviour of ice.

If an ice sample is subjected to a constant compressive load, it is readily seen that strain can be divided into several components. Initially the sample will compress elastically. This elastic strain ϵ_e, should be time-independent and is considered to be instantaneous. If the load is maintained for an extended period of time the sample will continue to compress. This time-dependent strain can be further divided into permanent plastic deformation (creep strain ϵ_c) and a time-dependent recoverable response (delayed elastic strain ϵ_d). The creep test which is described in the following section is one method for measuring these instantaneous and time-dependent components of strain.

Typically, each creep test was comprised of a 20 s load pulse followed by a 10 min relaxation. Each sample was subjected to a series of loadings starting with 0.25 MPa and increasing in increments of 0.25 MPa. Following each subsequent increase in stress a 0.25 MPa load was reapplied, thus providing a history of increasing damage.

The elastic strain is seen as a sudden step at the instant of loading or unloading. Provided the sample does not suffer any damage during the test, the instantaneous elastic strain ϵ_e for both the load and unload should be equal. As the test proceeds the strain will grow with time. As previously mentioned, this time dependant strain is comprised of delayed elastic strain and permanent creep. If the sample is then permitted to relax completely, the remaining strain is the permanent creep. It should be noted that given the stress levels and loading time of these tests, the permanent creep component is very small and not easily measured.

4.3 Test Apparatus

The uniaxial compression tests were conducted using an MTS load frame and feedback control system. The load frame (MTS model 312.21) has a capacity of 111 kN (12.5/25 kip) and is powered by a single hydraulic actuator. Movement of the actuator was controlled by the master control panel (MTS model 413) via the servo-valve and servo-controller and the desired load or displacement path was selected with an MTS model 410 digital function generator. Linear-variable differential transformers (LVDTs) provided actual values of strain and stroke while a load cell in the test frame produced a real-time load history. The load cell and LVDT signals were conditioned via Schaevitz model SCM 025 signal conditioners. These data were displayed on a Hewlett Packard 7046A X-Y recorder or an MTS digital indicator and as well a permanent record of the test data was stored on a personal computer. A schematic of the test system can be found in Figure 4.1.

4.4 Experimental Procedure

The samples for uniaxial compression testing were selected from ice collected on Hobson's Choice Ice Island during the 1990 field test program. This ice was cut from several test faces and included both intact, relatively undamaged, ice as well as ice from the highly damaged crushed layer. From the intact ice two samples were taken from vertical sections, while two were cut from horizontal sections. Thin sections of the vertical and horizontal planes were produced and the ice crystal structure characterized. The three crushed layer samples were taken horizontally. The ice in the crushed layer consisted of a conglomerate of finely pulverised ice,

surrounding larger ice particles (typically < 25 mm diameter), with no apparent preferred crystal orientation. This material can be considered to be isotropic and sample selection was performed to optimize material availability.

The samples were precision machined to a diameter of 54 mm ± 0.05 mm and the ends were finished flat and square with the overall length set at 135 mm ± 0.1 mm. To prevent the presence of cracks or formation of other such stress risers, the samples were finished with a polished surface. This was accomplished by removing the final layers of material with a chuck speed of 600 rpm or greater. Prior to testing, a latex membrane was placed over each sample. The sample was mounted on the lower platen of the MTS, with the upper platen then being fixed in place. The latex membrane also helped to secure the sample between the upper and lower platens. The LVDT collars were set on the sample and adjusted so that the LVDT's would be aligned vertically with the sample. The nominal gage length was set to 85 mm. Two thermistors, one at the top of the sample, and one at the bottom, were secured under the latex membrane. Finally the LVDT stroke was adjusted to zero with a slight positive offset. Figure 4.2 shows a fully instrumented sample ready for testing. All tests were performed at −10 °C ± 0.5 °C.

The MTS was either set in load control or strain control depending on the desired load sequence. For strain control tests, the signal generator was programmed to produce an inverted ramp with the strain rate given by:

$$\dot{\epsilon} = \frac{0.99 H_s}{l_g \tau} \tag{4.1}$$

where H_s is the desired stroke (mm), l_g is the actual gage length (mm) and τ is the period (s). In load control, the signal generator was set to produce a square wave

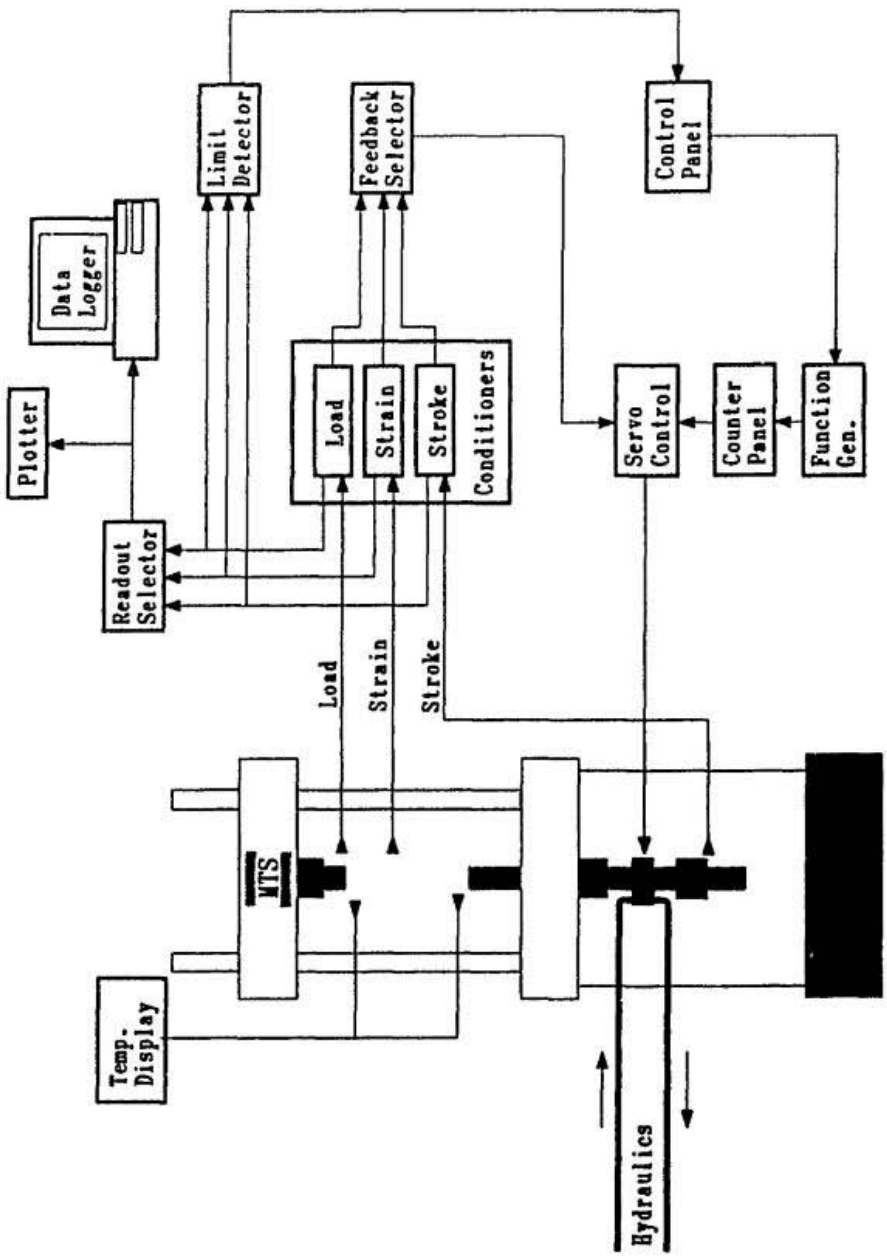

Figure 4.1: Feedback control system for uniaxial compression tests.

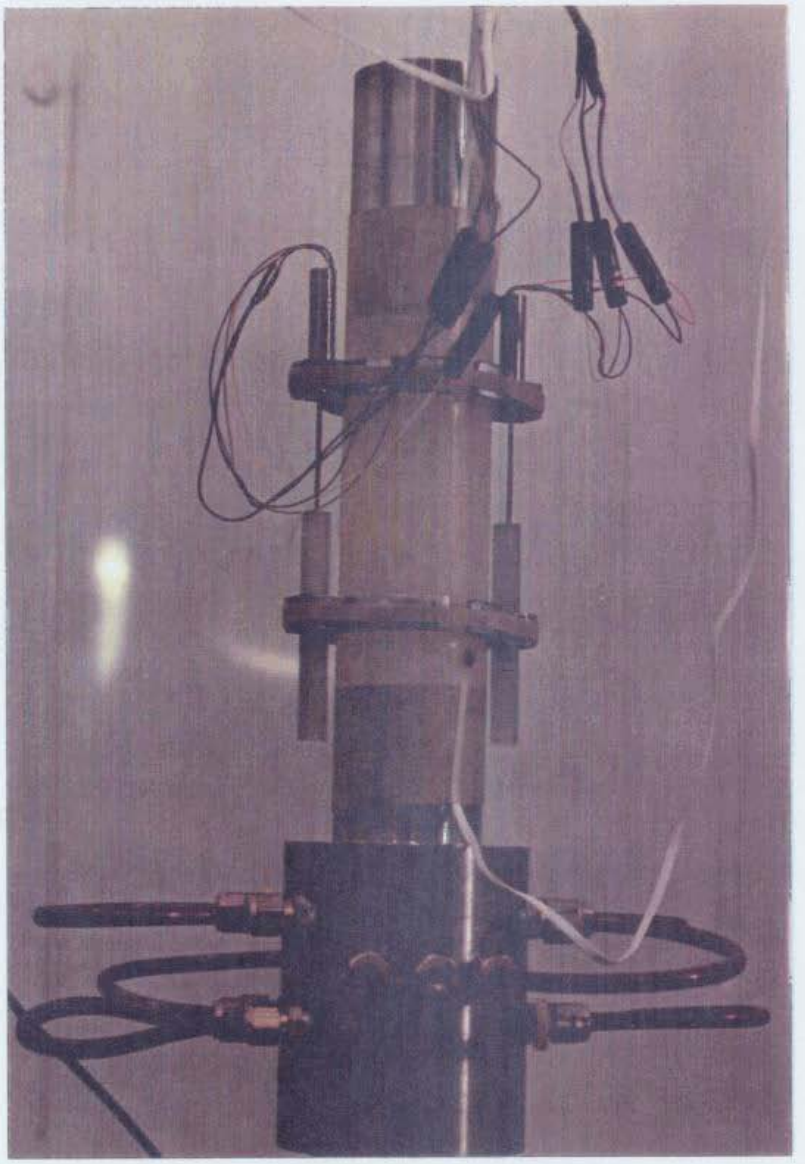

Figure 4.2: Ice sample before testing.

with a frequency of:

$$f = \frac{1}{0.5\tau} \tag{4.2}$$

where 0.5τ is the desired pulse time.

4.5 Data Collection

Data was recorded by means of a personal computer using an in-house data logging program. Upon completion of data recording, the binary data files were converted to a series of ASCII (American National Standard Code for Information Interchange) files containing the real time voltage data, which was once again converted to give real values of load, stress, strain, etc. Strain data was subsequently filtered using the low pass Butterworth digital filtering routine of The Math Works, PRO-MATLAB software package, with the cutoff frequency set at 10 Hz. The sampling rate was variable. The load control tests typically had a sampling rate of 286 Hz while the strain control tests were performed at approximately 190 Hz.

Axial strain data was measured by means of two 6.35 mm LVDT's (total stroke = 12.7 mm). The LVDT's were mounted in collars and aligned with the sample. The voltage output of each LVDT was fed into a voltage averager which gave one voltage reading to be input to both the MTS and the data recorder. The change in length of the sample was thus assumed to be equal to the average of the two LVDT's.

Values of axial load were acquired by means of a 90 kN load cell situated within the MTS load frame. To increase the resolution of the load cell, the load range could be adjusted from the MTS control panel. Experience showed that the strain control tests could be performed with a load range of 20 kN while the load control

tests were conducted with a load range of 10 kN.

Stroke of the hydraulic ram was also recorded. This was accomplished by means of a LVDT situated in the hydraulic actuator. Due to the elastic response of the load frame, this data was not used to calculate strain. However it did serve as a rough check of strain data.

4.6 Crystallographic Analysis

As discussed earlier, the field test program of 1990 on Hobson's Choice Ice Island was conducted in multi-year rafted sea ice. Analysis of cores taken at the test site revealed that the ice consisted of layers of snow ice, frazil ice, and columnar ice, with the salinity varying between 0 ‰ and 4 ‰ (Gagnon and Sinha, 1991).

The four intact ice samples were selected from indenter face SFR-01. The thin section of Figure 4.3, showed this ice to be in transition, containing both frazil and columnar ice. Furthermore, it should be noted that due to the rafting and consolidation processes the longitudinal axis of the columnar grains are no longer vertical and are now offset by approximately 37° from the vertical axis. The grain size can be classified as fine to extra large (Cammaert and Muggeridge, 1988) with some grains reaching 50 mm in length.

Following each compression test it was noted that the samples demonstrated preferential failure (i.e. the failure was concentrated at one end of the sample and was not uniform throughout), Figure 4.4 shows this behaviour. For test II1, failure occurred along a plane with an angle of 40° from the vertical axis, corresponding closely to the longitudinal axis of the columnar grains. The large grain size relative to the sample diameter, along with easy glide planes (basal planes) parallel to the

Figure 4.3: Ice crystal structure from test face SFR-01.

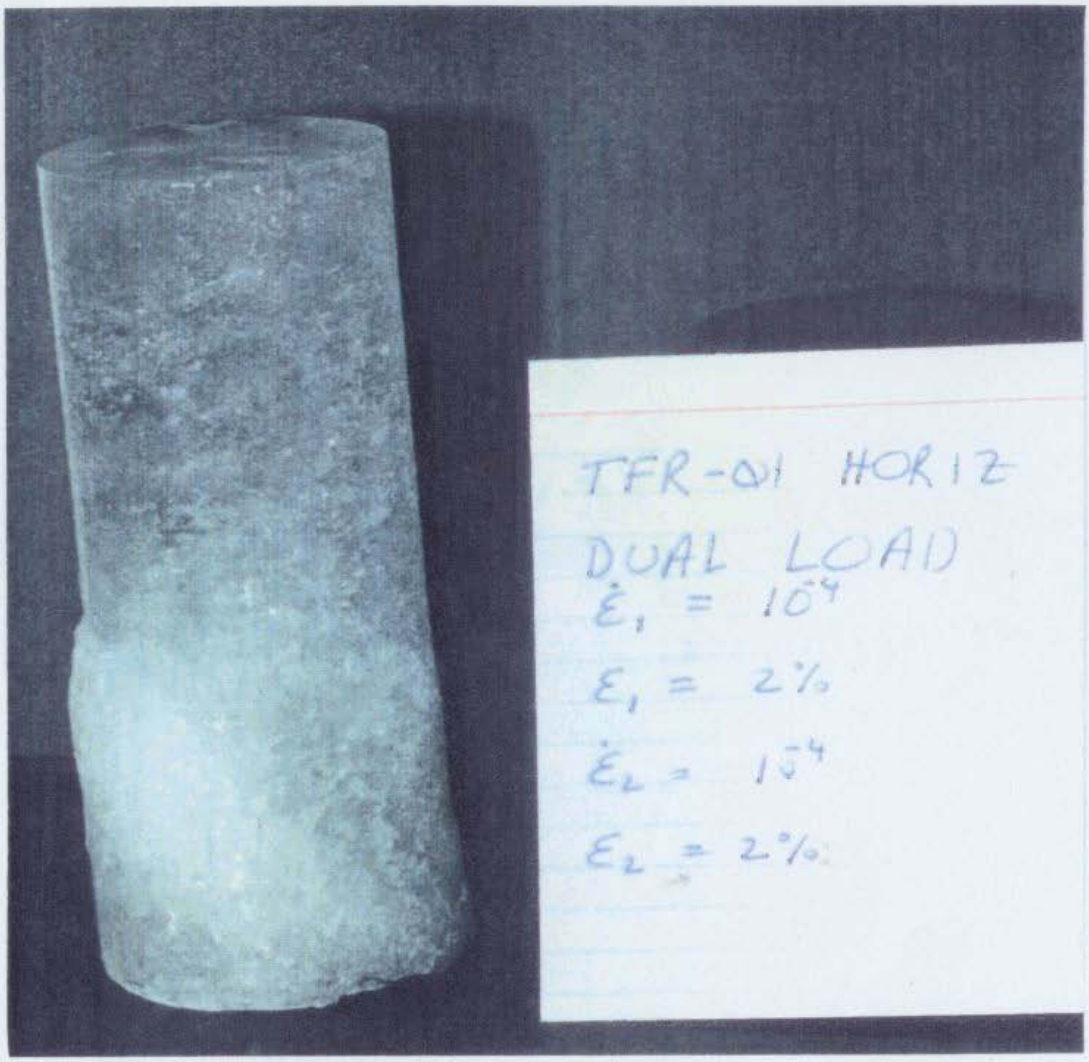

Figure 4.4: Preferential failure of ice sample from test II1.

Figure 4.5: Thin sections of ice sample from test II1; 25 mm and 100 mm from top.

columnar grains, contributed to this preferential failure.

Thin sections, taken at various elevations through the sample reveal the varying degrees of damage. Figure 4.5 shows thin sections at 25 mm and 100 mm from the top of sample SFR-01 following test II1. The damage in the top portion is slight with several intra-granular cracks (cracks within the grains) and isolated pockets of damage. The damage at the bottom of the sample however, is more extreme. Through the center of the thin section taken at 100 mm from the top of sample SFR-01, a band of finely crushed material is visible. This material resembles the fine pulverized ice found in the crushed layer, and appears to be the result of a grinding action as sliding occurs along the failure plane.

4.7 Constant Strain Rate Test Results

The intact ice samples were tested at three strain rates, 5×10^{-5} s^{-1}, 2.5×10^{-4} s^{-1}, and 5×10^{-4} s^{-1}. Neither strain rate was sufficiently large to cause brittle failure and thus the ductile to brittle transition could not be established. The stress strain curves for tests II1, II2, and II4, are shown in Figure 4.6, it can be seen from these curves that an increase in strain rate results in an increase in strength. Additionally, Figure 4.8 presents typical compressive strength data of multi-year sea ice, from various researchers.

The reload curves of the constant strain rate tests display some interesting characteristics. If at some point during a test, the load is removed and then reapplied, provided the strain rate is unchanged, the stress consistently returns to the previous path. When the stress strain curve is then constructed, it appears as if no interruptions occurred in the load history. It is therefore reasonable to suggest that

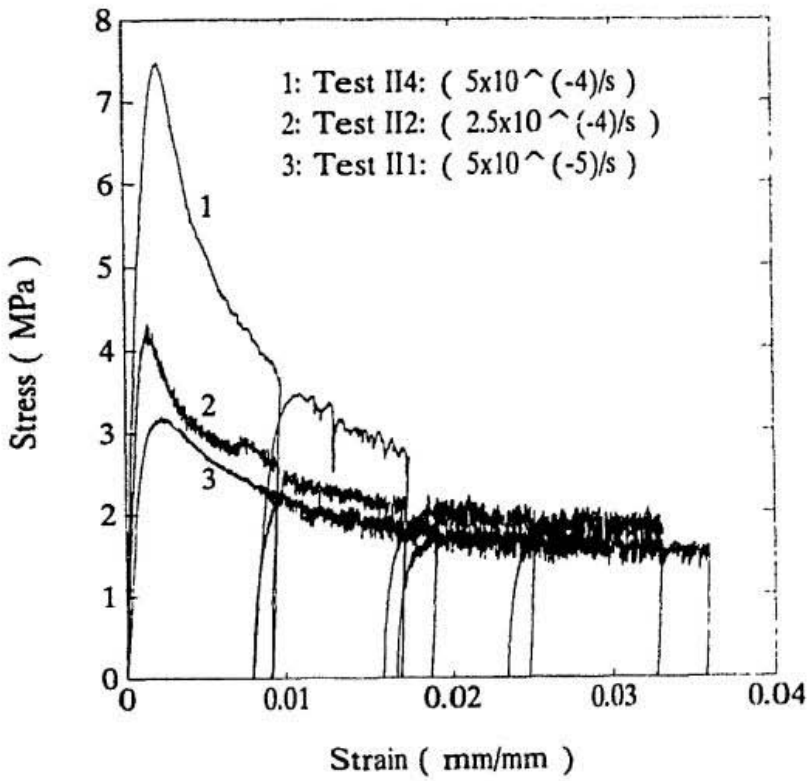

Figure 4.6: Stress-strain: tests II1, II2 and II4.

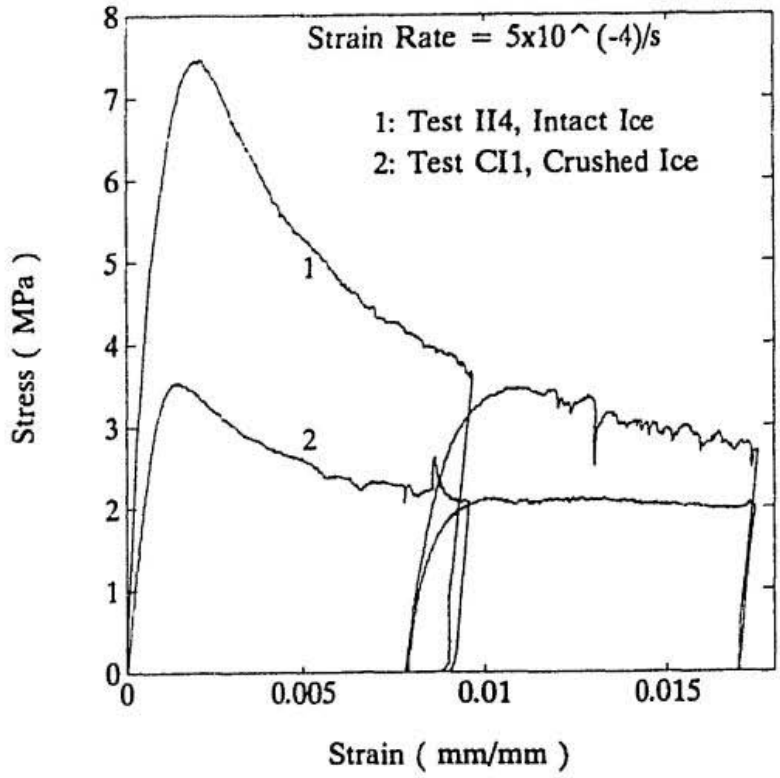

Figure 4.7: Stress-strain: tests II4 and CI1.

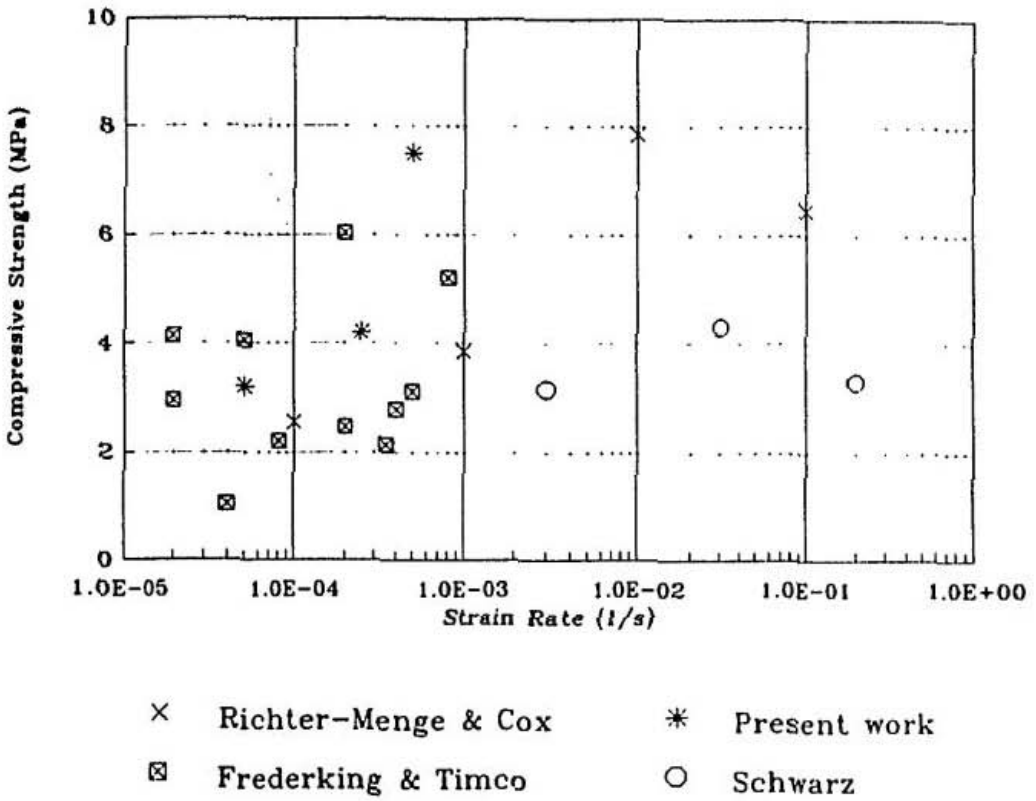

Figure 4.8: Compressive strength data from various authors (Frederking and Timco, 1983 and 1984; Richter-Menge and Cox, 1986; Schwarz, 1970).

the mechanical properties of the ice and its state of damage are a function of the stress or strain history. This behaviour can be seen in Figures 4.6 and 4.7.

If we compare the behaviour of the intact ice to the ice found in the crushed layer, Figure 4.7, we see that the ice in the crushed layer is much softer. At a strain rate of 5×10^{-4} s^{-1}, the ice from the crushed layer gave a peak stress of 3.49 MPa, only 53 % of the intact ice strength. This peak occurred at $\epsilon = 0.0015$, and the plateau was seen as approximately 2 MPa. Following two loadings of $\dot{\epsilon} = 5 \times 10^{-4}$ s^{-1} and $\epsilon = 0.01$, the strain rate was increased to $\dot{\epsilon} = 1 \times 10^{-3}$ s^{-1} (see Table 4.1 for a detailed loading scheme) and the second peak was found to be 2.54 MPa.

Test CI3 did not produce a characteristic load trace. With a strain rate of $\dot{\epsilon} = 2.5 \times 10^{-4}$ s^{-1} an initial peak of 1.1 MPa was reached, this occurred at $\epsilon = 0.0007$. The load dropped to approximately 0.9 MPa and once again began to increase. This gradual increase in stress continued until the load was removed at $\epsilon = 0.01$. Upon reloading the stress increased to approximately 1.43 MPa and remained fairly constant.

4.8 Creep Test Results

The creep tests, as discussed in Section 4.2, were performed on: intact ice, predamaged ice (damaged to $\epsilon = 0.02$), and crushed ice (ice taken from the highly damaged crushed layer). These tests were conducted with the applied loads varying between 0.25 MPa and 1.0 MPa. These tests can be used to determine the individual components of strain, i.e. elastic strain, delayed elastic strain, and permanent viscous flow. This section summarizes the mechanical response of the ice samples under the previously described load conditions.

Values of elastic modulus, measured from both the loading and unloading portion of the load cycle, did not always correspond precisely, and in one case the difference reached 21 %. This was an extreme case but typically the values were in very good agreement. When considering the complete data set, these values were found to be within 0.5 % of one another.

Table 4.2: Elastic modulus data.

Ice Type	E_{max} (GPa)	E_{min} (GPa)	$\overline{E}$ (GPa)
Intact	7.10	5.31	6.61
Predamaged	6.93	5.34	5.92
Crushed	5.47	3.56	4.35

As expected, the intact ice samples gave the highest value of elastic modulus, with the average being E = 6.61 GPa. The average value of elastic modulus for the predamaged samples was E = 5.92 GPa, while the crushed ice gave the lowest average value of elastic modulus, E= 4.35 GPa. Table 4.2 contains a brief summary of this elastic modulus data. These values of elastic modulus, particularly those of the intact ice, are lower than expected. Ideally, the elastic modulus should be approximately 9.5 GPa. Increased porosity of the natural sea ice would tend to lower this value. Additionally, the test apparatus can influence these results. The MTS cannot produce a perfect step load; a finite time is required to apply the load and slight overshoots in load are typical.

With a simple damage model, damage of the elastic modulus can be expressed as $E = (1 - D)E_o$, where E_o is the reference elastic modulus and D is the damage parameter. If the intact ice is assumed undamaged, then the predamaged samples have been damaged by 10.5 % (D=0.105) and the crushed ice samples have been damaged by 34.4 % (D=0.344).

Time dependant strain (creep) includes both permanent viscous flow and delayed elastic components. Experimentally these components of strain are difficult to distinguish, however the following assumptions have been used. With a low level of stress and a short loading time, the permanent viscous creep strain, ϵ_c of an undamaged sample will be very small and the delayed elastic strain, ϵ_d will dominate. The strain-time curve of test II3 can be used to demonstrate this point (refer to Appendix A). The undamaged strain-time trace of test II3 shows that any permanent deformation of the sample is unmeasureable. It is therefore reasonable to assume that the time dependant strain is primarily delayed elastic. A slight downward slope of these strain time traces is noticeable however this is attributed to signal conditioner drift.

Plotting total creep strain against stress for each time interval reveals a slight nonlinearity and an estimate of the exponent of stress was determined from the slope of log-log plots of stress and strain, see Figure 4.9. The value of the exponents for undamaged, predamaged and intact ice are presented in Table 4.3 and the average value is found to be 1.33. It should be noted that increasing damage appears to have very little influence on the exponent. These values are in agreement with those presented by C-Core (1990).

Damaging the ice sample not only reduces the elastic modulus, but also acts

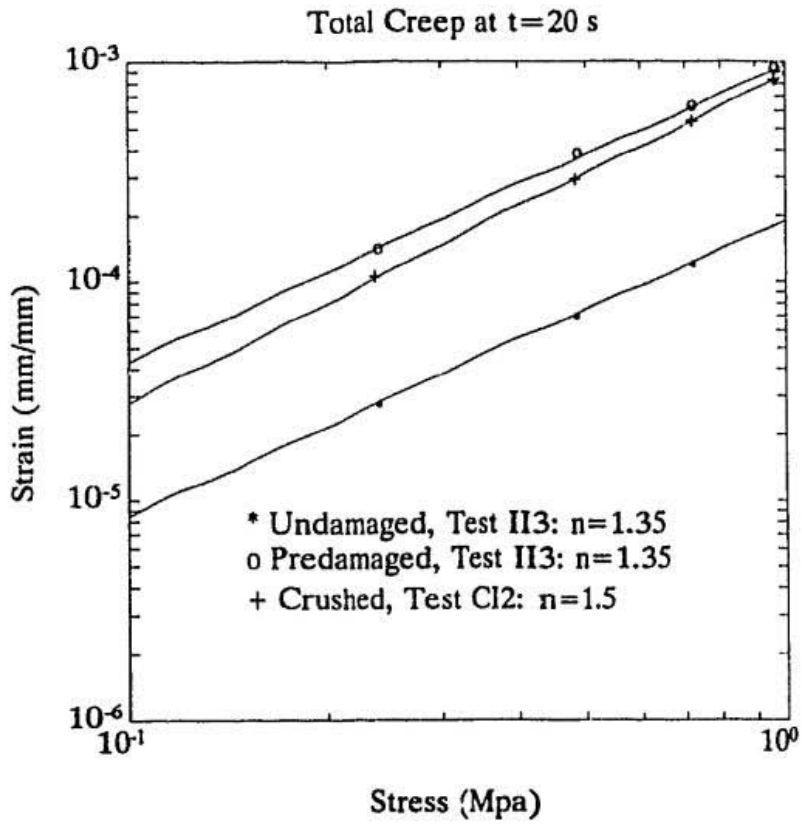

Figure 4.9: Log-log plot of stress vs. strain at 20 s.

Table 4.3: Slopes of Log(σ) vs. Log(ϵ).

Ice Type	2.5 s	10 s	15 s	20 s
Undamaged	1.11	1.32	1.36	1.35
Predamaged	1.18	1.35	1.47	1.35
Crushed	1.22	1.34	1.37	1.50

to enhance creep and delayed elastic strain. From the damaged creep tests of II3 and II4, (again refer to Appendix A), permanent deformation can be measured with all loads of 0.5 MPa or greater. In these tests, creep strain is estimated as the unrecovered portion of strain. Likewise, ice samples taken from the highly damaged crushed layer show similar behaviour.

Table 4.4 presents a summary of the strain component data for each nominal loading and ice type. Additionally, to roughly quantify creep enhancement, a ratio of $(\epsilon_d + \epsilon_c)$ to ϵ_e is presented. Furthermore, the effect of damage on the elastic modulus and the enhancement of delayed elastic and creep strain is graphically represented in Figure 4.10. Plots of strain vs. time for each ice type; undamaged, predamaged and crushed, are superimposed upon one another for loadings of 0.25 MPa and 0.75 MPa. It is clearly shown that increasing damage not only affects the elastic component of strain but also greatly enhances creep and the delayed elastic strain.

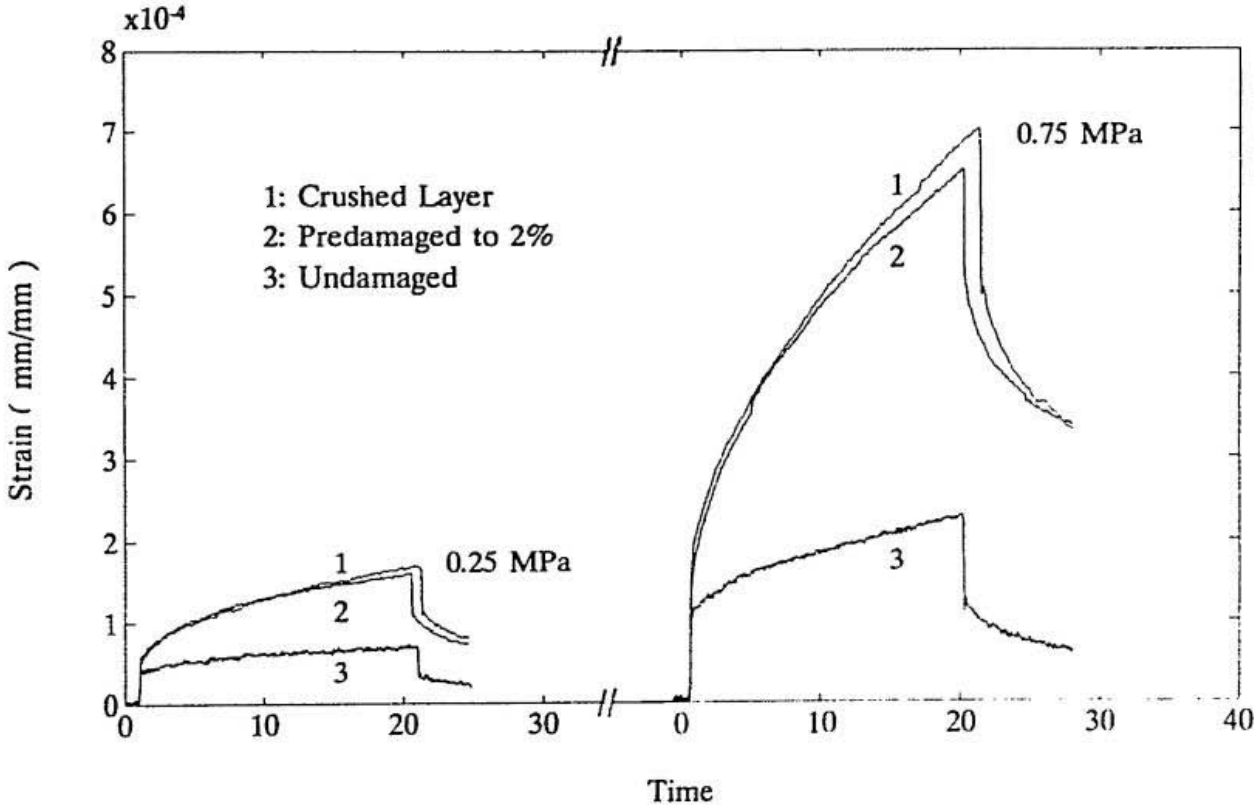

Figure 4.10: Creep of undamaged, damaged and crushed ice with constant loads of 0.25 MPa and 0.75 MPa.

Table 4.4: Strain component data at 20 s.

Ice Type	σ_{nom} (MPa)	$\overline{\epsilon_e}$ (mm/mm) ($\times 10^{-4}$)	$\epsilon_d + \epsilon_c$ (mm/mm) ($\times 10^{-4}$)	$\frac{\epsilon_d + \epsilon_c}{\epsilon_e}$
Undamaged	0.25	0.361	0.260	0.720
	0.50	0.815	0.690	0.847
	0.75	1.04	1.19	1.14
Predamaged	0.25	0.410	1.27	3.10
	0.50	0.855	3.91	4.57
	0.75	1.25	5.79	4.63
	1.00	1.59	8.52	5.36
Crushed	0.25	0.530	1.06	2.00
	0.50	1.06	2.92	2.75
	0.75	1.70	5.35	3.15
	1.00	2.55	8.29	3.25

Chapter 5

Finite Element Analysis of Ice-structure Interaction

Complex ice feature geometries, sophisticated constitutive models and a wide variety of structural geometries dictate the use of numerical modelling techniques for the solution of many ice-structure interaction problems. Even with state-of-the-art modelling techniques, the realistic behaviour of many natural phenomena cannot be reproduced rigorously. In all modelling routines, the engineer is required to make simplifying assumptions and to idealize natural processes. Such is the case for the following analysis.

The ultimate goal of the present work is to model the load fluctuations or dynamic response experienced during ice-structure interactions. Such a model would require a detailed knowledge of the structure, the ice feature and the fracture processes. This model must be capable of simulating the clearing and extrusion of the pulverized ice must also be addressed. Additionally, hydrodynamic effects could influence this model. At this time such a task would be overwhelming. However it is possible to simulate many individual aspects of the process.

In the proceeding chapters, the readers attention has been focused on the ex-

istence of an intermediate layer of highly damaged or crushed ice. Additionally, it has been shown that ice-induced vibrations often accompany ice-structure interactions. At this time, the influence of the intermediate layer on the global load will be investigated. It should be noted that this analysis is intended to reproduce the load upswing of one typical crushing cycle.

This analysis has been performed for several material models. These included: purely elastic, damaging viscoelastic and damaging viscoelastic with a viscous intermediate layer. Additionally, simulations were conducted to account for a reduction in effective contact area. The results of each simulation were compared to actual medium scale test data. Test NRC-06 of the 1989 Ice Island experimental program was chosen as the verification test. Unfortunately, the load-time traces of the 1990 Ice Island test series are not yet released to the public domain and hence could not be presented at this time.

"ABAQUS" was utilized to perform the finite element analysis. This software package provided the facilities to generate the mesh, specify the boundary conditions and describe the indenter characteristics. A damaging viscoelastic model was not available in ABAQUS and so a user-defined subroutine was used to describe the material properties of ice. This user-defined subroutine, "DILAT" was written and implemented by McKenna et al. (1990a and 1990b). Difficulties also arose in specifying the material properties for the intermediate crushed layer. It was postulated that varying the input parameters of the user-defined subroutine DILAT could provide an acceptable approximation of a highly viscous layer but this hypothesis required verification.

5.1 Verification of Viscous Behaviour

5.1.1 Verification Model

Kheisin et al. (1976) proposed that the intermediate layer could be conceptualized as a Newtonian fluid between two rigid plates. Closed-form solutions describing this behaviour can be found in the literature but difficulties arise when converting these closed-form equations to the finite element model. ABAQUS does not contain the facilities necessary to model a purely viscous layer and therefore material models must be modified to approximate this behaviour. If the idealized viscoelastic model for ice (see Figure 2.3) is examined, it can be seen that viscous strain will dominate if the elastic moduli are very stiff relative to the viscous flow component. The following model was developed to verify wether or not ABAQUS, with modified constitutive equations, could approximate a very viscous fluid.

Assuming the intermediate layer behaves as a fluid implies that this layer will flow under any applied shear stress. Additionally, this assumption suggests that the volume change due to an applied load must be very small or negligible. Furthermore, the Newtonian fluid assumption infers a linear relationship between applied shear stress and shear rate. Typically, for ice, the viscous flow component of strain follows a power law relationship with an exponent $n = 3$. Water is considered to be a Newtonian fluid, that is $n = 1$. It is reasonable to expect that the viscous component of crushed ice would follow a power law with an exponent in the range of $n = 1$ to $n = 3$ but unfortunately, an acceptable value of this exponent is yet to be established. In this analysis, the intermediate layer is treated as a non-Newtonian fluid i.e., the effective viscosity μ is a function of stress with $n = 3$.

Using the case of a fluid between two rigid plates, the following analysis was

performed. McKenna et al. (1990a and 1990b) developed a damaging viscoelastic model for ice and produced a user defined subroutine DILAT, for use with the finite element analysis program ABAQUS. By varying input parameters, DILAT could produce a highly viscous material response. A 50 mm thick layer of viscous material, as described by DILAT, was placed between two 1 m wide plates. The plates were assumed to be infinitely long in the vertical direction. This allowed extrusion in the horizontal plane only (plane strain state of stress). Corresponding to test NRC-06 of the 1989 test series, the plates were brought together at a rate of 20 mm/s.

Due to symmetry it was only necessary to model one quarter of the system, refer to Figure 5.1. This segment was discretized into 125 equally sized elements (5 rows of 25 elements) using 4 noded plane strain elements (ABAQUS type CPE4R). A rigid surface described the indenter and interface elements (ABAQUS type IRS21) were utilized to provide the stress distribution across the contact face.

For a viscous fluid, particle velocity at contacting surfaces must be zero. To meet this criteria, boundary conditions were set to restrict relative movement between the rigid surface and all nodes contacting the rigid surface. Additionally, since only one quarter of the system was required, boundary conditions were set so that the model would be symmetrical about the X and Y axis. The layer was squeezed from 50 mm to 45 mm at a rate of 20 mm/s. This corresponded to a total time of 0.25 s. Again, since the model was symmetrical about the X axis the rigid surface need only translate a total of 2.5 mm.

With lubrication theory and the configuration shown in Figure 5.1, a Newtonian

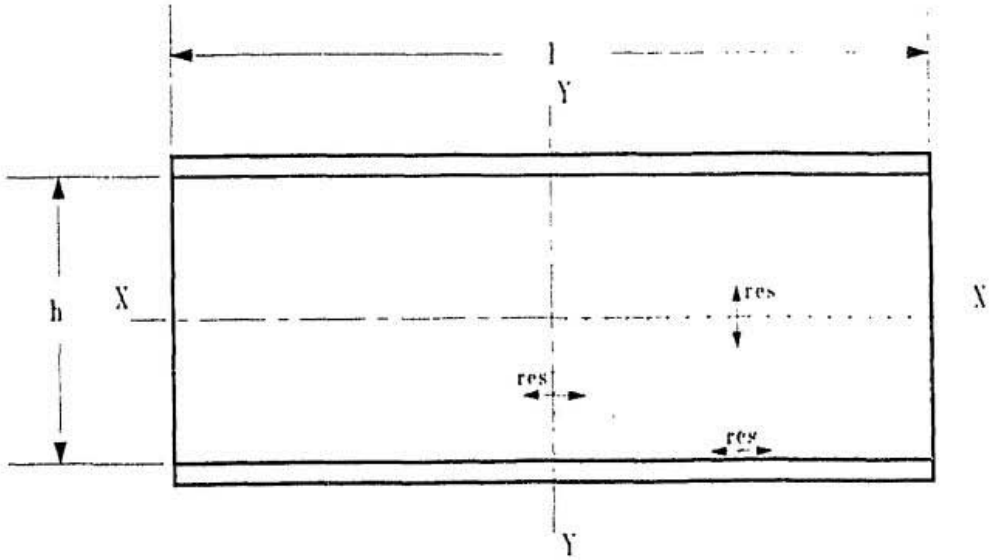

Figure 5.1: Idealized viscous layer.

fluid will produce a parabolic pressure distribution where;

$$P_x = \frac{6u\mu}{h^3}[\frac{l^2}{4} - x^2] \tag{5.1}$$

and u is the indentation velocity while μ is the viscosity. A complete derivation of this expression can be found in Jordaan and Timco, (1988).

5.1.2 Verification Results:

It has been postulated that an intermediate viscous layer could be produced by modifying the constitutive equations of the damaging viscoelastic model. Using the previously described finite element model and three sets of material properties, this hypothesis was investigated. Estimates of each component of the viscoelastic model, for crushed ice, were acquired from the uniaxial compression test program (Test CI2). These values were considered to be a reasonable starting point for the

Table 5.1: Material properties of crushed layer.

Parameter	Value		
	Trial 1	Trial 2	Trial 3
Elastic Modulus (Maxwell unit)	5900 MPa	5900 MPa	5900 MPa
Elastic Modulus (Kelvin unit)	2360 MPa	2360 MPa	2360 MPa
Poisson's Ratio	0.3	0.3	0.3
Grain Size	4 mm	4 mm	4 mm
Temperature	-10 °C	-10 °C	-10 °C
Permanent Viscous Creep Parameter at 1MPa and -10 °C	2.64×10^{-5} s^{-1}	2.64×10^{-4} s^{-1}	2.64×10^{-3} s^{-1}
Delayed Elastic Strain Parameter at 1 MPa and -10 °C	7.92×10^{-5} s^{-1}	7.92×10^{-4} s^{-1}	7.92×10^{-3} s^{-1}

analysis. The spring constants of the Maxwell and Kelvin units were held constant for all trials, but to soften the dashpots, the creep constants were increased by factors of 10 and 100 for trials 2 and 3 respectively. A summary of the material constants for each of the three trial runs are presented in Table 5.1. It should be noted that although a damaging viscoelastic model was used, the damage parameters were set such that the material properties do not change throughout the simulations.

The resulting pressure distribution of each simulation is shown in Figure 5.2. It is clearly shown that increasing the creep parameters of the Kelvin and Maxwell units produces two dominant effects. These are, the peak stress is reduced and the pressure distribution appears more parabolic i.e., the material portrays a more viscous behaviour. From trial 1, the pressure remains uniform for the first 0.25 m, suggesting an elastic response, beyond which a more viscous behaviour is evident. The pressure distributions of trials 2 and 3 are characteristic of a viscous fluid.

Although the shape of the pressure distributions are reasonable, peak stresses are higher than anticipated. Field measurements suggest that peak stresses should be of the order of 50 to 100 MPa while the simulations predicted peak stresses of 189 to 481 MPa. For this simulation the crushed layer is being squeezed between two rigid plates. With full scale ice indentations the crushed layer is situated between an indenter (or structure) and the ice feature and peak stresses are partially dictated by the deformation response of the ice.

The influence of element size is also a concern. It is expected that extrusion of the crushed layer will be hindered if the element size approaches the crushed layer thickness. A slight modification to the model has been used to demonstrate the influence of element size. Initially, the model was discretized such that 10 elements (5 elements for 1/2 the layer) comprised the crushed layer thickness. The number of elements across the layer were reduced to 2 and the total decreased from 125 to 5. Figure 5.3 demonstrates that an insufficient number of elements enhances the modal stiffness and impedes the mobility of the crushed layer. It should be noted that this simulation was performed with the creep parameters of trial 3.

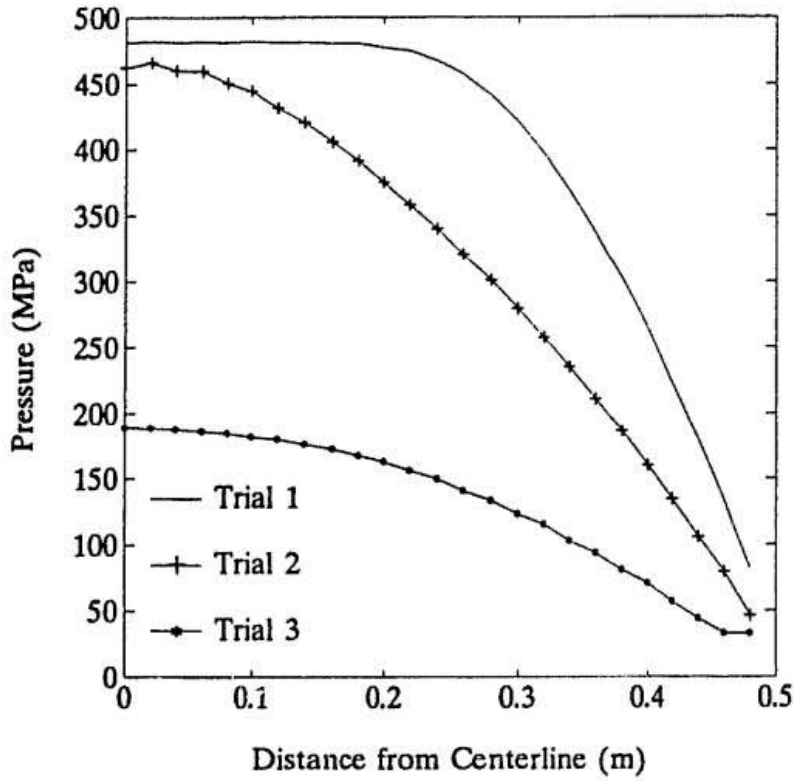

Figure 5.2: Pressure distributions for various sets of material parameters.

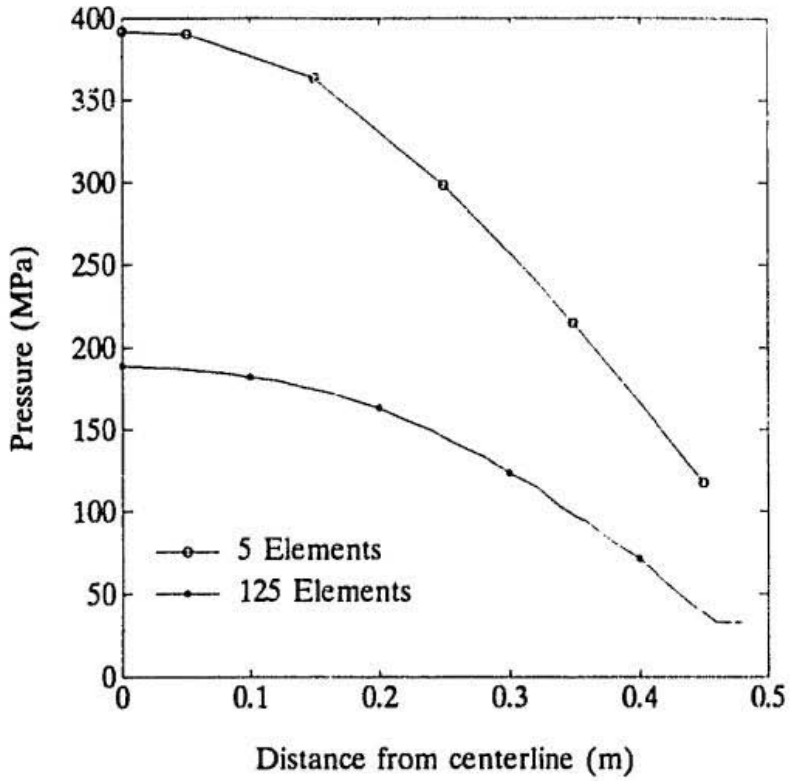

Figure 5.3: Influence of element size on crushed layer extrusion.

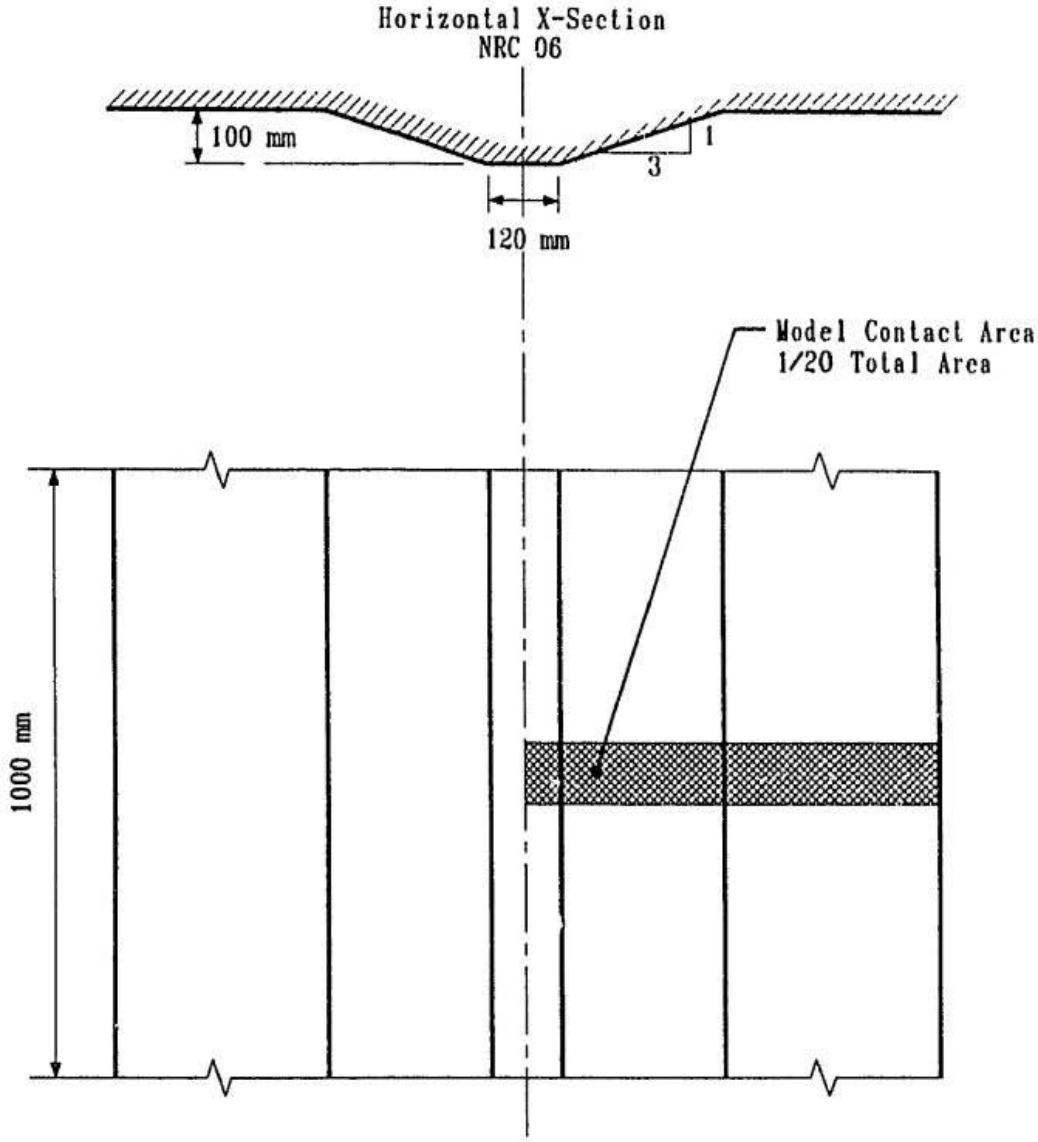

Figure 5.4: NRC-06 test face geometry.

5.2 Description of Test NRC-06 (1989)

Test NRC-06 was performed with the single actuator configuration of the indentation system described in Chapter 3. The indentor was flat and circular with a 1 m diameter. The test face, as shown in Figure 5.4, consisted of a truncated vertical wedge with an initial contact width of 120 mm and sides sloping at 3:1. The system was set to penetrate the ice face 30 mm at a rate of 20 mm/s.

Figure 5.5 displays the resulting load-time trace with the peak load reaching 1.8 MN. It is interesting to note that the amplitude and period of each crushing cycle appears to increase with time. The power spectrum of Figure 5.6 shows the dominant crushing frequency to be approximately 15 Hz. From the load-time trace, it can be noted that the characteristic saw-tooth pattern is superimposed on a long period wave of approximately 2 Hz. The total energy input for test NRC-06 was determined to be 18 kJ and the energy increased in a series of steps which correspond with each load fluctuation, refer to Figure 5.7.

5.3 NRC-06 Simulation

5.3.1 Finite Element Model of NRC-06

As previously stated, this finite element analysis model was intended to simulate the load upswing of one crushing cycle. Additionally, several material response models were investigated, these include:

- purely elastic material response;
- damaging viscoelastic material response;

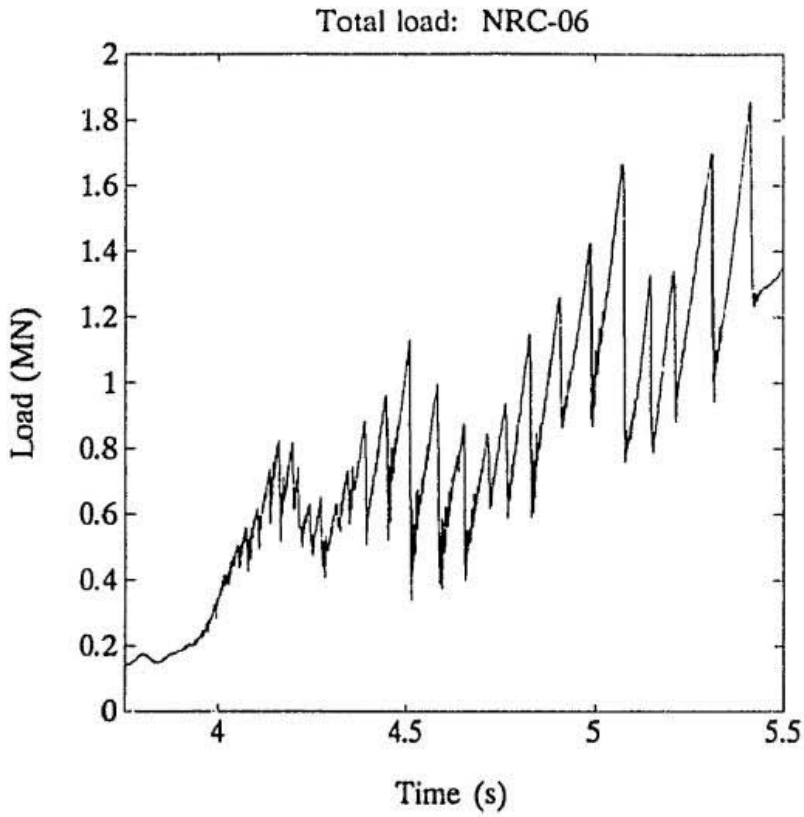

Figure 5.5: Load-time trace of NRC-06.

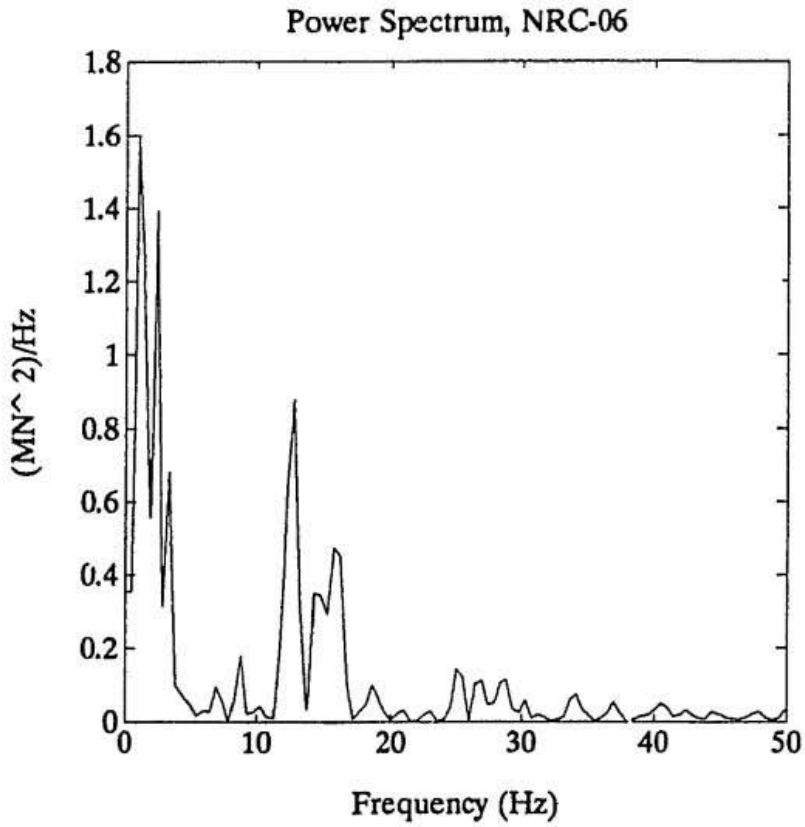

Figure 5.6: Power spectrum of NRC-06.

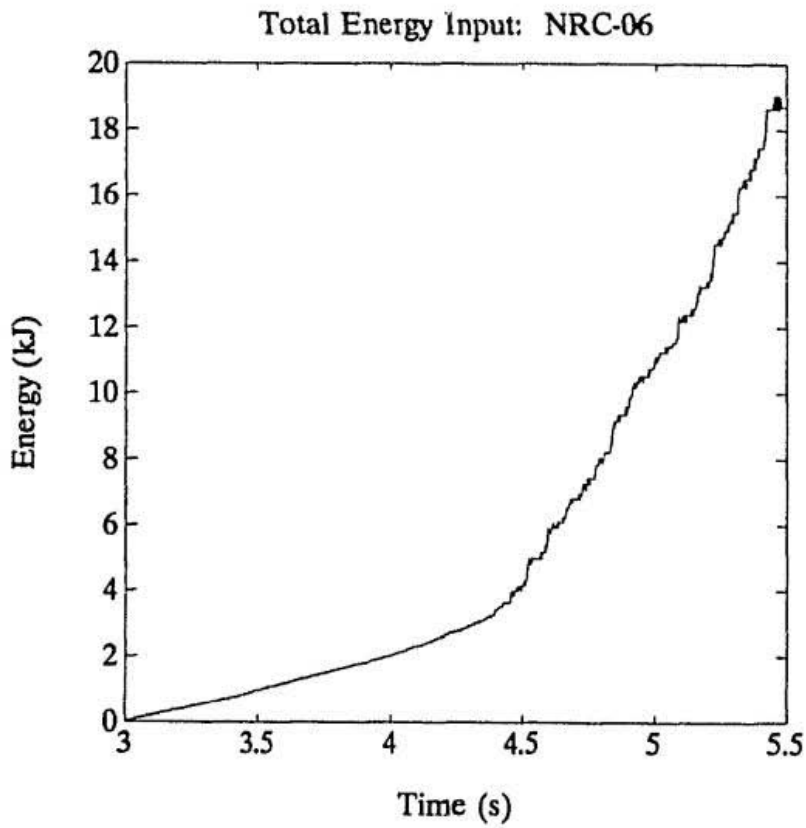

Figure 5.7: Total energy input of NRC-06.

- damaging viscoelastic response with a intermediate crushed layer (three crushed layer viscosities were utilized).

The test face configuration of NRC-06 is shown in Figure 5.4. A thin horizontal section through the center of the test face can be assumed to be under a plane-strain state of stress. If end effects at the indenter top and bottom are neglected, this horizontal section can represent the full test face. For this model, a 100 mm thick horizontal section was chosen, representing an area $1/10^{th}$ of the nominal contact area. Additionally, it can be seen that the model is symmetrical about the vertical centerline. Due to this symmetry it is only necessary to reproduce 1/2 of the test face. The model area has now become $1/20^{th}$ of the nominal contact area (see Figure 5.4). The pressure distribution at the ice-indenter interface will be equivalent to that of the model but the predicted total load must be increased by a factor of 20.

To allow extrusion of the crushed layer a very fine mesh was placed alongside the indentor. In this location each element was approximately 3 mm × 3 mm. The overall model measured 1500 mm × 1500 mm and to reduce the total number of elements multi point constraints (MPC) [1] were utilized. The indentor is represented by a rigid surface and interface elements are used to provide pressure distributions along the indentor. All elements were four nodded plane strain elements (ABAQUS type CPE4R), with reduced integration and hourglass control. A rigid surface represented the indentor and interface elements (ABAQUS type IRS21) provided the pressure distribution at the contact surface. The model is shown in Figure 5.8.

[1] A very fine mesh is required in the vicinity of the indentor but if this element size is maintained over the entire model, the required CPU time would be extraordinary. The MPC is one technique available in ABAQUS which allows the user to place large elements adjacent to smaller elements.

The ice was modelled as a damaging viscoelastic material, after McKenna et al. (1990a and 1990b), using the user defined subroutine DILAT. In this model, the ice was treated as a continuum and unfortunately discrete events such as spalling or flaking were not considered. The input parameters which describe the material properties are found in Table 5.2, these were taken from Xiao (1991). In cases where a crushed layer was present, an element set was defined adjacent to the indentor. This element set was provided with independent material properties. The crushed layer properties have been chosen from the uniaxial compression test data and additional simulations were performed with the creep parameters increased by a factors of 10 and 100. These parameters can be found in Table 5.1. ABAQUS contains facilities to model the purely elastic case and the elastic modulus for this run was set at 8000 MPa.

Ideally the model is conceptualized as a semi-infinite plate, although in reality, it must have some finite size. If the model is large relative to the contact area and the penetration a semi-infinite state can be approximated. For this model, the ratio of the maximum contact length to the length of the front edge was 1/10. Additionally, with increasing distance from the indentor, strain in the ice would approach zero. Therefore, the boundary conditions were set such that the back and right edges are fully restrained. The model was also symmetrical and the central axis was appropriately restrained (ie. movement of the left edge is restricted in direction 1, see Figure 5.8). The front edge was treated as a free surface except where it came in contact with the indentor. The friction coefficient between the ice and the indentor was assumed to be 0.15. Finally, the indentor was only permitted

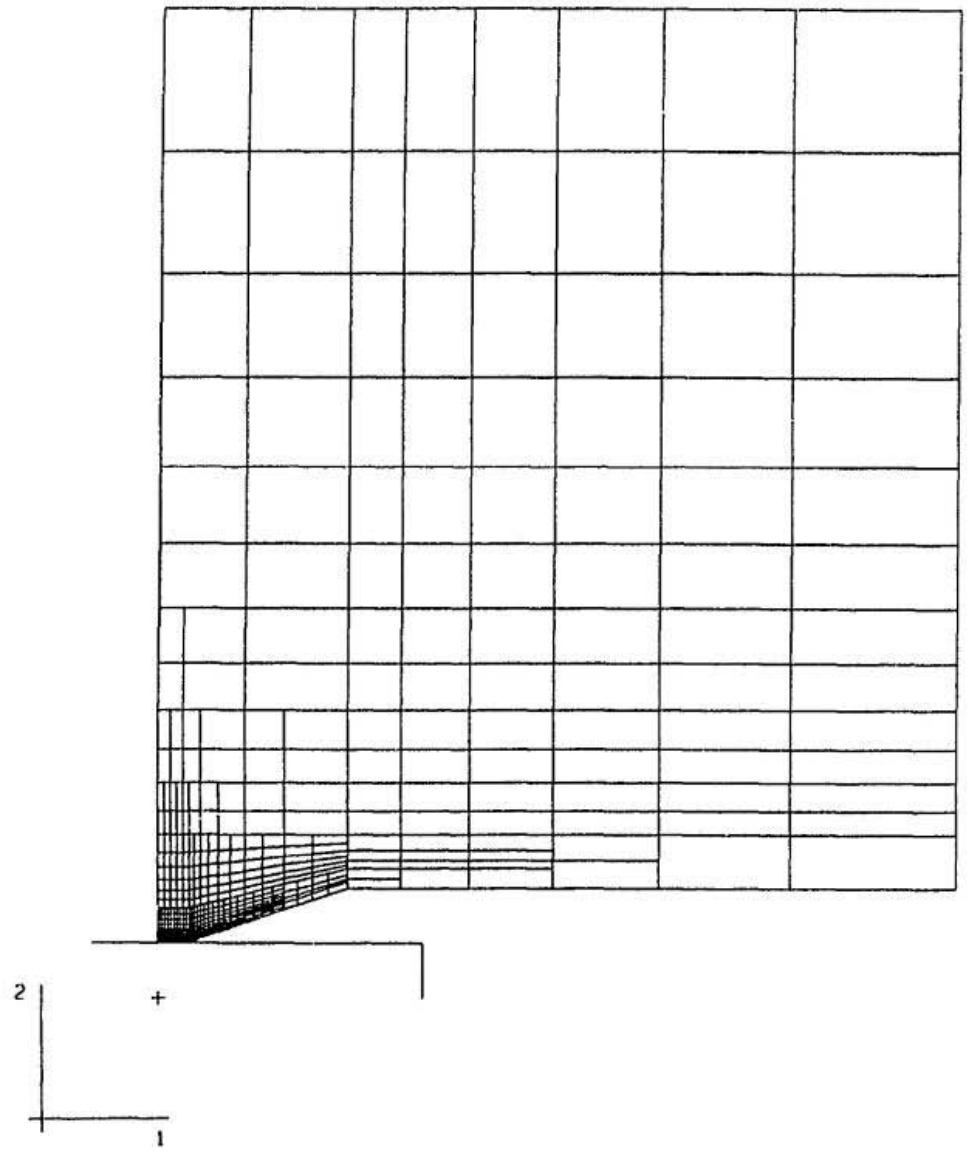

Figure 5.8: Finite element model of NRC-06.

Table 5.2: Material properties of sea ice (Xiao 1991).

Parameter	Value
Elastic Modulus (Maxwell unit)	8000 MPa
Poisson's Ratio	0.3
Grain Size	4 mm
Temperature	-10 °C
Permanent Viscous Creep Parameter @ 1 MPa and -10 °C	3.52×10^{-7} s^{-1}
β_c	18
Elastic Modulus (Kelvin unit)	3550 MPa
Delayed Elastic Strain Parameter @ 1 MPa and -10 °C	8.80×10^{-6} s^{-1}
β_d	8
Critical Stress for Cracking	3 MPa
Reference Crack Number	20,000
Dilat 1	0.25
Dilat 2	1.5

to translate directly into the ice face (all degrees of freedom,except direction 2, were restrained).

5.3.2 NRC-06 Simulation Results

As previously discussed, the purpose of this analysis is to model one load upswing of a typical crushing cycle. Also of interest is the pressure distribution at the ice-indenter interface. Test NRC-06 of the 1989 field test program was chosen as the verification test. Additionally, various material response models were investigated. Observations from the 1990 field test program showed that within each test face there were zones where the crushed layer diminishes to zero. It has been suggested that these zones carry the majority of the load. To investigate this hypothesis, the effect of reducing the contact area has been included with this analysis.

The purely elastic case showed very poor agreement with the test results. This elastic analysis suggested that the peak load should approach 120 MN contrasting sharply with the measured value of 1.8 MN (see Figure 5.9). The rate of increase of load does not compare well either. Average rates of increase in load, on the load upswing of the crushing cycle, were approximately 8.5 MN/s while that of the purely elastic model reached 78 MN/s. Additionally, peak pressures measured at the ice indenter interface, were on the order of 75 MPa while predicted pressures of the elastic model, ranged from 600 MPa to 1600 MPa.

Prediction of total load from the damaging viscoelastic model can be seen in Figure 5.10. This model also over estimated the global load. From this simulation the maximum load was estimated to be 8.5 MN. The initial rate of increase in load was also relatively high, 75 MN/s, and approached that of the purely elastic case.

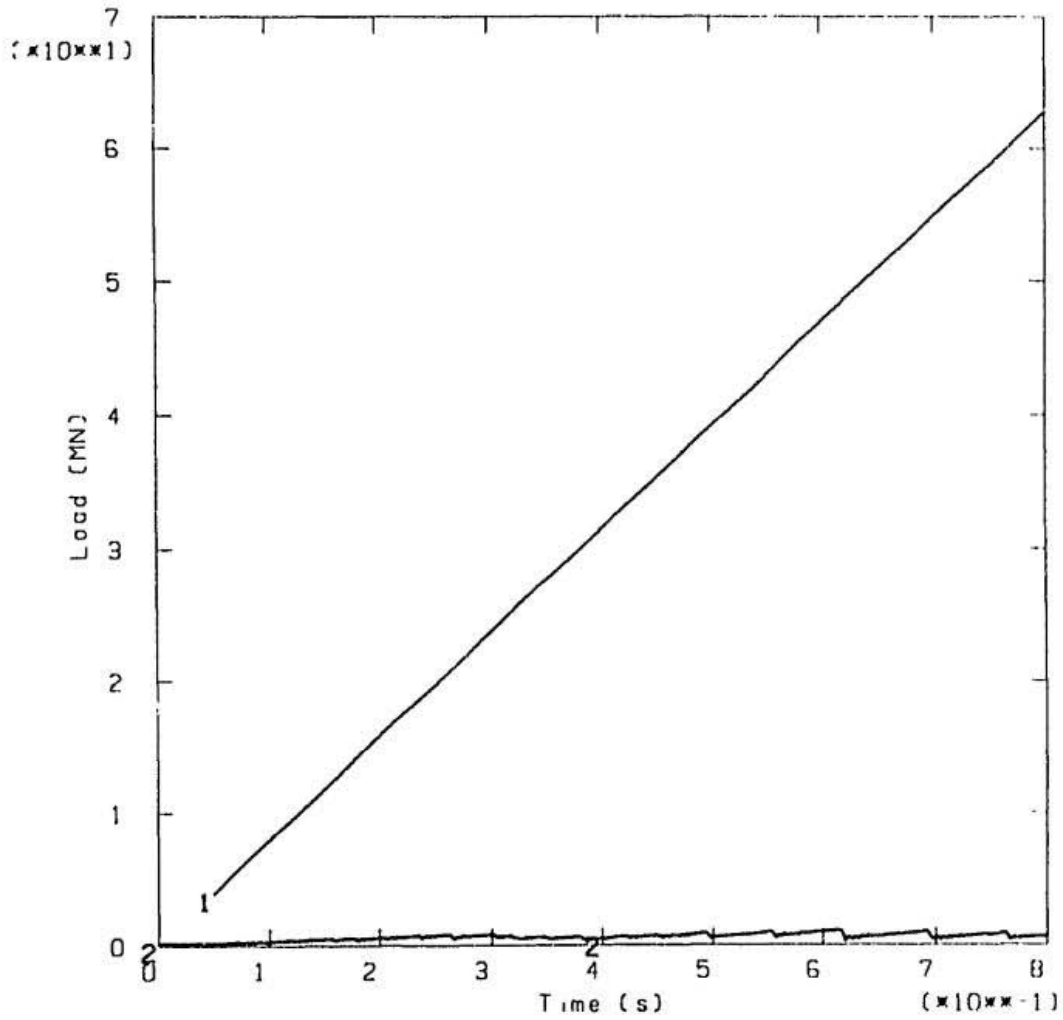

Figure 5.9: Purely elastic simulation of NRC-06 (1-Finite element prediction, 2 NRC-06 load history.)

After approximately 0.15 s, the ice began to creep. At this point, the predicted load remained fairly constant except for continuous, small fluctuations. It should be noted that these load fluctuations were associated with the model discretization and cannot be considered to be crushing cycles. Unfortunately this model did not consider discrete events such as spalling or flaking. In the work of Ian Jordaan and Associates (1991), it was shown that such events not only contributed to load fluctuations but also substantially influenced the global load.

The damaging viscoelastic model predicted peak pressures to be between 80 MPa and 90 MPa. These pressures occurred at about the 0.1 s time interval. The initial pressure distribution was very similar to that of the purely elastic model, with maximum pressures occurring at the outer edge of the contact face. As creep began to dominate, the pressure distribution became more parabolic with the maximum pressures occurring at the center (see Figure 5.11).

Three sets of creep parameters were utilized for those simulations which included a crushed layer (see Figures 5.12, 5.13 and 5.14). For each, the crushed layer thickness was assumed to be 60 mm. The best estimate of global load was achieved from the simulation with the lowest crushed layer viscosity. For this run, the creep parameters determined from the uniaxial compression tests were increased by a factor of 100 (Table 5.1, Trial 3) and the peak load in this case was determined to be 1.95 MN. When the measured creep parameters were utilized (Table 5.1, Trial 1), the peak load was found to be 8.5 MN and increasing these parameters by a factor of 10 (Table 5.3, Trial 2) gave a maximum force of 4.2 MN. The magnitude of contact pressures, for each simulation which incorporated a crushed layer, appeared to be reasonable. These values ranged from 13 MPa to 70 MPa. A summary of

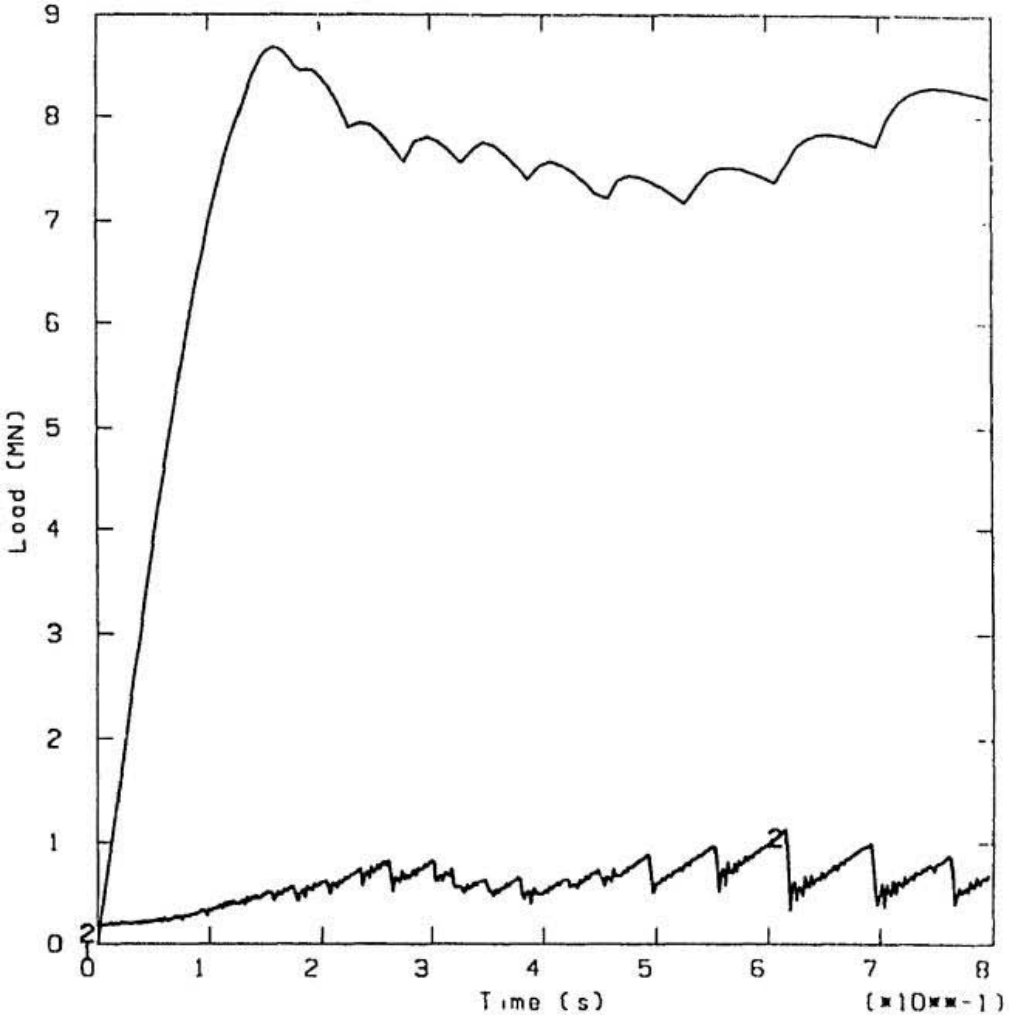

Figure 5.10: Damaging viscoelastic simulation of NRC-06 (1-Finite element prediction, 2-NRC-06 load history).

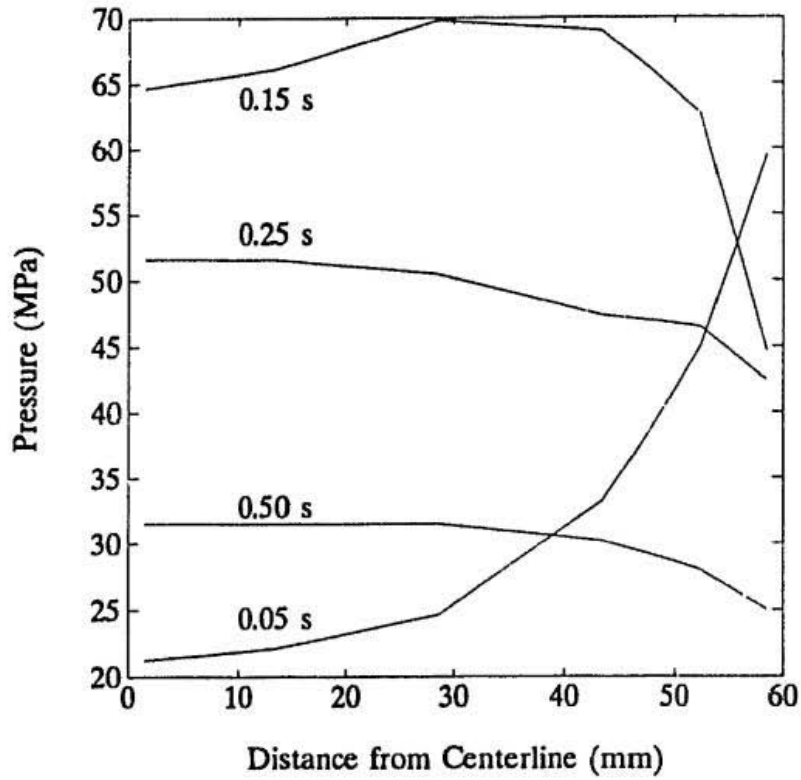

Figure 5.11: Pressure distribution of damaging viscoelastic model at selected times.

these results can be found in Table 5.3.

Although the order of magnitude of the contact pressures is acceptable, the pressure distribution was not as expected. For each the maximum pressure occurs at about 60 mm from the centerline, corresponding to the initial edge of the contact face. This effect is believed to be influenced by the deformation of ice behind the crushed layer. Maximum levels of stress and damage are found at this location and as well the confining pressures are minimum. Additionally, on the sloping ice face, the indenter is continuously contacting new, undamaged ice. This finite element analysis treats the ice as a continuum, and it is not yet capable of clearing the highly damaged material. As a result, the ice which would normally be ejected from the interface remains and contributes to the load.

Thus far, this analysis assumed that the load is distributed over the nominal contact area. The appearance of the test face coupled with medium-scale measurements of contact pressures suggested that the load is concentrated at discrete segments of the contact face. From Chapter 3, estimates of effective contact area implied that the load is carried by a zone which is approximately 35 % of the nominal contact area. With slight modifications to the finite element model, the influence of effective contact area was investigated. It was assumed that the contact zone would be situated at the geometric center of the test face. By using the "*MODEL CHANGE" facility of ABAQUS, several rows of elements were removed and the effective contact area reduced. Corresponding with field measurements this area was reduced to 35 % of the nominal and the analysis was repeated for the purely elastic and damaging viscoelastic models.

Once again the purely elastic model overestimated the global load. The overall

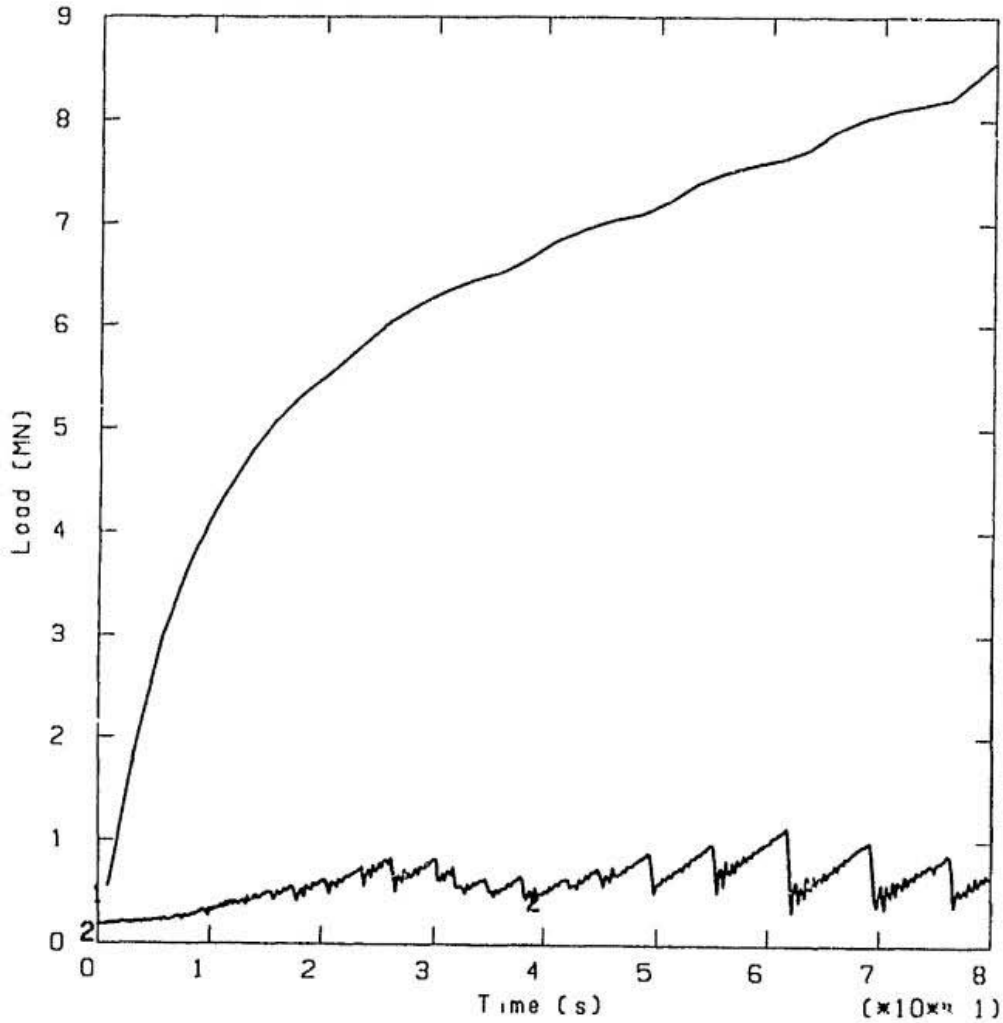

Figure 5.12: Viscous layer simulation of NRC-06: Creep parameters $\times 1$ (1–Finite element prediction, 2–NRC-06 load history).

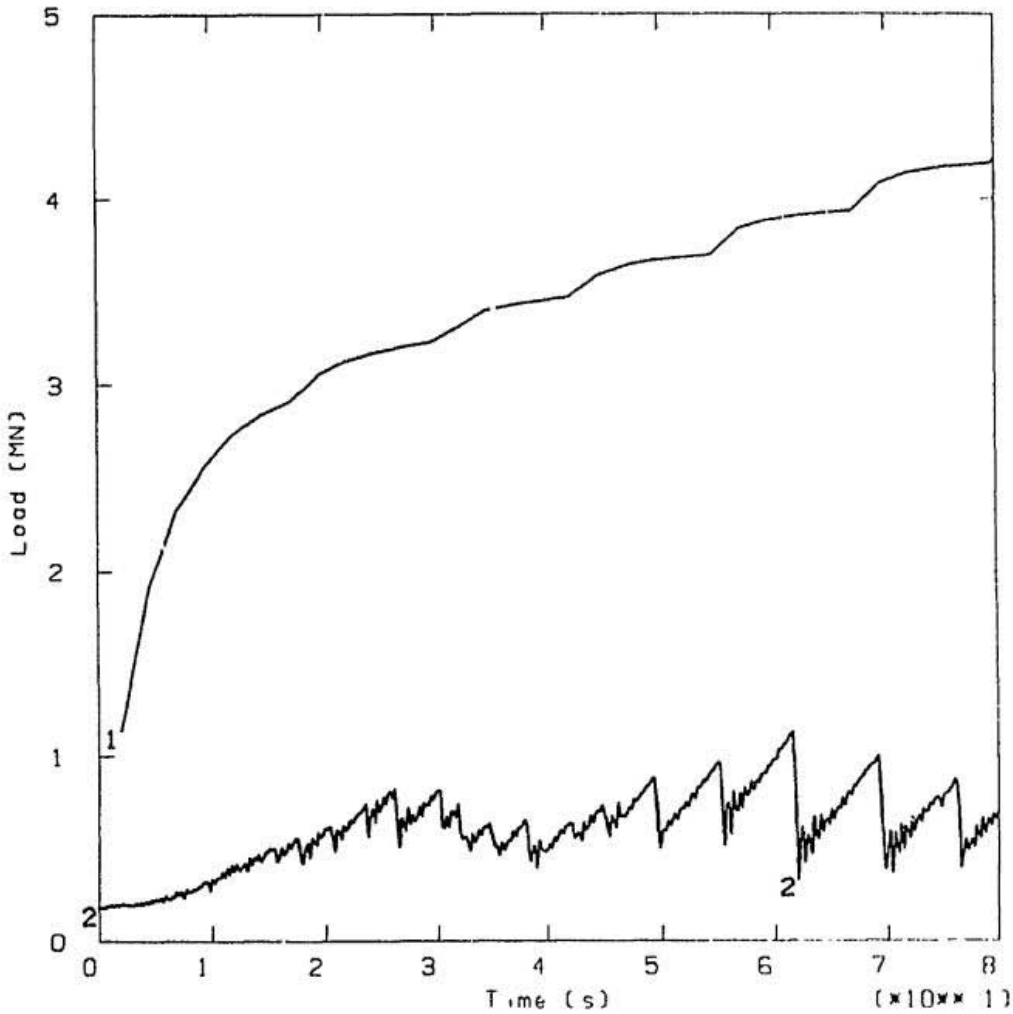

Figure 5.13: Viscous layer simulation of NRC-06: Creep parameters ×10 (1–Finite element prediction, 2–NRC-06 load history).

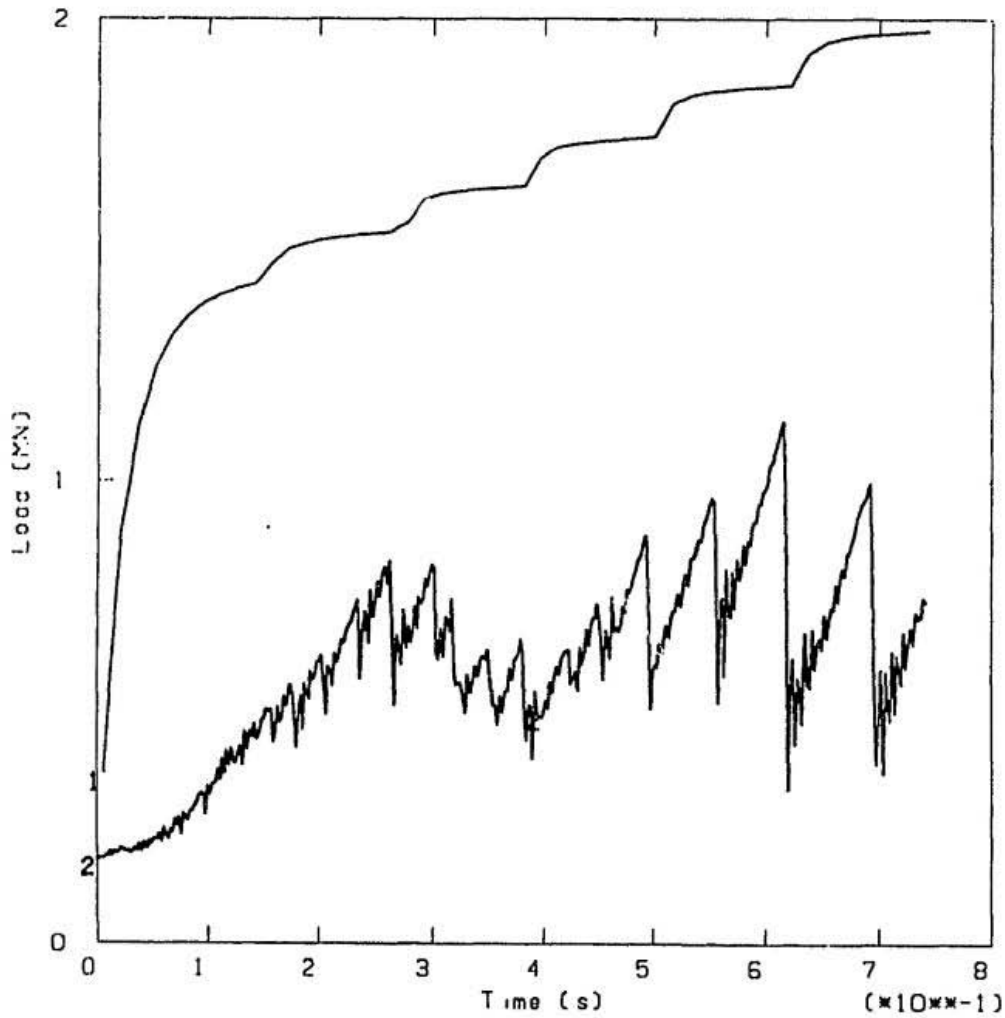

Figure 5.14: Viscous layer simulation of NRC-06: Creep parameters ×100 (1–Finite element prediction, 2–NRC-06 load history).

load approached 65 MN with a loading rate of 59 MN/s. Peak pressures were also much higher that expected: 500 to 1800 MPa.

The damaging viscoelastic model with reduced effective contact area gave a reasonable prediction of peak load, 3.2 MN but the initial loading rate of 57 MN/s was excessive. The order of magnitude of the contact pressures was also acceptable and ranged from 20 to 90 MPa. One particularly interesting characteristic of this load-time trace was a substantial drop in load (see Figure 5.15). Damage processes initiated at the outer edge of the contact zone and proceeded inward. This strain-softening resulted in a reduction of the global load. Crystallographic analysis from the medium-scale test program showed that ice taken from the areas of no apparent crushed layer displayed a substantial degree of damage. Applying some initial damage state to the ice in the effective contact zone would most probably produce a reduction in loading rate.

The results of the previous analysis are summarized in Figure 5.16. The initial loading rates for the various material models are compared to a typical crushing cycle of test NRC-06. It is clearly evident that an elastic material response overestimates the measured load. This holds true even when the effective contact area is reduced.

One other aspect must be addressed before the purely elastic model can be dismissed. Nominally, the indentation rate was specified as 20 mm/s. However the displacement-time record revealed a variable indentation rate. As a result of the indentation system compliance, the indentation rate was shown to vary with the load fluctuations. Closer examination of the displacement-time record revealed that variations in the indentation rate corresponded to the load fluctuations. As the

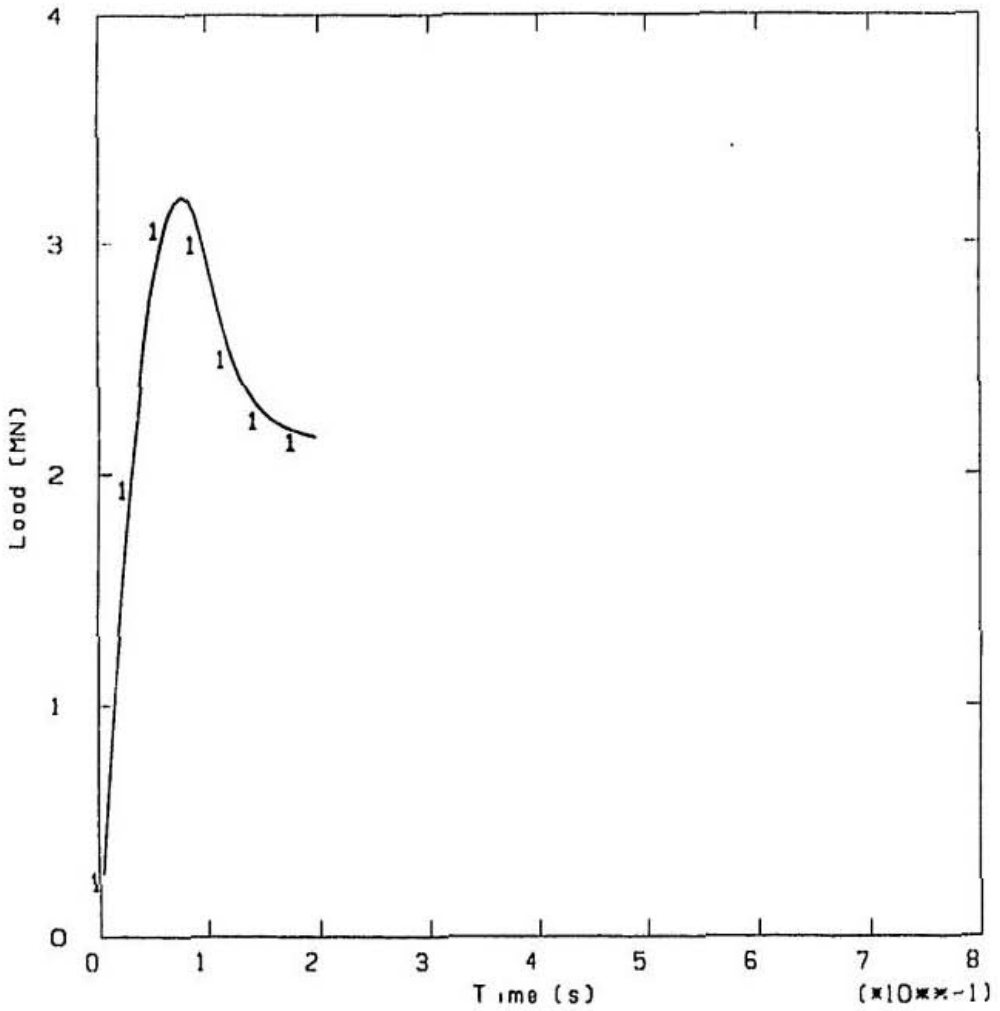

Figure 5.15: Predicted load-time trace from the damaging viscoelastic model with a reduced effective contact area.

Table 5.3: Summary of analysis results.

Model	Peak Load (@ 0.8 s) (MN)	Rate of Loading (MN/s)	Peak Pressure (MPa)	Area Compensation	
				Peak Load (@ 0.8 s) (MN)	Rate of Loading (MN/s)
Purely Elastic	64	78	1600	46	59
Viscoelastic	8.2	75	85	3.2*	57
Creep Parameter ×1	8.5	57	70	-	-
Creep Parameter ×10	4.2	32	36	-	-
Creep Parameter ×100	1.95	33	17	-	-
NRC-06	1.13	8.5	60	-	-

* Peak load predicted to occur at 0.08 s.

total load increased, the indentation rate was typically less than the nominal rate. However, as the load dropped, the indenter surged forward. Displacement rates, corresponding to load increases, were estimated to be approximately 12 mm/s. Analysis of the most extreme case (i.e. reduced contact area and reduced indentation rate), gave a loading rate of approximately 35 MN/s. Even under these conditions, the elastic model exceeds the measured value of 8.5 MN/s. Repeating these calculations for the damaging viscoelastic model gave a very similar result, i.e. the initial loading rate was determined to be 34.7 MN/s.

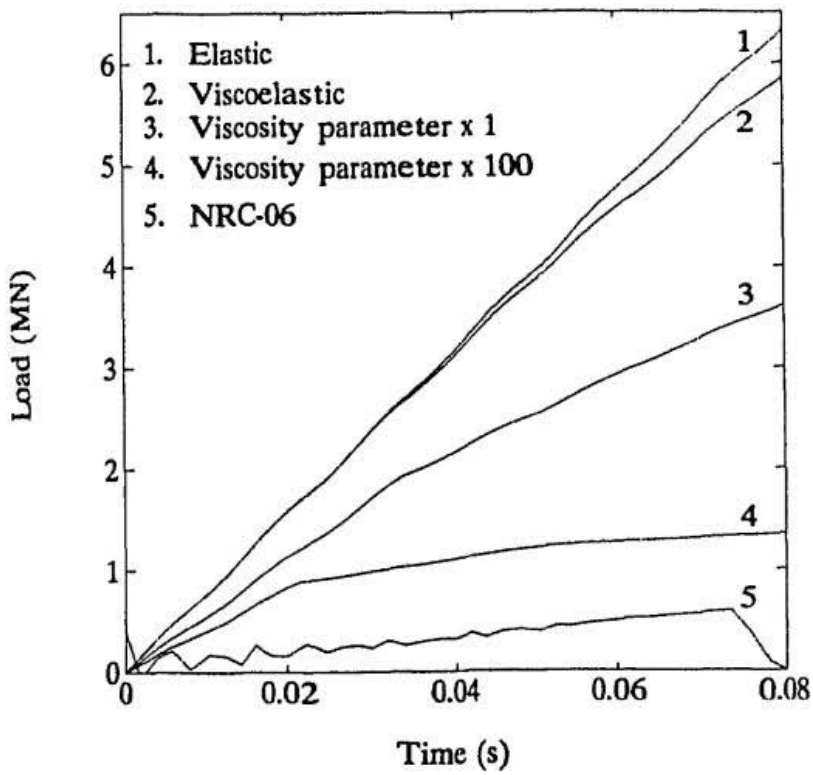

Figure 5.16: Estimates of loading rates for various material models.

Chapter 6

Discussion of Results and Conclusions

In may 1990 a medium-scale ice indentation tests program was conducted on Hobson's Choice Ice Island. The predominant failure mode exhibited during these indentation tests was crushing, although some spalling events were observed. Macroscopically, all failure surfaces portrayed some common attributes, these are: 1) spall areas, 2) zones of highly crushed or pulverized ice and 3) regions of no apparent crushed layer. The physical characteristics of the failure surface suggests that high pressure zones should correlate with those areas where the pulverized layer is thinnest; superimposing the final measured peak pressures on the failure surface did not to reveal such a phenomena. Comparative density analysis of the crushed layer and the intact ice showed that substantial dilatation had occurred during the damage process. Additionally, the density of the crushed layer appeared to be heavily influenced by the confining pressure. That is the density of the pulverized ice was highest at the centre of the crushed face, where the confining pressure was highest, and gradually decreased towards the periphery. Measurements of the crushed layer showed that its average thickness was on the order of 50 mm while the

measured maximum approached 173 mm. Additionally, microscopic examinations of the extruded particles revealed that pressure or friction melting and sintering processes were active during the crushing event; in-situ temperature measurements supported this hypothesis (Gagnon and Sinha 1991).

If observations of the failure surfaces are compared to typical load-time histories, several anomalies arise. Examination of test NRC-06 of the 1989 field test program showed the average crushing frequency to be approximately 15 Hz. With the nominal indentation rate being 20 mm/s, a theoretical crushed layer thickness of 1.3 mm was estimated. This value is much lower than typical measurements of crushed layer thickness. Furthermore, the peak pressure location does not necessarily correspond to zones where the crushed layer is apparently nonexistent. Observations of the physical characteristics of the test face suggests that the major portion of the load is carried by regions with no crushed layer but superimposing final measurements of peak pressure, on the test face, shows that the pulverized ice must possess substantial load carrying ability. Density measurements of the crushed layer also support this claim.

The uniaxial compression tests showed that increasing the damage state contributed to creep enhancement. Microscopic examination of the ice behind the zone of no apparent crushed layer revealed a very high level of damage (Kenny et al 1991). It is therefore reasonable to expect this material to be dominated by creep but triaxial compression tests are required to verify this assumption. The finite element analysis also showed that a uniform viscous layer is a reasonable assumption. This layer produces an averaging effect which allows an acceptable prediction of the global load but it cannot address the problems of large pressure gradients or

localized zones of high pressure.

Finally, it can be expected that the crushing and extrusion process follows a mixed mode. Recall from Chapter 5 that the load time trace of test NRC-06 consisted of a 15 Hz load cycle superimposed upon a longer period wave of 2 Hz. It is postulated that the long period cycle is associated with the formation and extrusion of the pulverized layer, while random, localized zones of high pressure contribute to the higher frequency crushing cycle.

6.1 Conclusions

As a result of the investigations presented herein, the following conclusions have been established:

- When ice is failing by crushing, a layer of highly damaged or pulverized ice exists adjacent to the structure or indentor and the deformation of this layer is dominated by creep and viscous flow processes.

- Modelling the crushed layer as a purely elastic material is unacceptable, even for very short loading periods.

- Zones in the contact face with an indistinguishable crushed layer, have typically been associated with high pressures. It may be more realistic to consider these zones to be centers of extrusion. In this manner, potential high pressure sites are not restricted to these areas.

- Increasing the level of damage in ice produces substantial creep enhancement. Furthermore, damage appears to have a much greater influence on creep rate than on elastic modulus.

- The pulverized layer possesses substantial load carrying abilities and high pressures are not restricted to areas where the pulverized layer thickness diminishes to zero.

- The uniform viscous layer assumption produces a reasonable estimate of global load but it cannot address the problems of large pressure gradients or localized zones of high pressure.

6.2 Recommendations for Future Work

In recent years substantial advances have been made in the area of ice-structure interactions and the availability of computing resources has encouraged the application of damage mechanics to this problem. Additionally, the medium scale field indentation programs, coupled with the vast supply of laboratory test data has contributed to the knowledge of ice-structure interactions. However, many questions still remain.

Although, under uniaxial states of stress, the stress-strain behaviour of ice is very well defined, additional work could be performed to measure damage states at incremental steps along the stress-strain curve. Full and medium scale test data have shown that confining pressures can exceed 70 MPa. Confined compression tests with hydrostatic pressures in excess of 50 MPa are rare but essential.

At the present time, knowledge of the behaviour of crushed or pulverized ice is mainly speculative. Very little such data are available in the public domain and the range of conditions, under which this material has been tested, is limited. Once again, confined compression tests, with hydrostatic pressures exceeding 50 MPa are essential. These tests should measure the mechanical response of the pulverized ice

and as well, attempt to simulate the conditions necessary for pressure melting at particle interfaces.

The model of ice-structure interaction, described within this work, defines an intermediate layer of pulverized ice adjacent to the structure. Unfortunately, the transition of ice from a continuum to a mass of discrete particles is not well understood and the criteria which govern such a process have not been established.

Field observations have shown that for full scale ice-structure interactions, average contact pressures are substantially lower than the uniaxial compressive strength of ice. Conversely, zones of very high pressure exist at the interface. Additionally, estimates of an effective contact area have been included. A more reliable estimate of the effective contact area, especially in cases where the ice is failing by crushing, would enhance the understanding of the ice-structure interaction process. One possible technique would be to utilize PVDF film (refer to Chapter 3) over an entire indenter face. This would provide a real-time pressure history for a continuous contact area.

With respect to finite element modelling of the ice-structure interaction process, clearing of highly damaged ice is not easily accomplished. Presently ABAQUS does not allow automatic removal of such highly damaged elements. Manually manipulating the finite element models and removing elements with a predefined level of damage may produce a more realistic load-time curve. Furthermore, discrete events such as spalling or flaking are very difficult to model. These occurrences are inherent components of ice-structure interactions and they have been shown to contribute substantially to the load-time histories.

References

Abele, G. and Frankenstein, G. (1967). "Snow and Ice Properties as related to Roads and Runways in Antarctic", *U.S. Army CRELL*, Technical Report No.176, 643 p.

Airaksinen, K. (1974). "Free Beam Tests and Friction Tests at Pond Inlet, N.W.T." *Polarforschung*, Vol. 44, No. 1, pp 71-75.

Anderson, D.L. (1962). "Elastic Properties of Sea Ice from Dynamic Measurements", *Air Force Surveys in Geophysics*, Summary Report - Project Ice Way, No. 145, Mass., pp. 153-172.

Björk B. (1981). "Ice-Induced Vibration of Fixed Offshore Structures, Part 2: Experiences with Baltic Lighthouses", *Marine Structures and Ships in Ice*, Report No.: 81-06/2, Norway.

Blenkarn K.A. (1970). "Measurement and Analysis of Ice Forces on Cook Inlet Structures", Proceedings *Offshore Technology Conference*, Houston, Texas, Vol II, pp. 365-378.

Budiansky, B. and O'Connell, R.J. (1976). "Elastic Moduli of a Cracked Solid", *International Journal of Solids and Structures*, Vol.12, pp. 81-97.

Butkovich, T.R. (1959). "On the Mechanical Properties of Sea Ice, Thule, Greenland, 1957", U. S. Army Snow Ice and Permafrost Research Establishment, Corps of Engineers, Research Report 54, Wilmette, Illinois, USA.

C-Core, (1990). *Developments of New Ice Load Models*, Centre for Cold Ocean Resources Engineering, Memorial University of Newfoundland, St. John's, Newfoundland, 65p.

Calcote, L.R. (1968). "Introduction to Continuum Mechanics", D. Van Nostrand Company, Inc., Princeton, New Jersey, pp. 179-189.

Cammaert, A.B. and Muggeridge, D.B. (1988). "Ice Interaction with Offshore Structures", Van Nostrand Reinhold, New York, U.S.A., 43p.

Cox, G.F.N, Richter, J.A., Weeks W.F. and Mellor, M. (1984). "A Summary of the Strength and Modulus of Ice Samples from Multi-Year Pressure Ridges", *ASME, Third International Offshore Mechanics and Arctic Engineering Symposium*, New Orleans, LA., V.3, pp. 126-133.

Dykins, J.E. (1971). "Ice Engineering – Material Properties of Saline Ice for a Limited Range of Conditions", *Naval Facilities Engineering Command*, Technical Report R720, Port Hueneme, California, USA.

Engelbrektson A. (1977). "Dynamic Ice Loads on a Lighthouse Structure", Proceedings *Fourth International Conference on Port and Ocean Engineering Under Arctic Conditions*, St. John's, NF. Canada, Vol. II, pp. 654-663.

Enkvist, E. (1972)."On the Resistance Encountered by Ships Operating in the Continuous Mode of Icebreaking". *The Swedish Academy of Engineering Sciences in Finland*, Helsinki, Finland, Report No. 24, 57 p.

Frederking, R. and Timco, G.W. (1983). "Uniaxial Compressive Strength and Deformation of Beaufort Sea Ice", Proceedings *Seventh International Conference on Port and Ocean Engineering Under Arctic Conditions*, Helsinki, Finland, pp. 89-98.

Frederking, R.M.W. and Timco, G.W. (1984). "Compressive Behavior of Beaufort Sea Ice Under Vertical and Horizontal Loading",Proceedings *Third International Offshore Mechanics and Arctic Engineering Symposium*, New Orleans, Louisiana, USA., Vol. III, pp. 145-149.

Frederking, R.M.W. (1990). personal communication.

Fung, Y.C. (1969). *A First Course in Continuum Mechanics*, Prentice-Hall, Inc., Englewood Cliffs, New Jersey, pp. 174-179

Gale, A.D., Sego, D.C. and Morgenstern, N. R. (1986). "Behaviour of Cohesionless Broken Ice", Proceedings *Third Canadian Conference on Marine Geotechnical Engineering*, St. John's NF, Canada, pp. 485-500.

Gale, A.D., Wong, T.T., Sego, D.C. and Morgenstern, N.R. (1987). "Stress-Strain Behaviour of Cohesionless Broken Ice", Proceedings *Ninth International Conference on Port And Ocean Engineering Under Arctic Conditions*, Fairbanks,Alaska, USA., pp. 109-119.

Gagnon, R.E. and Sinha, N.K. (1991). "Energy Dissipation Through Melting in Large Scale Indentation Experiments on Multi-Year Sea Ice." Proceedings, *OMAE*, in press.

Glen, J.W. (1955). "The Creep of Polycrystalline Ice", Proceedings *Royal Society of London*, Piccadilly, London, W., Ser. A, Vol. 228, pp. 519-538.

Grothues-Spork, V.H. (1974). "Aufmessung der Stromungen unter dem Eis des Eclipse Sound (Bafin Island) und Bestimmung von Reibungskoeffizienten zwischen Stahl und Eis", *Polarforschung*, Vol. 44, No. 1, pp 76-82.

Hallam, S.D. and Pickering J.G. (1988). "Modelling of Dynamic ice Loading on Offshore Structures", Proceedings *Polartech*, Vol. 1 pp. 235-248.

Horii, H. and Nemat-Nasser, S. (1983). "Overall Moduli of Solids with Microcracks: Load Induced Anisotropy" *Journal of Mechanics and Physics of Solids*, Vol.31, No.2, pp. 155-171.

Ian Jordaan and Associates, (1991). *Modelling of Fracture and Production of Discrete Ice Pieces*, pp. 32-36.

Iyer, S.H. (1983). "Size Effects in Ice and their Influence on the Structural Design of Offshore Structures." Proceedings, *Seventh International Conference, POAC*, Helsinki, Finland, V. 3, pp.414-432.

Jefferies, M.G. and Wright, W.H. (1988). "Dynamic Response of "Molikpaq" to Ice-Structure Interaction", Proceedings *Seventh International Conference on Offshore Mechanics and Arctic Engineering*, Houston, Vol IV, pp. 201-220.

Jordaan, I.J. (1986). "Numerical and Finite Element Techniques in Calculation of Ice-Structure Interaction" Proceedings *International Association of Hydraulics Research*, Iowa City, Iowa, Vol II, pp. 405-441.

Jordaan, I.J. and McKenna, R.F. (1988). "Constitutive Relations for Creep of Ice", Proceedings *International Association for Hydraulics Research*, Ice Symposium, Sapporo, Japan, pp. 47-58.

Jordaan, I.J. and Timco, G.W. (1988). "Dynamics of the Ice-Crushing Process." *Journal of Glaciology*, Volume 34, Number 118, pp.318-326.

Jordaan, I.J., Kennedy, K.P., McKenna, R.F. and Maes, M.A. (1990). "Loads and Vibration Induced by Compressive Failure of Ice." Proceedings, *Sixth International Specialty Conference, Cold Regions Engineering*, ASCE - CRREL, Editor Devinder S. Sodhi, Hanover, NH, pp.638-649.

Kennedy, K. P., (1991). "Dynamic Activity and Crushed Ice Behavior in Medium-Scale Ice-Structure Interactions", *M.Eng thesis*, Faculty of Engineering and Applied Science, Memorial University of Newfoundland, 45 p.

Kenny, S., Meancy, R., and Stone, B. (1991). "Failure Zone Characterization, Medium-Scale Field Indentation Program, Hobson's Choice Ice Island", Memorial University of Newfoundland, Ocean Engineering Research Centre, St. John's, Newfoundland, Canada.

Kheisin, D.E. and Cherepanov, N.V. (1973). "Change of Ice Structure in the Zone of Impact of a Solid Body Against the Ice Cover Surface". *Problems of the Arctic and Antarctic*, Jerusalem, Israel Program for Scientific Translations, Issues 33-35, pp.239-245.

Kheisin, D.E. and Likhomanov, V.A. (1973). "An experimental Determination of the Specific Energy of Mechanical Crushing of Ice by Impact". *Problems of the Arctic and Antarctic*, Vol 41, pp. 69-77.

Kheisin, D.E., Likhomanov, V.A., and Kurdyumov, V.A. (1976). "Determination of the Specific Breakup Energy and Contact Pressures Produced by the Impact of a Solid Against Ice". *U.S. Army Cold Regions Research and Engineering Laboratory*, CRREL TL 539, pp. 210-219.

Lainey, L. and Tinawi, R. (1981). "Parametric Studies of Sea-Ice Beams Under Short and Long Term Loadings", Proceedings *International Association for Hydraulic Research*, International Symposium on Ice, Quebec, Canada, Vol II, pp. 607-619.

Lainey, L. and Tinawi, R. (1984). "The Mechanical Properties of Sea Ice - A Compilation of Available Data", *The Canadian Journal of Civil Engineering*, Vol. 11, No. 4, pp. 884-923.

Langleben, M.P. (1962). "Elastic Properties of Sea Ice at Ultrasonic Frequencies", *Air Force Surveys in Geophysics*, Summary Report - Project Ice Way, No. 145, Mass., pp. 173-182.

Lindholm, J.E., Riska, K. and Joensuu, A. (1990). "Contact Between Structure and Ice: Results from ice crushing tests with a flexible indentor." *Laboratory of Naval Architecture and Marine Engineering*, Report M-101, Helsinki University of Technology, Helsinki, Finland, 30 p.

Määttänen M. (1975a). "Experiences of Ice Forces Against a Steel Lighthouse Mounted on the Seabed, and Proposed Constructional Refinements", Proceedings *Second International Conference on Port and Ocean Engineering Under Arctic Conditions*, Vol. 4, pp. 857-869.

Määttänen M. (1975b). "Ice Forces and Vibrational Behaviour of Bottom-Founded Steel Lighthouses", Proceedings *Third International Symposium on Ice Problems*, International Association of Hydraulic Research, Hanover, New Hampshire, pp. 345-355.

McKenna, R., Jordaan, I.J., Xiao, J. (1990a). "Analysis of Damage and Energy Flow in the Crushed Layer During Rapid Ice Loading", Proceedings *Ninth IAHR Ice Symposium*, Espoo, Finland, V.3, pp 231-245.

McKenna, R., Jordaan, I.J., and Xiao, J. (1990b). "Finite Element Modelling of the Damage Process in Ice", Proceedings *ABAQUS Users' Conference*, Newport, RI., in press.

Molgaard, J. (1989a). "A Study of the Friction of Ice", *National Research Council of Canada, Institute for Marine Dynamics*, Report No. CR-1989-33, St.John's, Nf., Canada.

Molgaard, J. (1989b). "Mechanisms of Ice Friction", Proceedings *IUTAM/IAHR, Symposium on Ice Structure Interaction*, St. John's, Nf., Vol. 2, pp. 385-403.

Richter-Menge, J.A. and Cox, G.F.N. (1986) "Mechanical Properties of Multi-year Sea Ice", *Workshop on Extreme Ice Features, National Research Council of Canada*, pp. 121-149.

Riska, K. (1989). "Theoretical Modelling of Ice–Structure Interaction." Proceedings, *IUTAM/IAHR Symposium on Ice–Structure Interaction*, St. John's, NF, Canada, in press.

Sanderson, T.J.O. (1988). *Ice Mechanics: Risks to Offshore Structures*, Graham and Trotman Limited, London, UK., 141p.

Schwarz, J. (1970). "The Pressure of Floating Ice-Fields on Piles", Proceedings *International Association for Hydraulic Research, Ice Symposium*, Reykjavik, Iceland, pp. 6.3, 1-11.

Schwarz, J. (1975). "On the Flexural Strength and Elasticity of Saline Ice", International Association of Hydraulics Research, Proceedings *Third International Symposium on Ice Problems*, Hanover, New Hampshire, pp. 373-385.

Sinha, N.K. (1978). "Rheology of Columnar-grained Ice", *Experimental Mechanics*, Westport, USA., Vol. 18, No. 12, pp. 464-470.

Sinha, N.K. (1981). "Deformation Behaviour of Ice-Like Materials in Engineering Applications", Proceedings, *International Symposium on the Mechanical Behaviour of Structural Media*, Ottawa, Canada, Part A, pp. 419- 430.

Sinha, N.K. (1983). "Creep Model of Ice For Monotonically Increasing Stress", *Cold Regions Science and Technology*, Amsterdam, Vol. 8, No. 1, pp. 25-33.

Sinha, N.K. (1984). "Intercrystalline Cracking, Grain-Boundary Sliding, and Delayed Elasticity at High Temperatures", *Journal of Material Science*, London, Vol.19, pp. 359-376.

Tabata, T. and Tusima, K. (1981). "Friction Measurements of Sea Ice on Some Plastics and Coatings", Proceedings *Sixth International Conference on Port and Ocean Engineering under Arctic Conditions*, Quebec, Canada, Vol. I, pp. 526-535.

Timco, G.W. and Frederking, R.M.W. (1982). "Compressive Strength of Multi-Year Ridge Ice", Proceedings *Workshop on Sea Ice Ridging and Pile-up*, Calgary, Alberta, National Research Council of Canada, Associate committee on Geotechnical Engineering, Technical Memorandum No. 134, pp. 52-61

Timco, G.W. and Jordaan, I.J. (1987). "Time-Series Variation in Crushing." Proceedings, *Ninth International Conference on Port and Ocean Engineering Under Arctic Conditions*, Fairbanks, AK, U.S.A., Volume 1, pp.13-20.

Tusima, K. and Tabata, T. (1979). "Friction Measurements of Sea Ice on Flat Plates of Metals, Plastics and Coatings", Proceedings *Fifth International Conference on Port and Ocean Engineering Under Arctic Conditions*, Trondheim, Norway, Vol. 1, pp. 741-755

Weeks, W.F. and Anderson, D.L. (1958). "An Experimental Study of Strength of Young Sea Ice", Transactions *American Geophysical Union*, Vol. 39, No. 4, pp. 641-647.

Wong, T.T., Gale, A.D., Sego, D.C. and Morgenstren, N.R. (1987). "Shear Box Tests on Broken Ice", Proceedings *Ninth International Conference on Port and Ocean Engineering Under Arctic Conditions*, Fairbanks, Alaska, USA., pp. 97-107.

Xiao, J. (1991). *Finite Element Modelling of Damage Processes in Ice-Structure Interaction*, M.Eng. Thesis, Faculty of Engineering and Applied Science, Memorial University of Newfoundland, St. John's, Newfoundland, in preparation.

Appendix A

Uniaxial Compression Test Data

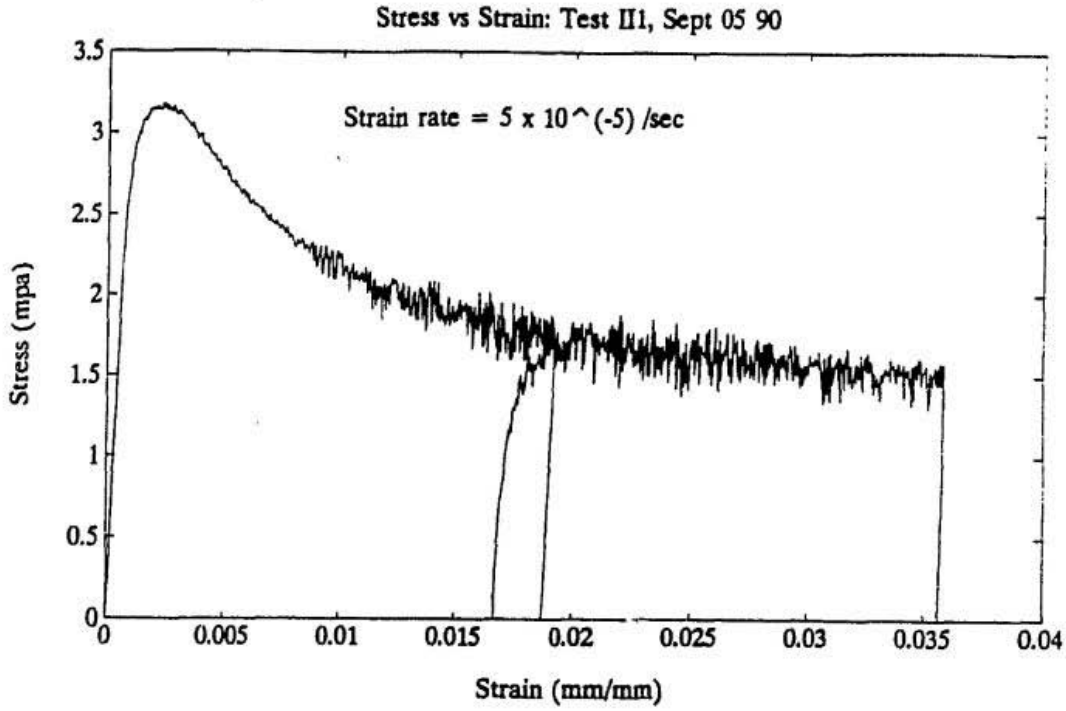
Stress vs Strain: Test II1, Sept 05 90
Strain rate = 5 x 10^(-5) /sec
Stress (mpa)
Strain (mm/mm)
3.5
3
2.5
2
1.5
1
0.5
0
0
0.005
0.01
0.015
0.02
0.025
0.03
0.035
0.04

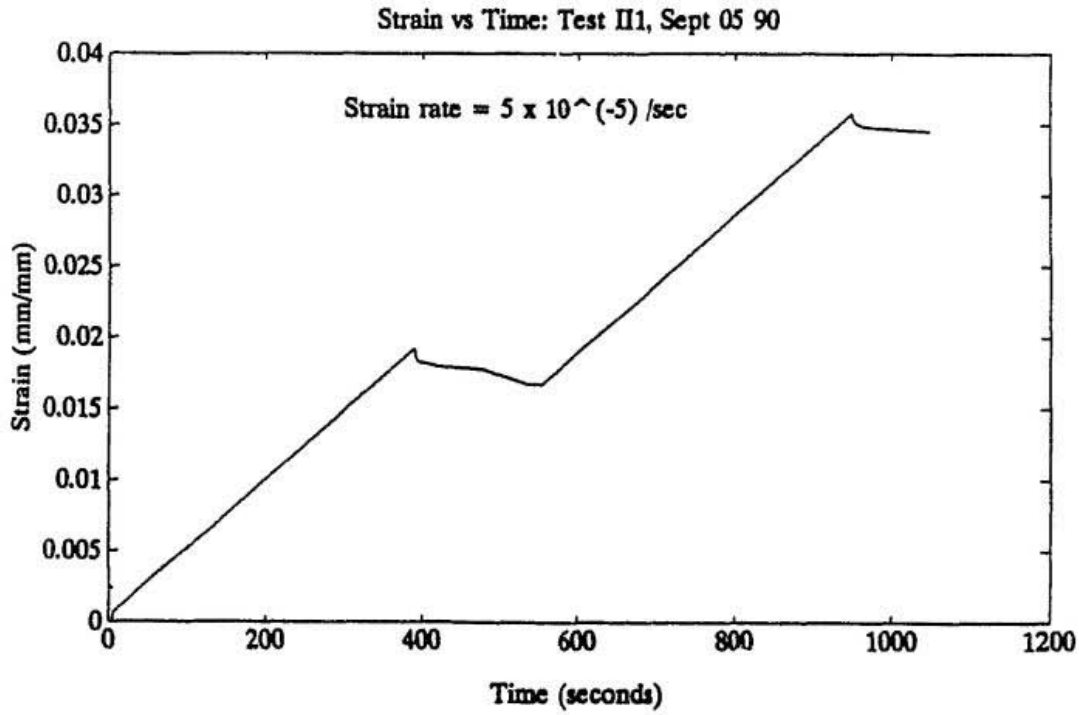
Strain vs Time: Test II1, Sept 05 90
Strain rate = 5 x 10^(-5) /sec
Strain (mm/mm)
Time (seconds)
0.04
0.035
0.03
0.025
0.02
0.015
0.01
0.005
0
0
200
400
600
800
1000
1200

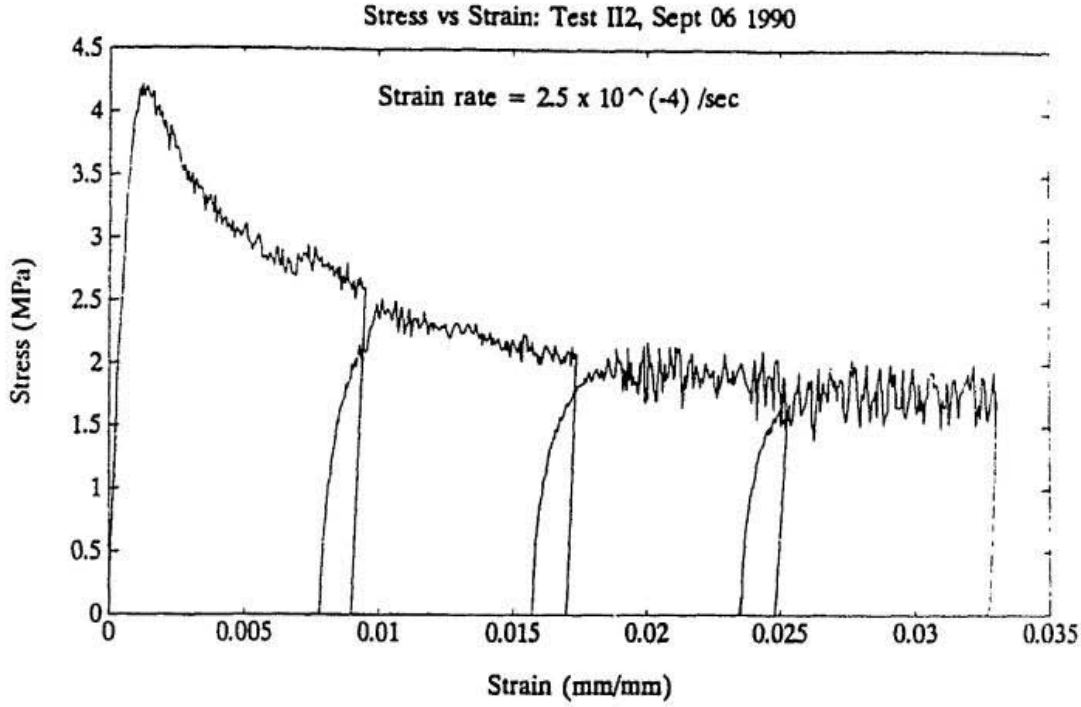
Stress vs Strain: Test II2, Sept 06 1990
Strain rate = 2.5 x 10^(-4) /sec
Stress (MPa)
Strain (mm/mm)
0
0.5
1
1.5
2
2.5
3
3.5
4
4.5
0.005
0.01
0.015
0.02
0.025
0.03
0.035

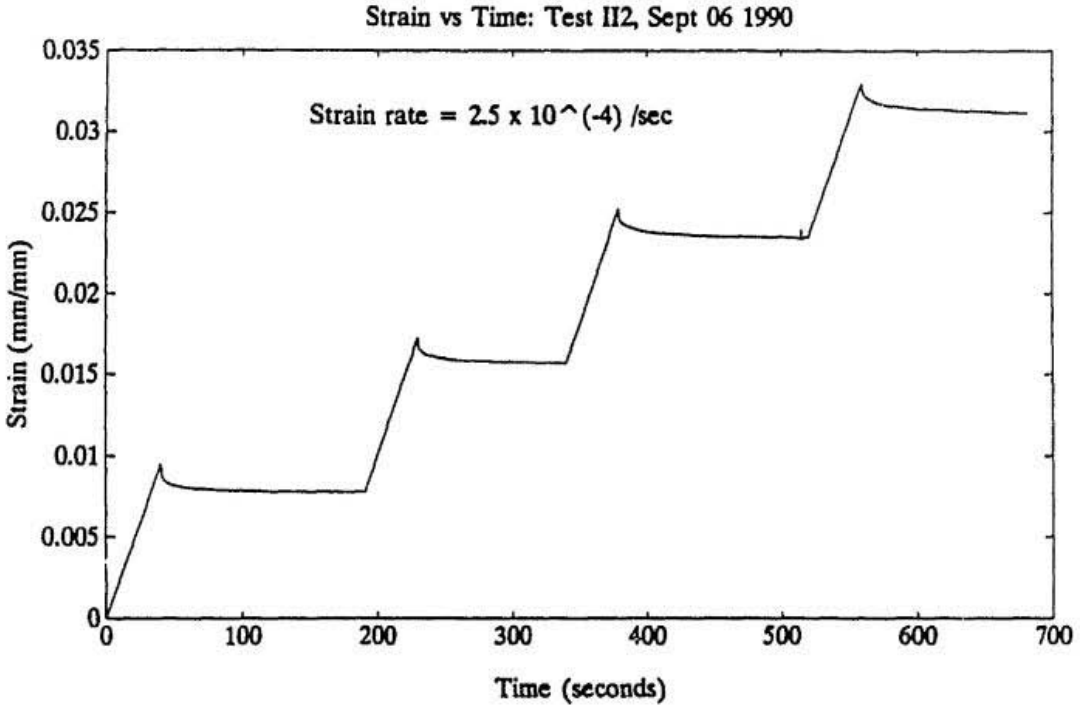
Strain vs Time: Test II2, Sept 06 1990
Strain rate = 2.5 x 10^(-4) /sec
Strain (mm/mm)
Time (seconds)
0
0.005
0.01
0.015
0.02
0.025
0.03
0.035
100
200
300
400
500
600
700

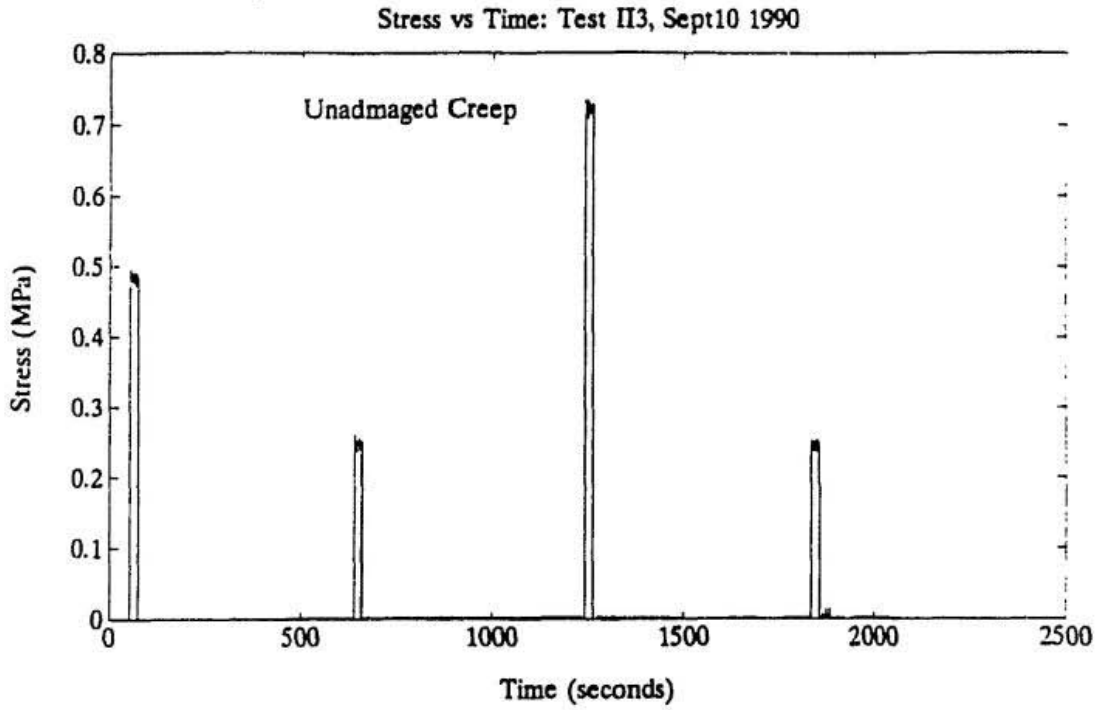
Stress vs Time: Test II3, Sept10 1990
Unadmaged Creep
Stress (MPa)
0.8
0.7
0.6
0.5
0.4
0.3
0.2
0.1
0
0
500
1000
1500
2000
2500
Time (seconds)

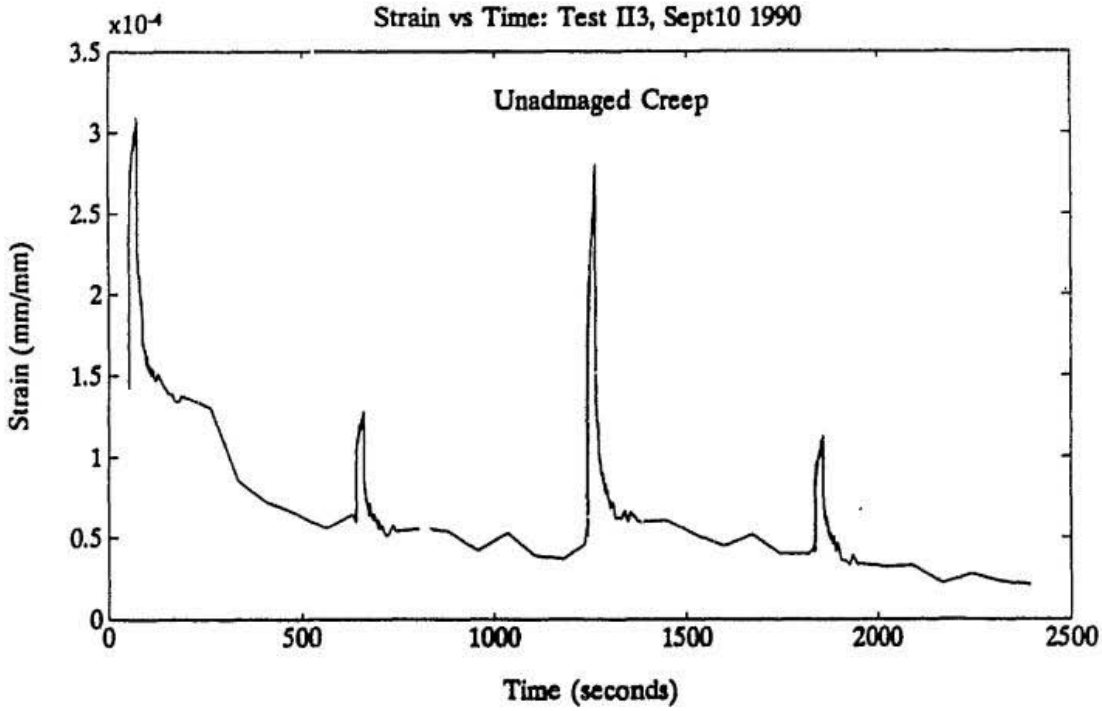
Strain vs Time: Test II3, Sept10 1990
x10-4
Unadmaged Creep
Strain (mm/mm)
3.5
3
2.5
2
1.5
1
0.5
0
0
500
1000
1500
2000
2500
Time (seconds)

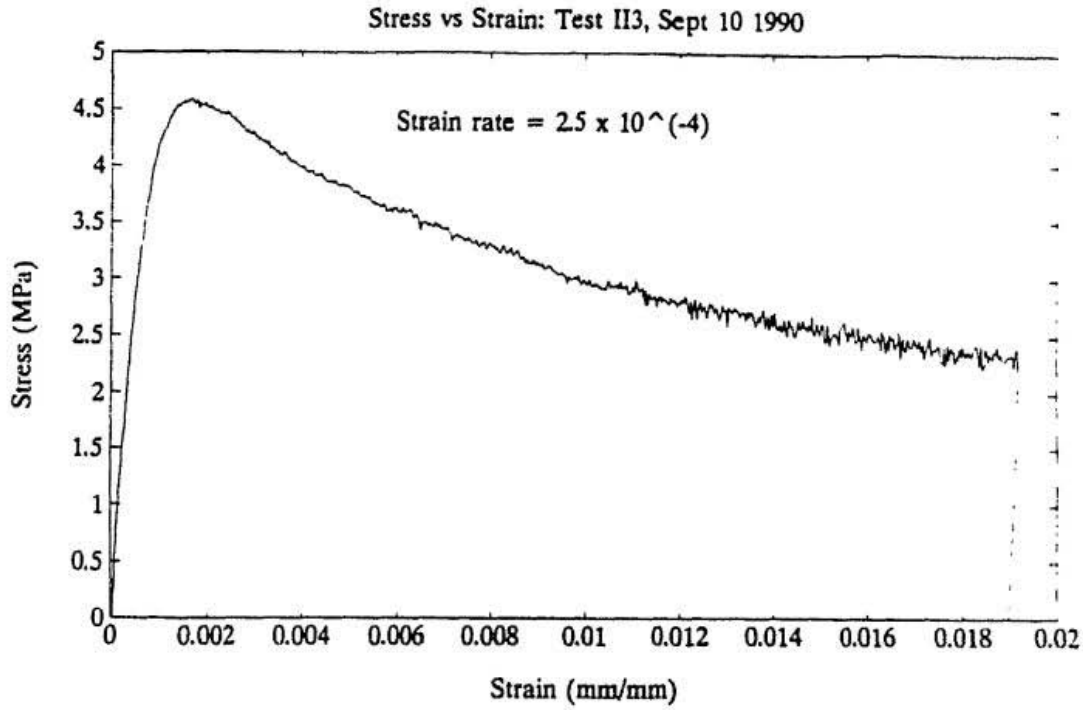
Stress vs Strain: Test II3, Sept 10 1990
Strain rate = 2.5 x 10^(-4)
Stress (MPa)
Strain (mm/mm)
0
0.5
1
1.5
2
2.5
3
3.5
4
4.5
5
0.002
0.004
0.006
0.008
0.01
0.012
0.014
0.016
0.018
0.02

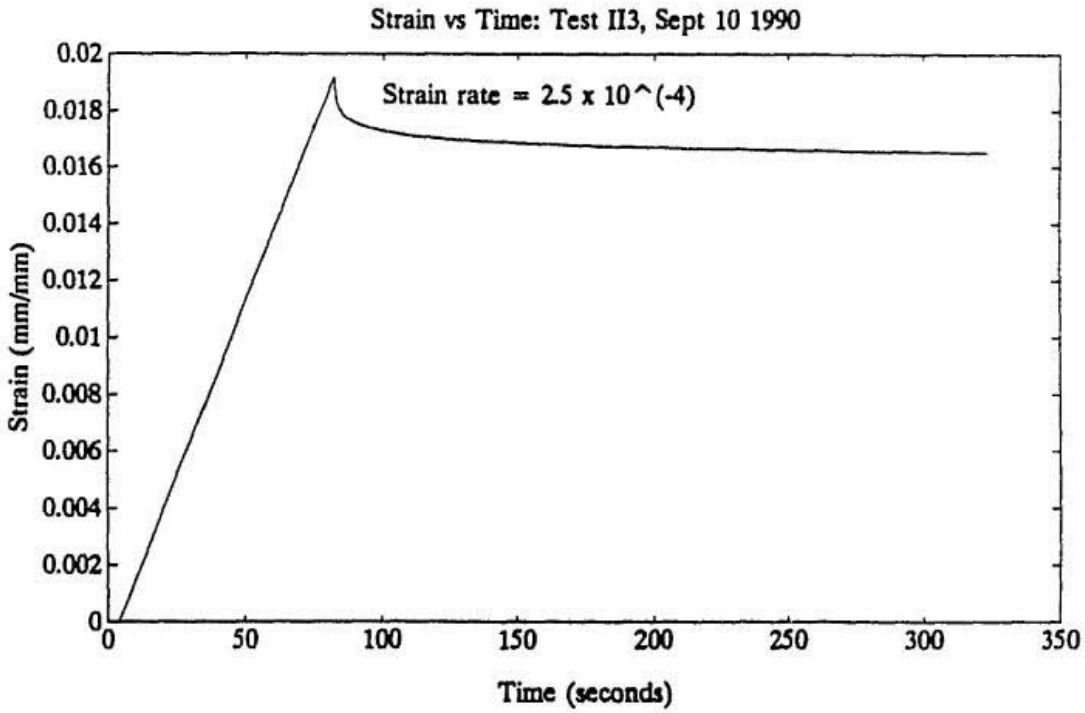
Strain vs Time: Test II3, Sept 10 1990
Strain rate = 2.5 x 10^(-4)
Strain (mm/mm)
Time (seconds)
0
0.002
0.004
0.006
0.008
0.01
0.012
0.014
0.016
0.018
0.02
50
100
150
200
250
300
350

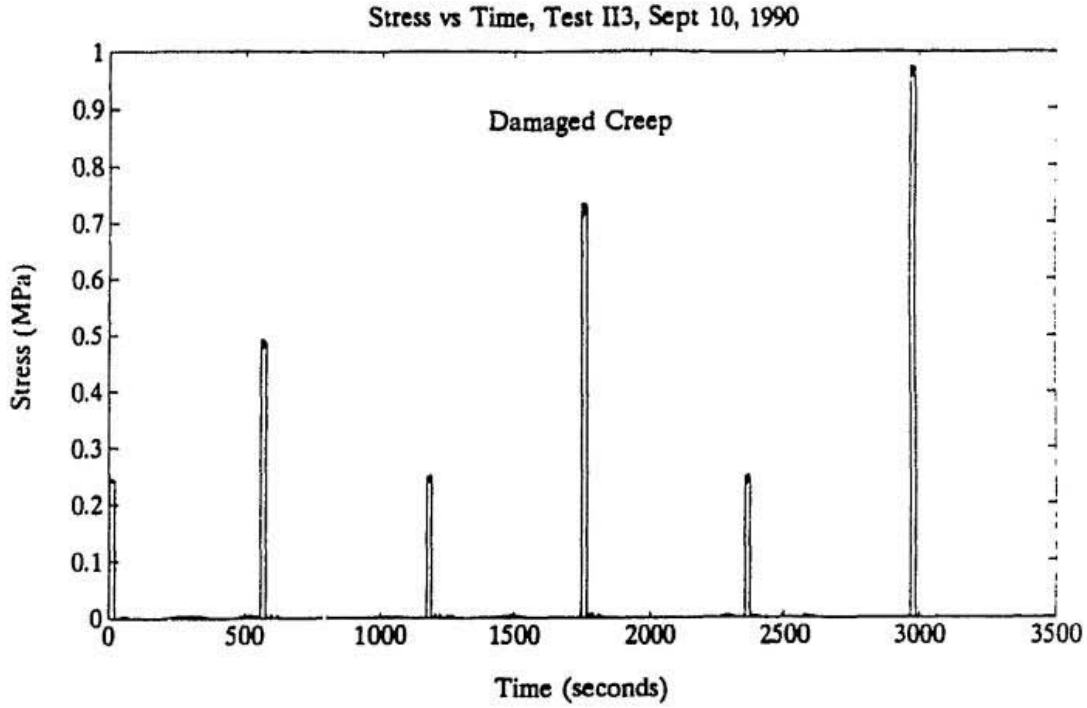
Stress vs Time, Test II3, Sept 10, 1990
Damaged Creep
Stress (MPa)
Time (seconds)
0
0.1
0.2
0.3
0.4
0.5
0.6
0.7
0.8
0.9
1
0
500
1000
1500
2000
2500
3000
3500

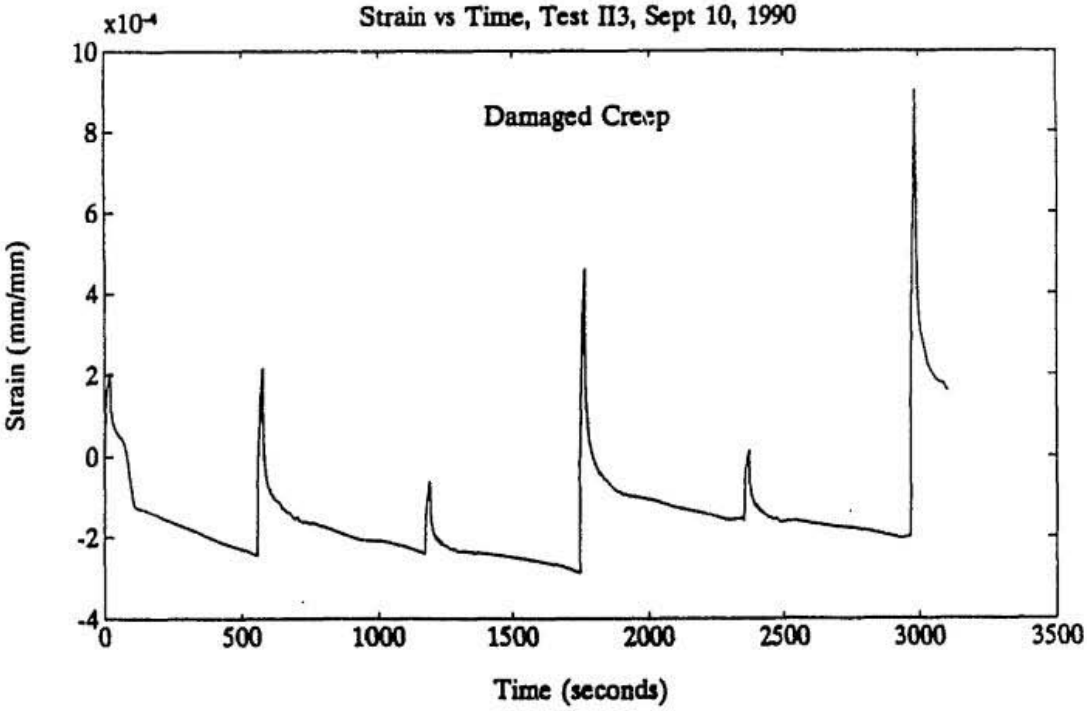
Strain vs Time, Test II3, Sept 10, 1990
x10⁻⁴
Damaged Creep
Strain (mm/mm)
Time (seconds)
10
8
6
4
2
0
-2
-4
0
500
1000
1500
2000
2500
3000
3500

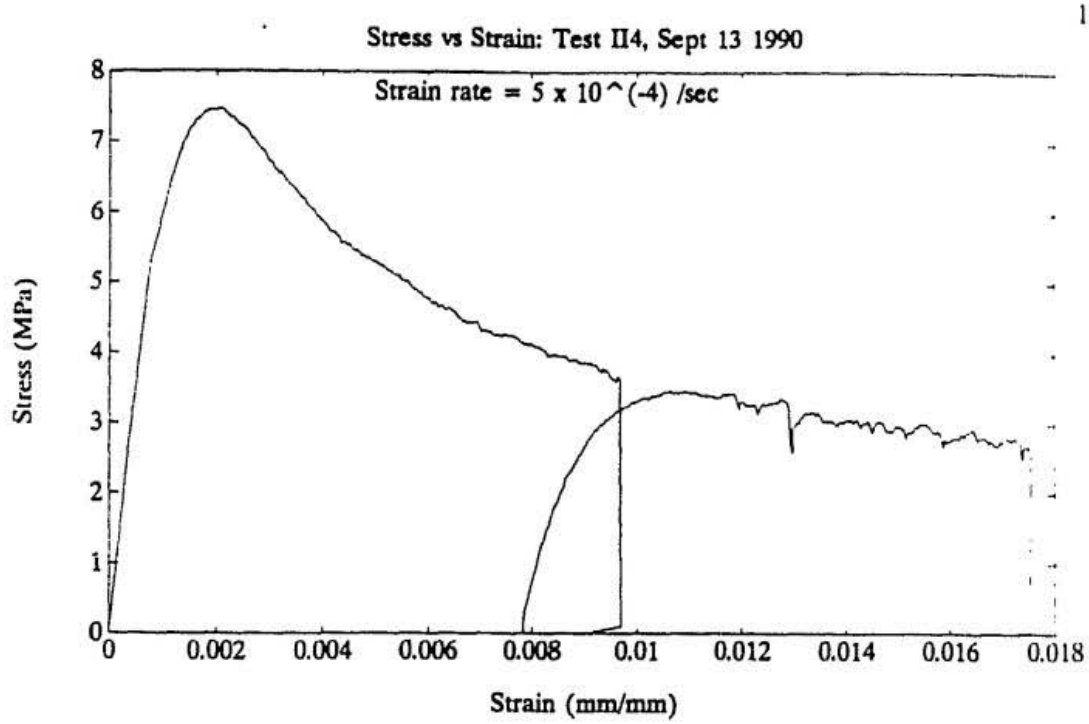
Stress vs Strain: Test II4, Sept 13 1990
Strain rate = 5 x 10^(-4) /sec
Stress (MPa)
Strain (mm/mm)
0
1
2
3
4
5
6
7
8
0.002
0.004
0.006
0.008
0.01
0.012
0.014
0.016
0.018

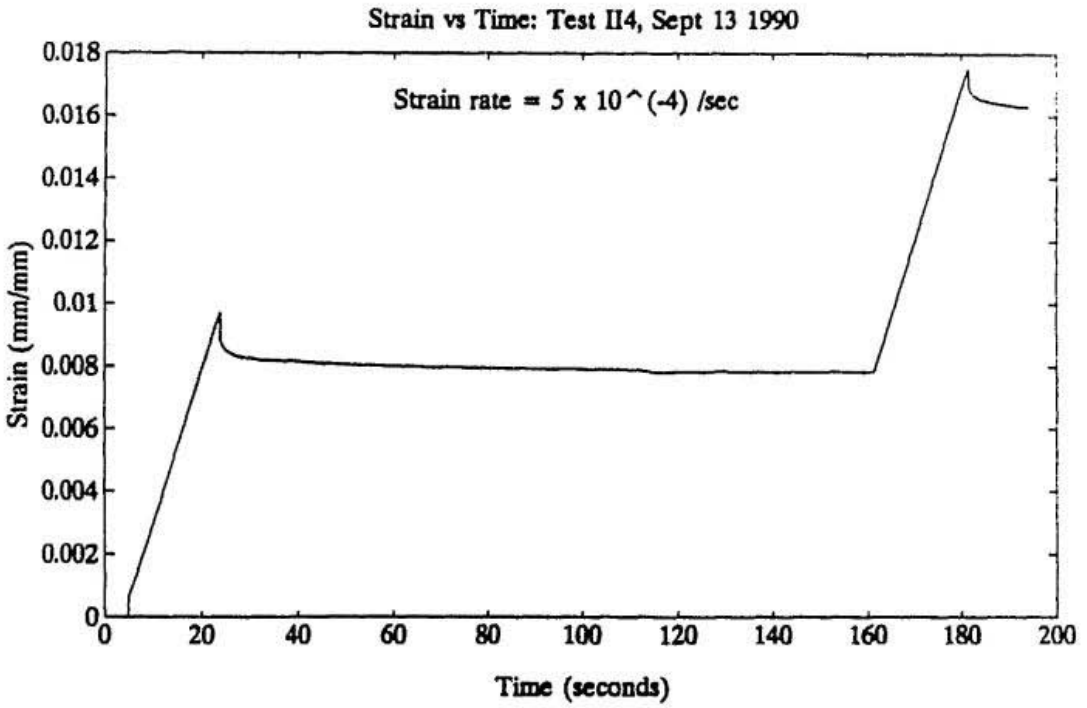
Strain vs Time: Test II4, Sept 13 1990
Strain rate = 5 x 10^(-4) /sec
Strain (mm/mm)
Time (seconds)
0
0.002
0.004
0.006
0.008
0.01
0.012
0.014
0.016
0.018
20
40
60
80
100
120
140
160
180
200

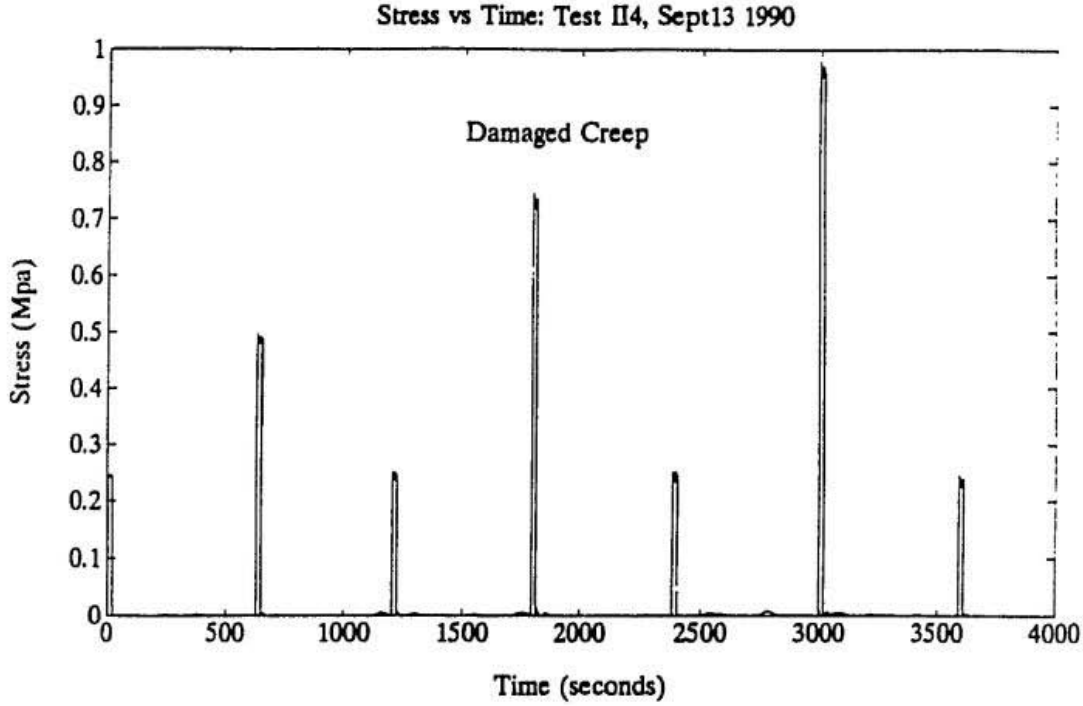
Stress vs Time: Test II4, Sept13 1990
Damaged Creep
Stress (Mpa)
Time (seconds)
0
0.1
0.2
0.3
0.4
0.5
0.6
0.7
0.8
0.9
1
0
500
1000
1500
2000
2500
3000
3500
4000

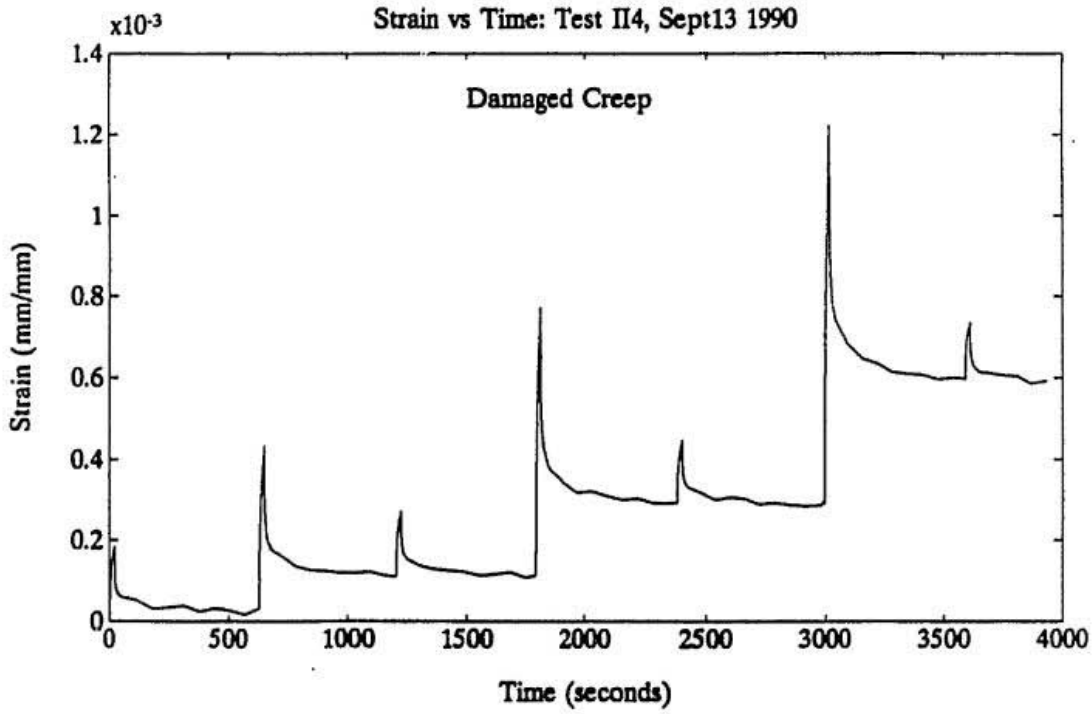
x10-3
Strain vs Time: Test II4, Sept13 1990
Damaged Creep
Strain (mm/mm)
Time (seconds)
0
0.2
0.4
0.6
0.8
1
1.2
1.4
0
500
1000
1500
2000
2500
3000
3500
4000

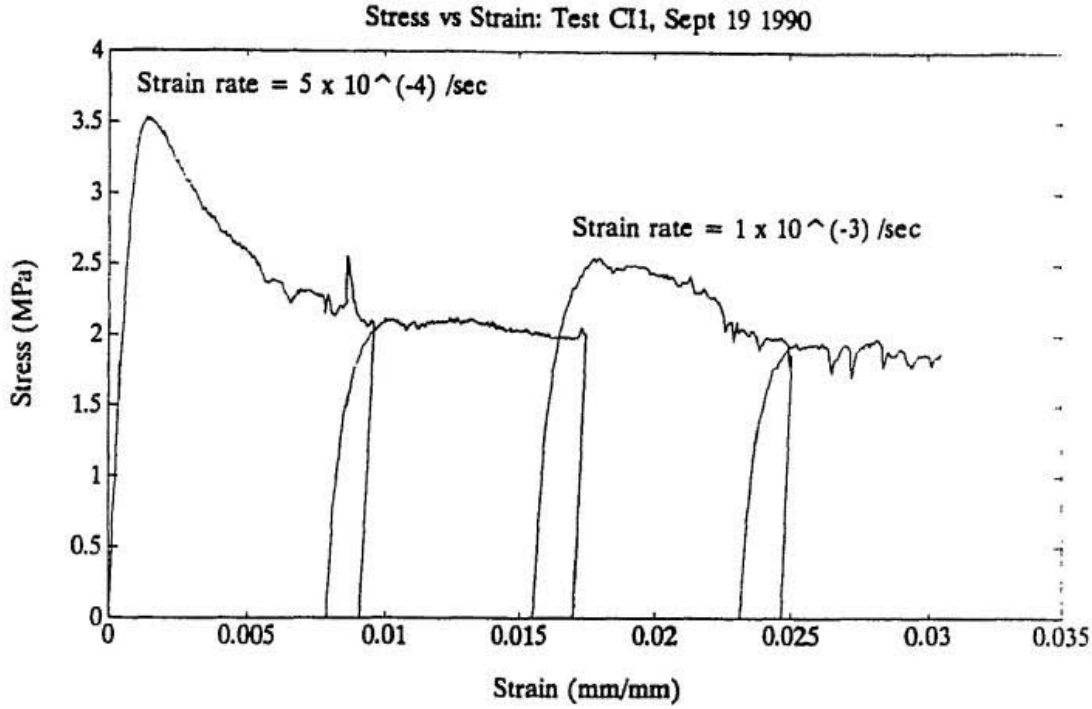
Stress vs Strain: Test CI1, Sept 19 1990
Strain rate = 5 x 10^(-4) /sec
Strain rate = 1 x 10^(-3) /sec
Stress (MPa)
Strain (mm/mm)
0
0.5
1
1.5
2
2.5
3
3.5
4
0.005
0.01
0.015
0.02
0.025
0.03
0.035

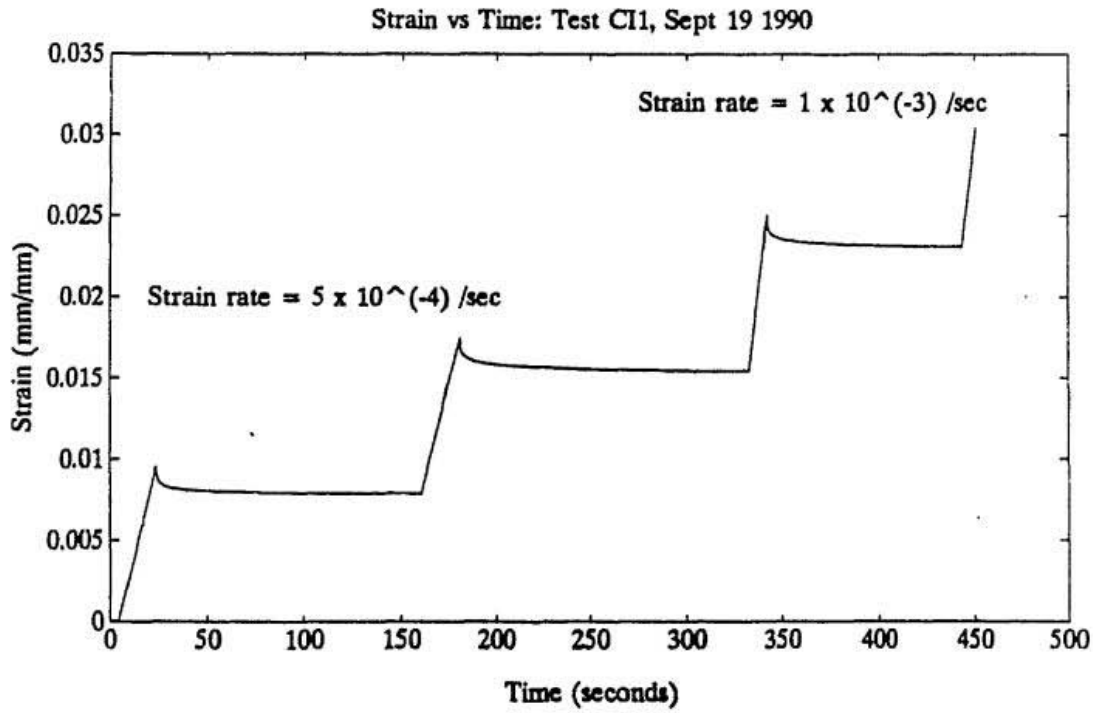
Strain vs Time: Test CI1, Sept 19 1990
Strain rate = 1 x 10^(-3) /sec
Strain rate = 5 x 10^(-4) /sec
Strain (mm/mm)
Time (seconds)
0
0.005
0.01
0.015
0.02
0.025
0.03
0.035
50
100
150
200
250
300
350
400
450
500

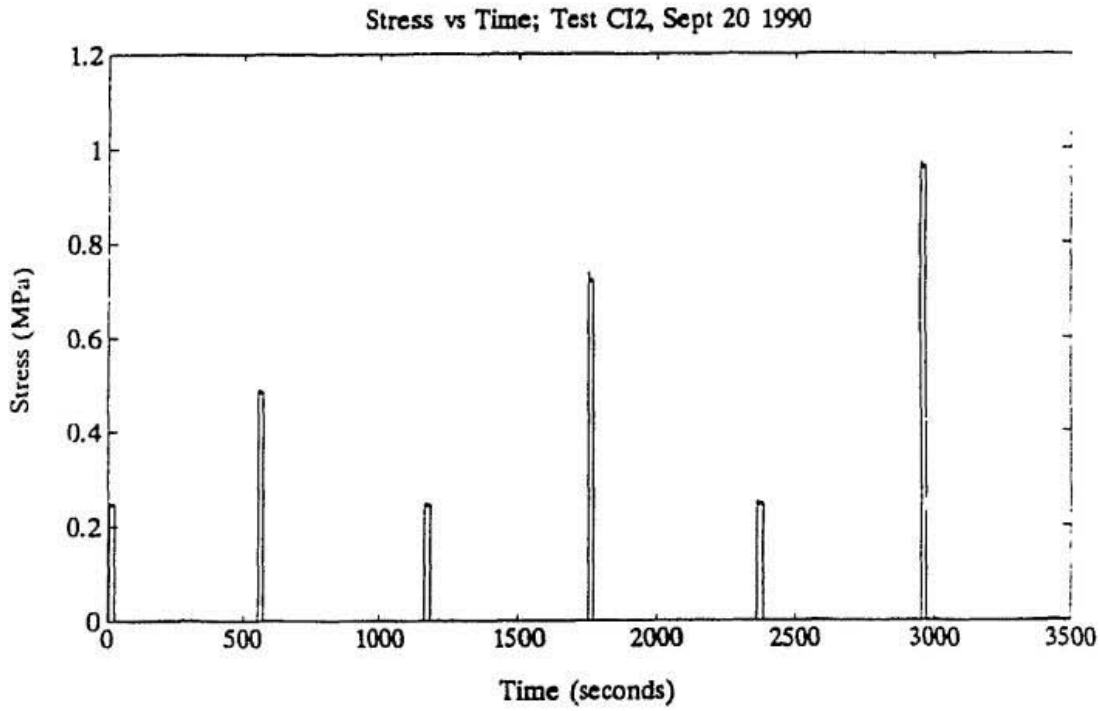
Stress vs Time; Test CI2, Sept 20 1990
Stress (MPa)
1.2
1
0.8
0.6
0.4
0.2
0
0
500
1000
1500
2000
2500
3000
3500
Time (seconds)

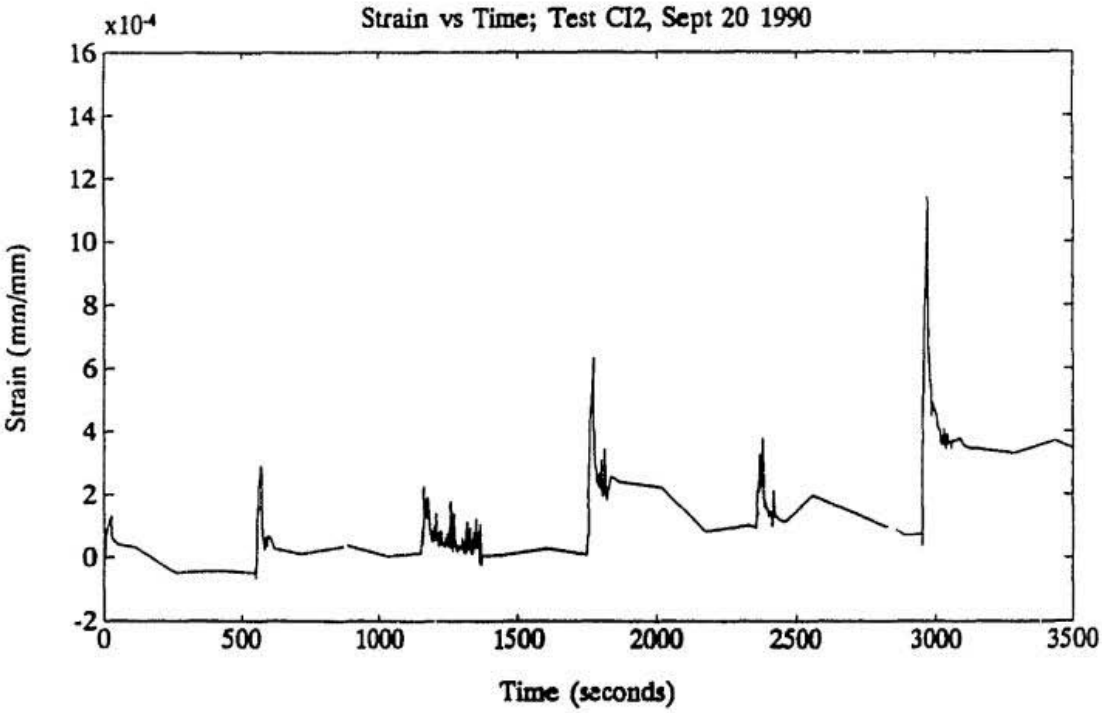
Strain vs Time; Test CI2, Sept 20 1990
x10-4
Strain (mm/mm)
16
14
12
10
8
6
4
2
0
-2
0
500
1000
1500
2000
2500
3000
3500
Time (seconds)

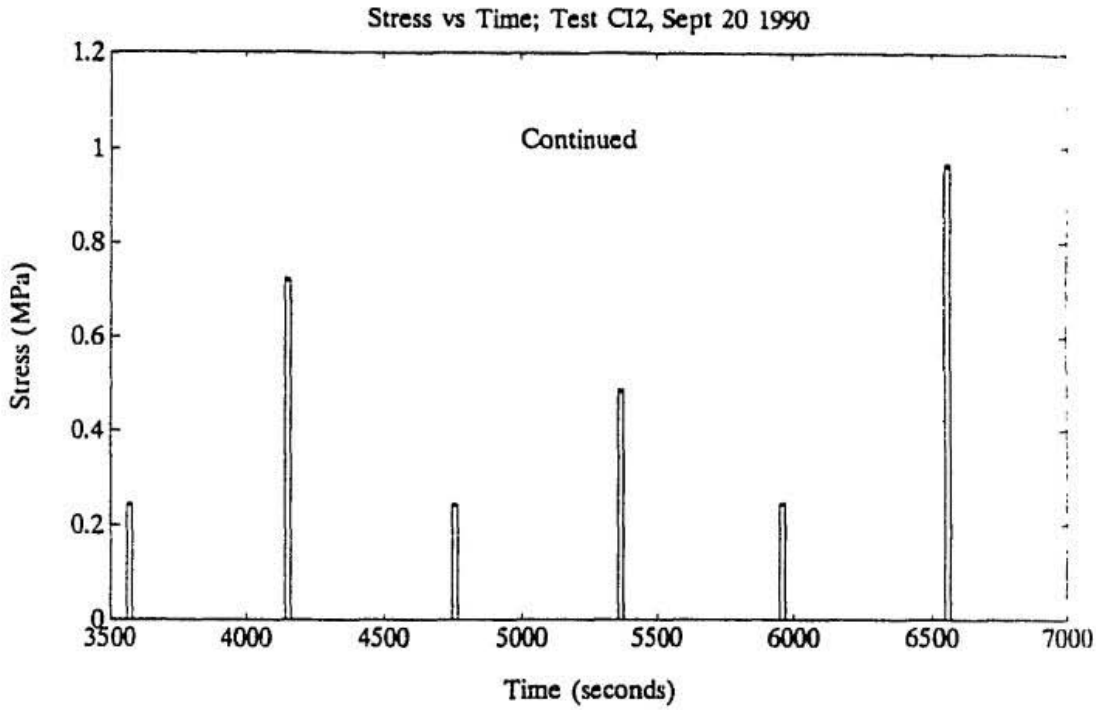
Stress vs Time; Test CI2, Sept 20 1990
Continued
Stress (MPa)
1.2
1
0.8
0.6
0.4
0.2
0
3500
4000
4500
5000
5500
6000
6500
7000
Time (seconds)

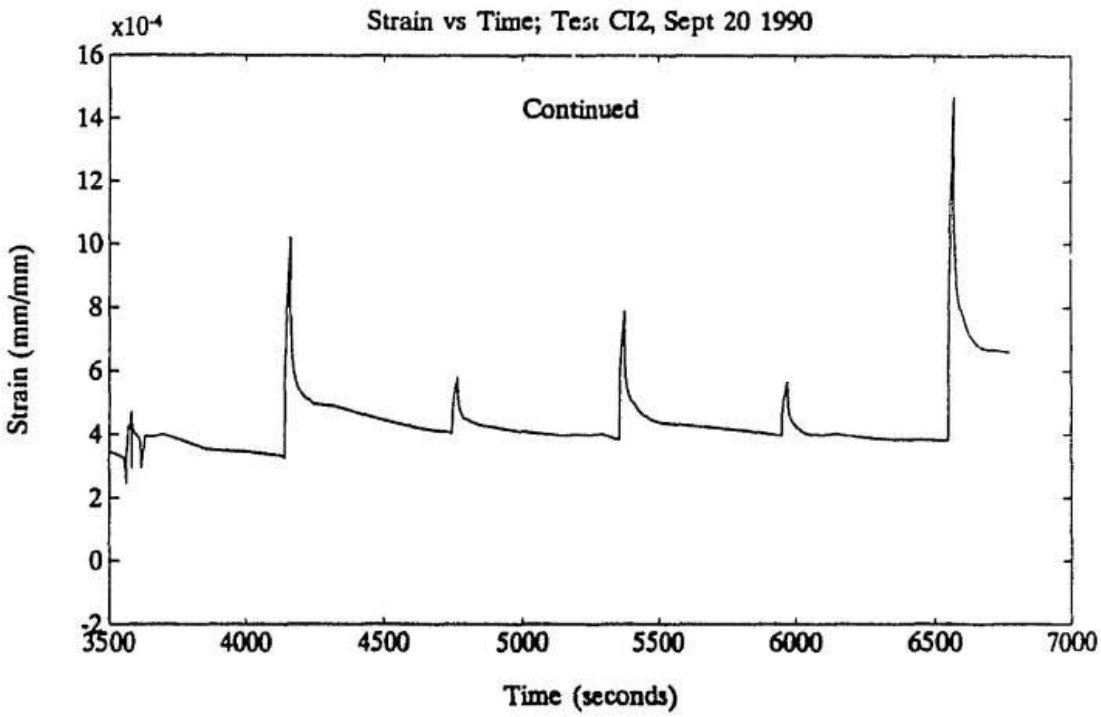
Strain vs Time; Test CI2, Sept 20 1990
x10⁻⁴
Continued
Strain (mm/mm)
16
14
12
10
8
6
4
2
0
-2
3500
4000
4500
5000
5500
6000
6500
7000
Time (seconds)

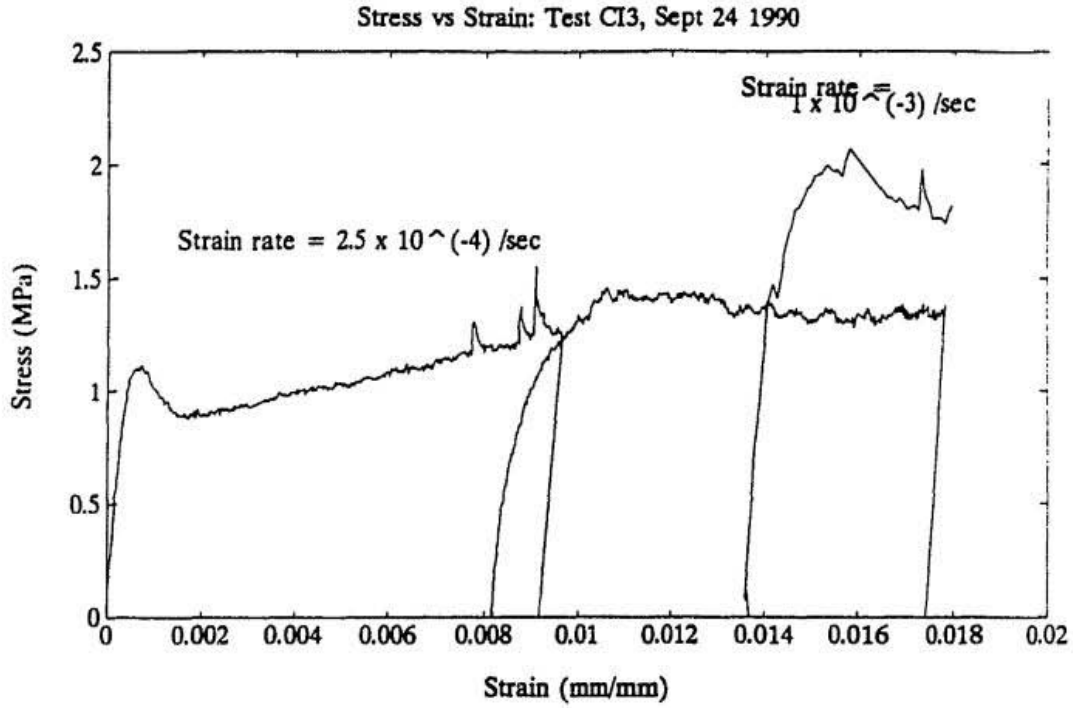
Stress vs Strain: Test CI3, Sept 24 1990
Strain rate = 1 x 10^(-3) /sec
Strain rate = 2.5 x 10^(-4) /sec
Stress (MPa)
Strain (mm/mm)
0
0.5
1
1.5
2
2.5
0.002
0.004
0.006
0.008
0.01
0.012
0.014
0.016
0.018
0.02

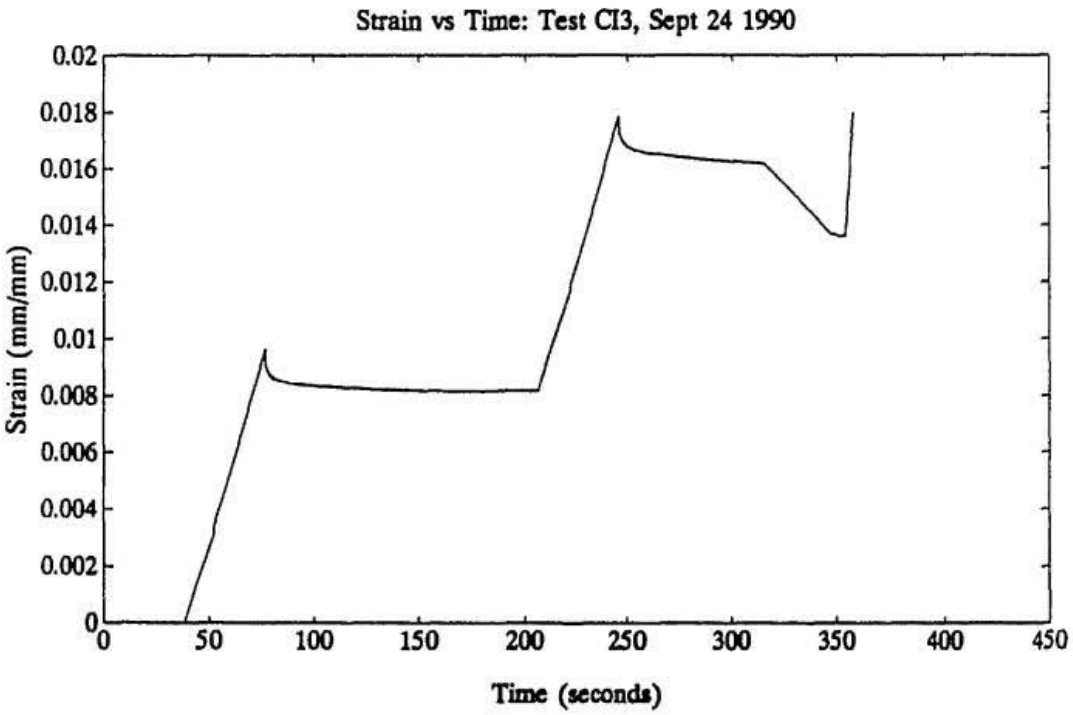
Strain vs Time: Test CI3, Sept 24 1990
Strain (mm/mm)
Time (seconds)
0
0.002
0.004
0.006
0.008
0.01
0.012
0.014
0.016
0.018
0.02
50
100
150
200
250
300
350
400
450

Appendix B

Input Data File for ABAQUS Version 4-8-4

```
**
**
**              SIMULATION OF TEST NRC-06 FROM THE
**              1989 FIELD TEST SERIES
**
**
*HEADING
SIMULATION OF TEST: NRC-06
DAMAGING VISCOELASTIC MODEL WITH
CRUSHED LAYER
**
**
*PREPRINT,HISTORY=NO
**
**
**              GENERATING NODES
**
**
*NODE,NSET=N101
101,0,0
*NODE,NSET=N121
121,0.060,0
*NODE,NSET=N141
141,0.360,0.100
*NODE,NSET=N147
147,1.5,0.100
*NFILL,BIAS=1,NSET=FACE1
N101,N121,20,1
*NFILL,BIAS=0.9,NSET=FACE2
N121,N141,20,1
*NFILL,BIAS=0.8,NSET=FACE3
N141,N147,6,1
*NSET,NSET=FACE
FACE1,FACE2,FACE3
*NCOPY,SHIFT,CHANGE NUMBER=400,OLD SET=FACE,NEW SET=COP
0,0.012,0

*NFILL,BIAS=1,NSET=ALL1
FACE,COP,4,100
*NODE,NSET=MID1
```

```
1701,0,0.200
*NODE,NSET=MID2
1721,0.060,0.200
*NODE,NSET=MID3
1741,0.360,0.200
*NODE,NSET=MID4
1747,1.5,0.200
*NFILL,BIAS=1,NSET=MID5
MID1,MID2,20,1
*NFILL,BIAS=0.9,NSET=MID6
MID2,MID3,20,1
*NFILL,BIAS=0.8,NSET=MID7
MID3,MID4,6,1
*NSET,NSET=MID
MID5,MID6,MID7
*NFILL,BIAS=.85,NSET=ALL2
COP,MID,12,100
*NCOPY,SHIFT,CHANGE NUMBER=1200,OLD SET=MID,NEW SET=BACK
0,1.500,0

*NFILL,BIAS=0.85,NSET=ALL3
MID,BACK,12,100
*NSET,NSET=ALL
ALL1,ALL2,ALL3
*NSET,NSET=CENT,GENERATE
101,2901,100
*NSET,NSET=RIGHT,GENE
147,2947,100
**
**
**                GENERATE ELEMENTS
**
**
*ELEMENT,TYPE=CPE4R,ELSET=MAIN1
1,101,102,202,201
200,701,703,803,801
250,721,722,822,821
300,1101,1105,1205,1201
330,1121,1123,1223,1221
400,133,134,334,333
```

```
410,137,138,538,537
420,533,534,634,633
450,537,538,738,737
470,1137,1139,1239,1237
482,141,142,742,741
483,142,143,1143,1142
484,143,144,1144,1143
485,144,145,1345,1344
486,145,146,1746,1745
487,146,147,1747,1746
488,1344,1345,1745,1744
490,1141,1142,1342,1341
500,741,742,1142,1141
530,1701,1705,1805,1801
550,1901,1909,2009,2001
560,1935,1937,2037,2033
580,2133,2141,2241,2233
600,1741,1742,1842,1841
680,2101,2117,2217,2201
700,2301,2333,2433,2401
**
*ELGEN,ELSET=MAIN2
1,32,1,1,6,100,32
*ELGEN,ELSET=MAIN3
250,12,1,1,4,100,12
*ELGEN,ELSET=MAIN4
200,10,2,1,4,100,10
*ELGEN,ELSET=MAIN5
300,5,4,1,6,100,5
*ELGEN,ELSET=MAIN6
330,8,2,1,6,100,8
*ELGEN,ELSET=MAIN7
400,4,1,1,2,200,4
*ELGEN,ELSET=MAIN8
410,4,1,1
*ELGEN,ELSET=MAIN9
420,4,1,1,6,100,4
*ELGEN,ELSET=MAIN10
450,4,1,1,3,200,4
*ELGEN,ELSET=MAIN11
```

```
470,2,2,1,6,100,2
*ELGEN,ELSET=MAIN12
490,3,1,1,3,200,3
*ELGEN,ELSET=MAIN14
530,10,4,1,2,100,10
*ELGEN,ELSET=MAIN19
550,4,8,1,2,100,4
*ELGEN,ELSET=MAIN20
560,2,4,1,2,100,2
*ELGEN,ELSET=MAIN15
580,1,,,8,100,1
*ELGEN,ELSET=MAIN16
600,6,1,1,12,100,6
*ELGEN,ELSET=MAIN17
680,2,16,1,2,100,2
*ELGEN,ELSET=MAIN18
700,1,,,6,100,1
**
*ELSET,ELSET=MAIN
MAIN1,MAIN3,MAIN4,MAIN5,MAIN6,MAIN7,MAIN8,MAIN9
MAIN10,MAIN11,MAIN12,MAIN14,MAIN15,MAIN16
MAIN17,MAIN18,MAIN19,MAIN20
**
*ELSET,ELSET=FACE
MAIN2,MAIN3,MAIN4,MAIN5,MAIN6
MAIN7,MAIN8,MAIN9,MAIN10,MAIN11
**
*ELSET,ELSET=LAY1
200,201,202,203,204,205,206,207,208,209
210,211,212,213,214,215,216,217,218,219
250,251,252,253,254,255,256,257,258,259
260,261,262,263,264,265,266,267,268,269
270,271,272,273
*ELSET,ELSET=LAYER
```

```
MAIN2,LAY1
**
**
**                SET MPC'S FOR MESH
**
**
*MPC
1,233,133,333
1,433,333,533
1,337,137,537
1,637,537,737
1,837,737,937
1,1037,937,1137
1,702,701,703
1,704,703,705
1,706,707,705
1,708,709,707
1,710,711,709
1,712,713,711
1,714,715,713
1,716,715,717
1,718,719,717
1,720,719,721
1,1103,1101,1105
1,1107,1105,1109
1,1111,1109,1113
1,1115,1113,1117
1,1119,1117,1121
1,1122,1121,1123
1,1124,1123,1125
1,1126,1125,1127
1,1128,1127,1129
1,1130,1129,1131
1,1132,1131,1133
1,1134,1133,1135
1,1136,1135,1137
1,1138,1137,1139
1,1140,1139,1141
1,541,141,741
1,941,741,1141
```

```
1,1241,1141,1341
1,1441,1341,1541
1,1641,1541,1741
1,742,142,1142
1,1144,144,1344
1,1544,1344,1744
1,1345,145,1745
1,1723,1721,1725
1,1727,1725,1729
1,1731,1729,1733
1,1735,1733,1737
1,1739,1737,1741
1,1905,1901,1909
1,1913,1909,1917
1,1921,1917,1925
1,1929,1925,1933
1,2109,2101,2117
1,2125,2117,2133
1,2137,2133,2141
1,2317,2301,2333
**
**
**              CREATE RIGID SURFACE AND INTERFACE
**              ELEMENTS FOR INDENTER SIMULATION
**
**
*NODE,NSET=REF
9999,0.0,-0.100
*ELEMENT,TYPE=IRS21
900,101,102,9999
*ELGEN,ELSET=INDENT
900,30,1,1
*INTERFACE,ELSET=INDENT
0.10
*FRICTION
.15,500,2000
**
*RIGID SURFACE,ELSET=INDENT,TYPE=SEGMENT
START,-0.500,-0.100
LINE,-0.500,0.0
```

```
LINE,0.500,0.0
LINE,0.500,-0.100
**
**
**                DEFINE BOUNDARY CONDITIONS
**
**
*BOUNDARY
BACK,1,2
CENT,1
9999,1
9999,6
RIGHT,1
**
**
**                DEFINE MATERIAL BEHAVIOUR
**
**
*MATERIAL,NAME=A1
**ELASTIC
**8000,0.3
**
*USER MATERIAL,CONSTANTS=24
** E0      v       dg        T        creepc    betac     csc       powsc
8000,     0.3,    0.004,    -10.0,   2,        18,       3.0,      1.0
**
** n       NO      dilat1    dilat2   creepd    betad     emoduf    dam0
3.0,      20000,  0.25,     1.5,     50,       8,        1,        0.0
**
** dum     dum     dum       dum      dum       dum       dum       dum
0.0,      0.0,    0.0,      0.0,     0.0,      0.0,      0.0,      0.0
**
*DEPVAR
19
**
*MATERIAL,NAME=A2
**
*USER MATERIAL,CONSTANTS=24
** E0      v       dg        T        creepc    betac     csc       powsc
```

```
5900,     0.3,     0.003,     -10.0,     15000,     0,     2.0,     0.5
**
** n      NO       dilat1     dilat2     creepd     betad  cmoduf   dam0
3.0,      0.0,     0.0,       0.0,       45000,     0,     0.9,     0.0
**
** dum    dum      dum        dum        dum        dum    dum      dum
0.0,      0.0,     0.0,       0.0,       0.0,       0.0,   0.0,     0.0
**
*DEPVAR
19
**
**
**                SET SECTION THICKNESS
**
**
*USER SUBROUTINE,INPUT=17
*SOLID SECTION,ELSET=MAIN,MATERIAL=A1
0.10
*SOLID SECTION,ELSET=LAYER,MATERIAL=A2
0.10
**
*RESTART,WRITE,FREQUENCY=60
**
**
**                SET STEP FOR INDENTATION AND PRINT
**                NECESSARY DATA
**
**
**DATA CHECK
*STEP,AMPLITUDE=RAMP,INC=500,CYCLE=12,NLGEOM
**
**
**                DEFINE INDENTATION PARAMETERS
**                MOVE NODE 9999 OF RIGID SURFACE 0.030 M
**                IN A TIME OF 1.5 SEC.
**                INDENTATION RATE:: 0.020 M/S
**
**
*STATIC,PTOL=1E-3
```

```
0.0001,1.5,1E-8,0.0015
**
*BOUNDARY
9999,2,,0.030
**
*PRINT,RESIDUAL=YES,CONTACT=YES,FREQUENCY=400
**
*EL PRINT,ELSET=MAIN2,SUMMARY=NO,FREQUENCY=20
MISES,S
*EL PRINT,ELSET=INDENT,FREQUENCY=20,SUMMARY=NO
S
*NODE PRINT,NSET=REF,FREQ=20
RF2,U2
*EL FILE,ELSET=MAIN,FREQUENCY=20
SDV
*EL FILE,ELSET=LAYER,FREQUENCY=20
SDV
*EL FILE,ELSET=INDENT,FREQUENCY=10
S
*NODE FILE,NSET=REF,FREQUENCY=10
RF,U
**
*END STEP
```